May 2019

The Role of Tbx5 in Sinoatrial Node Differentiation in Mouse Embryonic Stem Cell Derived Cardiomyocytes

Yunkai Dai
Clemson University, yunkaidai@gmail.com

THE ROLE OF TBX5 IN SINOATRIAL NODE DIFFERENTIATION IN MOUSE EMBRYONIC STEM CELL DERIVED CARDIOMYOCYTES

A Dissertation
Presented to
the Graduate School of
Clemson University

In Partial Fulfillment
of the Requirements for the Degree
Doctor of Philosophy
Bioengineering

---

by
Yunkai Dai
May 2019

Accepted by:
Dr Ann Foley, Committee Chair
Dr Agneta Simionescu
Dr Robin C. Muise-Helmericks
Dr Ying Mei

ABSTRACT

The sinoatrial node of the mouse embryo arises from the wall of the right atrium near the border of the sinus venosus. Early in development this region expresses the transcription factor Tbx5. Because of this, Tbx5 is thought to sit at the apex of a transcriptional cascade leading to sinoatrial node (SAN) differentiation. To test this we produced a mouse embryonic stem cell line B1 (pTripZ-mTbx5; αMHC::GFP) that conditionally overexpresses Tbx5, to determine if this would lead to enhanced SAN differentiation. We found that ES cells overexpressing Tbx5 showed enhanced overall cardiac differentiation and that cardiac cells showed increased beat rates as compared control embryos. Despite this, key genes associated with SAN differentiation including HCN4 and Shox2 increased in cells overexpressing Tbx5, while the percent of HCN4 or Shox2 positive myocytes did not alter. Faster beating cells showed a decreased expression of the chamber specific marker Cx43 and increased expression of Tbx3 and Tbx18. These data suggest that Tbx5 overexpression is not sufficient for SAN differentiation, although it does activate part of the transcriptional cascade that directs early steps in the SAN. Together these data suggest that Tbx5 cannot activate SAN differentiation alone but instead must synergize with other factors.

DEDICATION

This work is dedicated to my parents, my father YUQING DAI, my mother WENYAN MAO. Without constant supports from you, I would never be eligible to fulfill my goal to pursue my PhD degree. In 2017, I had my low-back problem which needs immediate surgery, so my dad flied from Shanghai to Charleston over 10,000km to look after me before and after my surgery by Dr John Glaser. Their help brought me back to normal life. Thanks you so much.

ACKNOWLEDGMENTS

I would like to first thank my PI, Dr Ann.C.Foley, who has supported and guided me through the past six years. In 2014, when I was the first phD student in Foley lab, Dr Foley not only showed me the professional way to perform cellular and molecular experiments, but also drove me to supermarkets for grocery shopping over the weekends when I do not have a car at that time. Her famous saying is “Devil in the details”, each steps of protocols hides a devil inside when you do not take care of your experiments seriously.

Working with my lab mate is so fun. Dr Andrew Hunter and Allison Reno built up MATLAB algorithm to calculate the beat rate automatically. Isabel Jia, she is a fast learner and a big help. Ray Deepe, he assisted me a lot for taking image on microscopy. I would also like to acknowledge other trainee of Foley lab and members of Mei lab and I really enjoyed discussing the projects with all these guys.

I would like to thanks all of my thesis committee members, Dr Simionescu, Dr Muise-Helmericks and Dr Mei, who helped me and guided me through my phD study. Special thanks to Dr Robin Muise-Helmericks, she gave me a great overview of MAP3K7 signaling pathway. They gave me deep insight into my project.

Finally, I would like to thanks my girlfriend, Bowen Sun, who is a beautiful girl from Harbin, China. We met together at Charleston, sounds like a miracle. She is a great cooker and always likes trying new recipe, so we both enjoyed the moment of tasting her delicious dinner. I hope this can stay forever. Love you so much, Bowen.

TABLE OF CONTENTS

Page

TITLE PAGE i

ABSTRACT ii

DEDICATION iii

ACKNOWLEDGMENTS iv

LIST OF TABLES ix

LIST OF FIGURES x

CHAPTER

I. LITERATURE REVIEW 1

Abstract 1
Introduction 1
Characteristics of an ideal population for cardiac Graft 3
Studies elucidating the molecular mechanisms of cardiac differentiation 4
Cardiac Progenitors 7
Progress and new challenges for cell-based therapies 10
Transcription Factor-Mediated Reprogramming 13
Engineering cardiovascular tissues 14
Heart Conduction System 22
Developmental Origin of the Sinoatrial Node 22
The transcriptional program that directs formation of the AVC and Purkinje system 26
Sinoatrial Node arrhythmias 27
Conclusions 27

II. SPECIFIC AIMS 28

Abstract 28
Specific aims 29

Table of Contents (Continued)

Page

III. MATERIAL AND METHODS 33

Cell culture 33
Plasmid transfection and Lentivirus production 33
Lentivirus Transduction and establishment of clonal cell lines 34
Embryoid Body (EB) Differentiation 35
Construct of pTripZ Vector, doxycycline-inducible-Gene of Interest (GOI)-overexpression Vector 35
Construct of pTET-ON Vector, doxycycline-inducible-GOI-overexpression Vector Flow Cytometry 36
List of vectors and mESCs line made 38
Real-time PCR 39
Flow Cytometry 42
Immunocytochemistry 42
Beat Rate data 43

IV. TBX5 OVEREXPRESSION ENHANCES CARDIAC DIFFERENTIATION AND INCREASES BEAT RATE BUT DOES NOT INCREASE THE FORMATION OF FULLY DIFFERENTIATED SINOATRIAL NODE CELLS 44

Introduction 44
Four independent clonal lines that conditionally overexpress Tbx5 were established 44
Addition of Doxycycline increased beat rate 47
Relative Tbx5 RNA Expression during EB differentiation 50
Tbx5 overexpression increases overall cardiac formation 55
Subtype of Differentiated Cardiomyocytes 58
Representative Image of ICC staining 62
Summary 70

V. THE ROLE OF MAP3K7/TAK1 OVEREXPRESSION DURING EB DIFFERNTIATION 71

Introduction 71
Cardiomyocytes derived from MAP3K7/TAK1 -overexpressing EBs display molecular characteristics of the SAN 71

Table of Contents (Continued)

Page

MAP3K7/TAK1 specifically upregulates the expression of markers for the cardiogenic endoderm. 75
MAP3K7/TAK1 Overexpression leads to up regulation of Shh and Gli2 76
MAP3K7/TAK1 Overexpression does not affect early mesoderm formation 79
Discussion 81

VI. SINGLE CELL ANALYSIS OF GENE EXPRESSION DURING MYOCARDIAL DIFFERENTIATION 82

Introduction 82
FACS Protocol 82
RNA Isolation and Reverse Transcription 85
Discussion 91

VII. DESIGN AND VERIFICATION OF OVEREXPRESSION LINES 92

Introduction 92
Independent clonal lines that conditionally overexpress Tbx3 were established 94
Independent clonal line that conditionally overexpress hIsl1 was established 99
Independent clonal line that conditionally overexpress hShox2 was established 104
Independent clonal line that conditionally overexpress hTbx18 was established 108
Independent clonal lines that conditionally overexpress MAP3K7/TAK1 were established 112
Independent clonal lines that conditionally overexpress Tbx5 were established 117
Summary 123

VIII. DISCUSSION 126

A transcriptional cascade that mediates SAN differentiation 126
ES cell lines with overexpression of Tbx3, Isl1, Shox2 and Tbx18 129

Table of Contents (Continued)

Page

Date Interpretation from Tbx5-overexpressing B1 EBs 130

IX. FUTURE RESEARCH 136

REFERENCES 137

LIST OF TABLES

Table		Page
3.1	GOI Primer was used to clone into downstream of TurboRFP motif into the pTripZ vector	37
3.2	GOI Primer was used to clone into downstream of pTight TET-Responnsive promoter into the pTET-ON vector	37
3.3	The detailed list of all vectors and mESCs made in Foley lab	38
3.4	qRT-PCR primers of Cx30.2, Cx43, GAPDH, HCN4, m/h Isl1, m/h Shox2, m/h Tbx18, MAP3K7, Tbx3, Tbx5, mCXCR4, mGPC1, mTm4sf2, mSox17, mSox2, mDkk1, mHhex, mCer1, Shh and Gli1-3	41
6.1	RNA concentration of FACS-sorted samples	86
6.2	cDNA concentration of FACS-sorted samples	86
6.3	Mean CP and CP Error collected from PCR machine	87
7.1	List of cell lines discussed in this chapter	93
7.2	List of all mESCs that I produce and all characteristics. NA, Not Applicable	125

LIST OF FIGURES

Figure Page

1.1 A graphical representation of cardiac differentiation showing the stages of cardiac differentiation, including characteristic markers of each stage 6

1.2 A graphical representation of a typical infarcted left ventricle (LV), showing wall thinning in the damaged area (yellow) 19

1.3 A comparison of cell-based therapies for heart repair with a hypothetical bioengineering approach. 19

1.4 Proposed model of TF interactions during SAN differentiation 25

4.1 Verification of B1 pTripZ-mTbx5; αMHC::GFP mouse embryonic stem cell line. 46

4.2 Manual beat data and automatic beat data. 49

4.3 Relative Tbx5 expression during EB differetiation. 51

4.4 Relative Tbx5 expression during B5 and B10 EB differetiation. 52

4.5 B1 or R1 EBs were cultured in standard differentiation Medium with either FBS #A87F82H or TET-free FBS #AC10251184 54

4.6 Cardiac differentiation analyzed by Flow Cytometry 56

4.7 Cardiac differentiation analyzed by Flow Cytometry at Day 19 and Day 21 57

4.8 The subtype of cardiomyocytes and relative transcripts of R1, B1, B1 Dox-treated EBs at Day 21 60

4.9 The subtype of cardiomyocytes and relative transcripts of R1, B1, B1 Dox-treated EBs at Day 19 61

List of Figures (Continued)

Figure Page

4.10 Representative Image of Immnuocytochemistry (ICC) Staining of Day 21 Cardiomyocytes of R1, MAP3K7 /TAK1-overexpressing, B1, B1 Dox-treated EBs.....64

4.11 Representative Image of Immnuocytochemistry (ICC) Staining of Day 19 Cardiomyocytes of R1, MAP3K7 /TAK1-overexpressing, B1, B1 Dox-treated EBs.....65

4.12 Representative Image of ICC staining of Day 21 Cardiomyocytes of R1, MAP3K7/TAK1 -overexpressing, B1, B1 Dox-treated EBs. 66

4.13 Representative Image of ICC staining of Day 19 Cardiomyocytes of R1, MAP3K7/TAK1 -overexpressing, B1, B1 Dox-treated EBs. 67

4.14 Representative Image of ICC staining of Day 21 Cardiomyocytes of R1, MAP3K7/TAK1 -overexpressing, B1, B1 Dox-treated EBs. 68

4.15 Representative Image of ICC staining of Day 19 Cardiomyocytes of R1, MAP3K7/TAK1 -overexpressing, B1, B1 Dox-treated EBs. 69

5.1 Relative Tbx18 expression during EB differetiation 74

5.2 Quantitative Real-Time PCR data showing transient up Regulation of the AVE markers Cerberus and hHex, as well as the pan-endodermal marker Sox17.....77

5.3 The effect of MAP3K7/TAK1 inhibitro 5z-7-oxozeaenol during EB differentiation 78

5.4 Quantitative Real-Time PCR data showing a strong, transient up regulation of Shh and Gli2 78

5.5 Summary of flow cytometry data 80

List of Figures (Continued)

Figure Page

6.1 Representative Image of FACS analyze data of R1 FACS Control, R1 αMHC::GFP and B1 pTripZ-mTbx5; αMHC::GFP at Day 21 84

6.2 HCN4, Shox2, Tbx3, Isl1, Cx43 relative transcription were assessed by qRT-PCR for Day 19 cardiac cell and Day 21 cardiac cell 89

6.3 HCN4, Shox2, Tbx3, Isl1, Cx43 normalized transcription were assessed by qRT-PCR for Day 19 cardiac cell and Day 21 cardiac cell. 90

7.1 Proposed model of SAN differentiation in MAP3K7/TAK1 Paper. 93

7.2 Verification of X1, X6 pTripZ-mTbx3; αMHC::GFP mouse embryonic stem cell line 96

7.3 Verification of DX5, DX9 pTET-ON-mTbx3; αMHC::GFP mouse embryonic stem cell line. 97

7.4 Relative Tbx3 expression during EB differetiation 98

7.5 Verification of I4 pTripZ-hIsl1; αMHC::GFP mouse embryonic stem cell line 101

7.6 Verification of DI1, DI3 pTET-ON-hIs1; αMHC::GFP mouse embryonic stem cell line 102

7.7 Relative Isl1, Tbx5, Tbx3, Nkx2.5 expression during EB differetiation. 103

7.8 Verification of S2 pTripZ-hShox2; αMHC::GFP mouse embryonic stem cell line 106

7.9 Verification of DS13, DS14 pTET-ON-hShox2; αMHC::GFP mouse embryonic stem cell line 107

List of Figures (Continued)

Figure Page

7.10 Verification of T2 pTripZ-hTbx18; αMHC::GFP mouse embryonic stem cell line 110

7.11 Verification of DT2, DT5 pTET-ON-hTbx18; αMHC::GFP mouse embryonic stem cell line 111

7.12 Verification of M8 pTripZ-MAP3K7; αMHC::GFP mouse embryonic stem cell line 115

7.13 Verification of DM11 pTET-ON-MAP3K7; αMHC::GFP mouse embryonic stem cell line 116

7.14 Verification of DB4, DB6 pTET-ON-mTbx5; αMHC::GFP mouse embryonic stem cell line 120

7.15 Cardiac differentiation analyzed by Flow Cytometry. 121

7.16 The subtype of cardiomyocytes of R1, DB6, DB6 Dox-treated EBs at Day 19 and relative transcripts at Day 17 122

8.1 Proposed model of TF interactions during SAN differentiation 128

8.2 Foley lab model of TF interactions during SAN differentiation 128

8.3 Beat Data and Tbx5 transcripts at Day 19 and Day 21 133

8.4 The relative transcripts of R1, B1, B1 Dox-treated EBs at Day 21 134

8.5 The subtype of cardiomyocytes of R1, MAP3K7/TAK1 overexpressing, B1, B1 Dox-treated EBs at Day 21 135

8.6 Sufficient expression of Tbx5 activates Shox2, Isl1, Tbx3, Tbx18 and HCN4 transcripts, but do not inhibits Nkx2.5 and Cx43 transcripts 135

CHAPTER ONE

LITERATURE REVIEW

Abstract

The heart is a large organ containing many cell types, all of which are necessary for normal function. Because of this, cardiac regenerative medicine presents many unique challenges. Each of the many types of cells within the heart has unique physiological and electrophysiological characteristics. Because of this grafts of donor cells must be well matched to the area of the heart into which they are grafted to avoid mechanical dysfunction or arrhythmia. In addition, grafted cells must be functionally integrated into the region of the graft to effective repair cardiac function. Because of its size and physiological function, the metabolic needs of the heart are considerable. Therefore grafts must contain not only cardiomyocytes but also a functional vascular network to meet their needs for oxygen and nutrition. Here we review progress on the use of pluripotent stem cells as a source for donor cardiomyocytes and highlight current unmet needs in the field. We will also examine recent tissue engineering approaches integrating cells with various engineered materials that should address some of these unmet needs.

Introduction

Despite the promise of regenerative medicine, cardiovascular disease remains the leading cause of death in the United States [1]. Indeed, cardiovascular regenerative medicine presents many unique challenges. First, unlike other muscles in the body, the

human myocardium possesses only limited cell division [2] and a very limited ability to repair itself after injury. A recent study using apical resection of neonatal mouse hearts suggested the murine hearts have significant regenerative capacity for some days shortly after birth. However, this capacity was lost within the first week of birth and a recent attempt to repeat these studies using a different inbred mouse strain showed only incomplete regeneration of heart tissue [3]. Together, this suggests that many as yet unknown factors may impact the regenerative capacity of the young mouse heart. To date, spontaneous regeneration of human hearts, on the scale that would be required to repair a typical myocardial infarction (MI), has not been observed. Indeed, it has been suggested that a typical infarct episode in the human heart might damage as many as one billion cells [4]; well beyond even the most optimistic estimates of the heart's ability to repair itself. Recent carbon dating experiments indicate that under normal conditions, cells within the adult human are renewed at a rate of about 1% per year until age 25 and at only 0.45% per year by age 70 [2], suggesting that there is minimal turnover of cells in healthy hearts. By contrast, the heart may be able to activate a program of renewal after injury. One study showed significant cell renewal in mouse hearts following pressure overload or infarct [5]; however spontaneous functional recovery of adult human hearts after a major cardiac event has not been observed. For these reasons, it has long been suggested that the most feasible approach to cardiac regeneration after MI would be the engraftment of cardiomyocytes or cardiac progenitors that have been expanded ex vivo from stem cell populations. Here we will review recent progress in the use of both transcription factor mediated reprogramming within the heart and the isolation of cardiac progenitors from pluripotent cells types such

as embryonic stem cells (ESCs) and human induced pluripotent stem cells (iPSCs). We will also examine how bioengineers are using tissue-engineering approaches that involve both cell grafts and hydrogels to improve the integration, differentiation and survival of cells to be grafted.

Characteristics of an ideal population for cardiac grafts

Cells that are useful as potential donors for cardiac repair should be readily available, expandable in culture, show an excellent natural ability for self-renewal and have contractile and electrophysiological characteristics consistent with their roles within the heart. Cells isolated from unrelated donors raise immunological concerns. In addition, the use of human ESCs raises ethical concerns. Because of this, non-cardiac contractile cells such as skeletal muscle cells and/or non-pluripotent stem cells derived from adult tissues were long considered to be the most desirable sources of potential donor cells for cardiac repair. More recently, the development of protocols to differentiate large numbers of bona fide cardiac cells from iPSCs, have overcome these ethical and immunological concerns while raising the hope that these cells may overcome the problems of functional integration and arrhythmias.

In recent years several protocols have been developed for the efficient production of cardiac cells from ESCs and these (or slight modifications of these) have proven to be equally effective for the differentiation of both mouse and human iPSCs. Most notably, co-culture of human ESCs (hESCs) with the visceral endoderm-like cell line (END2) [6] has been shown to induce 20-25% cardiac differentiation whereas protocols using either

carefully timed addition of growth factors [7] or a combination of growth factor addition and flow cytometry-based selection of cardiac progenitors [8] have been shown to activate 30% and 40-50% cardiac cells, respectively. These protocols are in turn based on a large body of work, done in frog, chick and mouse embryos, as well as in ESCs to elucidate the embryology and molecular genetics of heart induction.

Studies elucidating the molecular mechanisms of cardiac differentiation

The mammalian heart is made up of cells from at least three sources. First, multi-potent cardiac progenitors that form during gastrulation give rise to the original linear heart tube and are referred to as the first heart field (FHF). In addition to this, two groups of cells that lie outside this initial heart tube also contribute to the adult heart. The so-called second heart field (SHF) [9-14] and the neural crest [15]. We have previously reviewed the embryology and molecular genetics of primary (FHF) heart induction in detail [16, 17]. However, a few features that are particularly relevant to stem cell differentiation of cardiac cells should be mentioned here. Heart formation is a multistep process that begins with the formation of mesoderm during gastrulation. In all vertebrate embryos and in ESCs, the activities of Transforming Growth Factor beta (TGFβ) family members and Wnts are required for the formation of mesoderm as cells exit the primitive streak (or dorsal lip in amphibian embryos) [18-27] . Once formed, the mesoderm immediately begins to migrate away from the streak and toward its final position in the embryo where it will begin to differentiate according to its location within the embryonic axis [28, 29]. When Wnt signals are depleted for the endoderm of early mouse embryos, multiple beating hearts form all

along the embryonic axis [30], suggesting that there is a broad potential for cardiac formation within the mesoderm of the early embryo. These studies also suggest that Wnt signaling from the endoderm appears to actively repress myocardial formation outside of the normal heart field. Thus, the migration of mesoderm away from the primitive streak may serve, not only to bring cells into their final positions within the embryo but may serve to protect the future heart field from Wnt signals that are present in the primitive streak.

This finding is consistent with earlier studies in chick, frog, mouse and zebrafish demonstrating that the transition from uncommitted mesodermal cell to cardiac progenitor involves both cell migration away from the primitive streak (or its embryological equivalent) and presence of signals that inhibit Wnt [31-33]. In the embryo (and almost certainly also in differentiating ESCs), this signal comes from the adjacent endoderm. Later, other growth factors including FGF act on the myocardium to activate cell proliferation (reviewed in: [16, 17]. Thus a hallmark of FHF induction across all vertebrates is the transient activation of Wnt and TGFβ signaling to activate mesoderm formation from the pluripotent epiblast, followed by a period of Wnt inhibition that is necessary for mesodermal cells to adopt a cardiac fate (Fig 1.1) [34, 35]. As with mammalian embryos, a combination of Wnt and TGFβ signaling can be used to activate a primitive streak-like activity from ESCs [36] and timely modulation of TGFβ and Wnt signaling have proven to be necessary and sufficient to activate the formation of cardiac progenitors and beating cardiomyocytes formation from both mouse and human ES cells [7, 8, 13, 37-43].

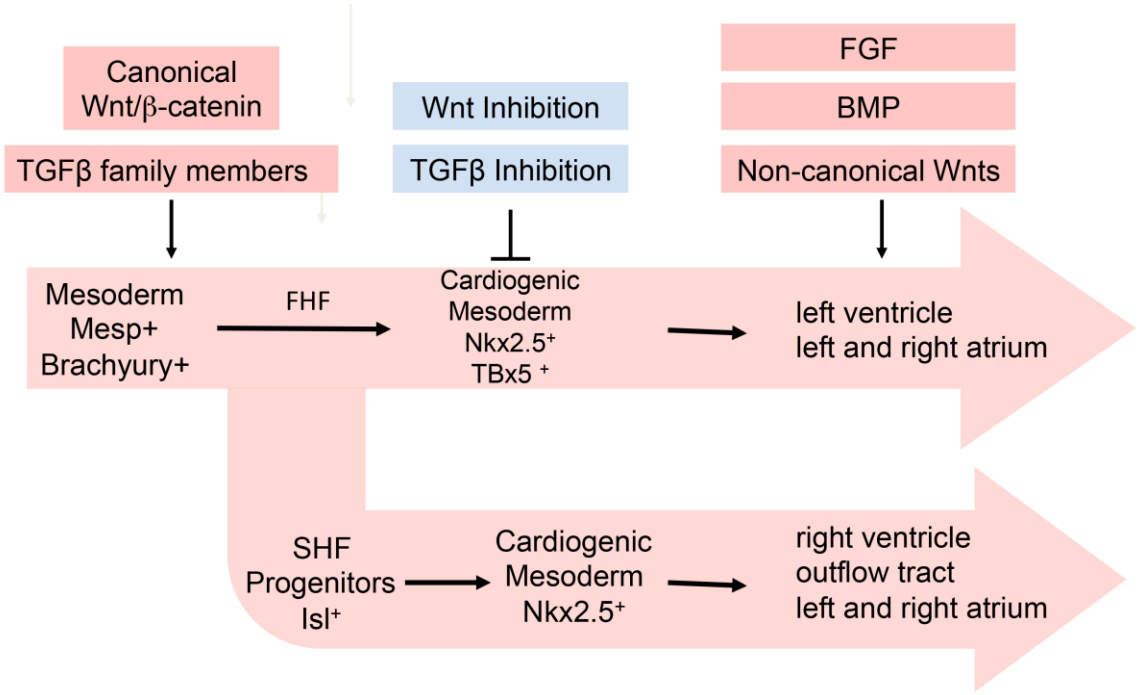

Fig 1.1 A graphical representation of cardiac differentiation showing the stages of cardiac differentiation, including characteristic markers of each stage. Also noted are key indicators that differentiate between the first heart field (FHF) and second heart field (SHF). Key regulators of each developmental step are indicated. BMP, bone morphogenic protein; FGF, fibroblast growth factor; TGF, transforming growth factor.

Differentiation of SHF cells toward the myocardial state is delayed as they proliferate and move toward the heart tube through a mechanism that is not fully understood. At about E8.5, SHF cells begin to contribute to the growing heart by migration through the arterial and venous poles of the heart. The right and left atria contain derivatives from both the FHF and the SHF. By comparison, the left ventricle develops primarily from the FHF and the right ventricle and outflow tract (OFT) primarily from SHF progenitors [12, 44, 45]. It is unclear whether there is an equivalent to FHF and SHF differentiation during cardiomyocyte differentiation from ESC. However, since the major force generating cardiomyocytes of the heart (left ventricular cardiomyocytes) are derived from the FHF, understanding the factors that mediate the switch between FHF and SHF development may lead to improved protocols for the *in vitro* differentiation of cardiac cells enriched for the left ventricular fate.

Cardiac Progenitors

When embryonic stem cells are differentiated as embryoid bodies (EBs), they readily form cardiac cells but they also produce many other cell types. A major area of research over the last decade therefore has been the search for markers that could identify a cardiac specific progenitor population (Fig 1.1). This would allow researchers to isolate, by flow cytometry, just those cells that had the potential to differentiate as myocardial cells.

Genetic fate-mapping experiments in the mouse indicate that both the FHF and SHF are derived from a progenitor population expressing Mesp1. Mesp1 (+) mesoderm emerges from the primitive streak of the mouse early during gastrulation (~E6.5) [46, 47] and

migrates around the epiblast cylinder, coalescing across the anterior midline to form the cardiac crescent at E7.5. By E8.5 the cardiac crescent has undergone a series of morphogenetic movement to form the beating linear heart tube. Mice lacking both Mesp1 and Mesp2 form axial mesoderm at the streak, as assessed by the expression of the pan-mesodermal marker Brachyury but these mice do not form the migratory "mesodermal wings" [48] and as such are devoid of most mesodermal lineages. When ESCs are differentiated as embryoid bodies (EBs), typically 2-3% of the cells develop into cardiac lineages. When Mesp1 is transiently overexpressed in EBs, this percentage increases to as much as 10%, suggesting that Mesp1 expressing cells encompass a cardiac progenitor population. However, since most mesodermal lineages are marked early on by the expression of Mesp1, this proved to be too non-specific to be an effective marker of cardiac progenitors [49].

Some of the earliest markers of the cardiac primordium are the transcription factors Nkx2.5 and Tbx5. Although there is considerable overlap between the expression patterns of these two genes, fate mapping reveals that Nkx2.5 is expressed in derivatives of both the FHF and SHF [50] whereas the expression of Tbx5 is biased to (but not exclusive to) the SHF[51]. Because of this, *Nkx2.5* was also examined as a potentially specific marker for cardiac progenitors. *Nkx2.5* expressing cells that are isolated either *in vivo* from mouse embryos or *in vitro* from differentiating ESCs are bi-potential and give rise to both cardiac and smooth muscle. In addition, this progenitor population can give rise to multiple cardiac lineages (based on cell shape and action potential morphology) including atrial, ventricular and conduction system [52].

At the cardiac crescent and linear heart tube stages, SHF cells, identified by the expression of *Isl1* [9, 11, 13, 53] and *Fgf10* [12], reside outside of the heart tube [11]. Initial genetic fate mapping experiments suggested that cells that have expressed *Isl-1* give rise to both the coronary vasculature and multiple cardiac lineage including cells in the atrium, ventricles, conduction system and outflow tract [11, 54, 55], with the majority of cells located in the right atrium and outflow tract and only a small contribution to the left ventricle [54, 56]. Similarly *Isl-1* expressing cells that are isolated from differentiating hESCs give rise to smooth muscle, cardiac and endothelial cells [53]. A recent reassessment of the Isl1 fate map suggests that Isl1 is expressed in all cardiac progenitors [50].

One marker that has proven to be extremely useful for the identification and isolation of cardiac progenitors is the *fetal liver kinase-1* (*Flk-1*). *Flk-1* is the major receptor for vascular endothelial growth factor A (VEGF-A). Because this, it was thought that it would primarily mark endothelial and hematopoietic lineages. However, Cre-mediate fate mapping in mouse embryos revealed, surprisingly, that Flk-1(+) cells also give rise to several mesodermal lineages [57, 58] and Flk-1(+) cells isolated from differentiating mESCs gave rise not only to endothelial cells but also to cardiac and smooth muscle cells [59-61]. Differentiating ES cells that are FACS sorted based on the simultaneous expression of both *Flk-1* and the chemokine receptor CXCR4 comprise a cardiopoietic lineage that is largely depleted of endodermal cell types [62]. Ultimately, the combination selection based on Flk-1 (KDR in humans) with addition of pro-cardiogenic growth factors proved to be the basis for the very efficient differentiation of cardiac cells from hESCs [8].

Unfortunately of the potential cardiac progenitor markers that have been identified to date, no single marker identifies cardiac and only cardiac lineages. Therefore the isolation of highly purified cardiac cells may require further steps. For example, sorting based on the expression of several markers might produce a population that is more enriched for cardiac cells or could be used to isolate specific sub-populations within the myocardium. Another potential problem with the protocols currently in use to activate heart formation from stem cell sources is that they all have the potential to activate the formation of multiple cardiac types, including atrial, ventricular and conduction system [63-65], raising the possibility of arrhythmias if cells with inappropriate electrophysiologies develop within grafts of cells.

Progress and new challenges for cell-based therapies

This concern is highlighted in recent work by, Murry and colleagues. Their recent work highlights the progress that has been made in generating donor cells from ES cells. They demonstrated the feasibility of large-scale production of cardiomyocytes from human ES cells that can be frozen in sufficient numbers and with sufficient subsequent viability for therapeutic applications in humans ($1X10^9$ cells). In addition, when these cells were injected directly into the infarct zone of a non-human primate MI model, these cells were retained within the heart for at least several weeks (and, in the one case that was assessed, for up to 3 months) and showed calcium transients that were synchronized with the rest of the myocardium suggesting functional engraftment [66]. During these studies, they made two observations that highlight the next major challenges for this field. First, although the

group size in this study was small, recovery of ventricular function was not statistically significant, which raises the possibility that these cells lacked some of the mechanical properties of mature ventricular cells. Indeed, myofibril alignment sarcomere registration and cardiomyocyte diameter, suggested that these cells were not fully mature. Advances in the field on physiological maturation of cardiomyoctyes were recently reviewed in: [67]. Electrophysiological maturation was not assessed in these cells, however grafts resulted in arrhythmias not observed in sham-injected animals suggesting either incomplete electrophysiological maturation or the presence of non-ventricular cardiac cells within the graft.

One of the great unmet needs in the field of cardiac regeneration is to determine the extent to which the characteristics of a cardiomyoctye are determined by its final position within the heart and what extent is determined by extrinsic factors. In short, when does a cardiomyocyte "know" that it will be part of the atrium, ventricle or conduction system? If a cell fated for the atrium is grafted into the ventricle what happens to it? Does it change its fate according to its new position? Does it die? Does fail to functionally integrate? Or, does it become a potential source of arrhythmias? Early fate maps in the chick embryo suggest that atrial and ventricular fates within the myocardium are sorted out before they exit the primitive streak [68]. This occurs at midblastula in the zebrafish [69]. Explants of the prospective chick heart field that are grown in isolation differentiate according to their fate. That is, an atrial specific myosin heavy chain is only expressed in posterior explants and not in anterior explants that are fated to become the ventricle [70]. Altogether these data suggest that some degree of lineage determination has occurred well before cell

differentiation as cardiomyocytes. That much said, there is also evidence that the fate of cardiac progenitors remains flexible for some time. For example explants of the future ventricle could be induced to express atrial markers by treating them with retinoic acid [71] and when cells fated to the atrium were grafted into the ventricle, they changed their rate of beating [72]. These studies suggested that plasticity was maintained throughout the cardiac progenitor phase and only ended after differentiation as beating cardiomyocytes. The implication for regenerative medicine is that it may be more therapeutically beneficial to transplant cardiac progenitors rather than beating cardiomyocytes. Although, as discussed above, we have not yet identified a progenitor population that gives rise exclusively to cardiac cells.

At present few groups have attempted to differentiate cells of specific cardiac lineages. The underlying assumption has been that cardiac progenitors function as generic cardiac cells that will develop mature electrophysiologies appropriate to their ultimate position within the heart. However this hypothesis has not been directly tested. Recently [73-75], it has been shown that a small molecule inhibitor of the canonical Wnt/β-catenin signaling pathway appears to direct cells with high preference to the ventricular fate. Interestingly other small molecule inhibitors of Wnt and the protein Dkk1 do not have this effect [74], suggesting that our understanding of the molecular genetics of this process is not yet fully understood. The ability to direct myocardial differentiation to specific cardiac cell types may represent an extremely important next step in realizing their full regenerative potential.

Transcription Factor-Mediated Reprogramming

Another area currently being explored for cardiac regenerative medicine is use of transcription factor mediated reprogramming of cells. The development of iPSCs [76], which demonstrated that essentially any differentiated cell could be restored to a pluripotent state by the activation of a small number of transcription factors, renewed interest in the concept that any cell might be converted to a different cell type by ectopic expression of the correct combination of transcription factors in that cell. Previously, work on genes such as *MyoD* and *Pax6*, had suggested that at least some cell fates might be controlled by single master regulatory genes. Indeed overexpression of the drosophila *Pax6* homolog, *eyeless*, in legs and wings was sufficient to induce ectopic eye formation [77]. Before that, *MyoD* was shown to be capable of converting fibroblasts to a myogenic state [78, 79]. However, further research quickly demonstrated that few, if any, cell fates are controlled by the activity of a single master regulatory gene. Current work in the field of transcription factor mediated reprogramming has focused on identifying minimal sets of transcription factors that might control given cell fates. With regard to the cardiac fate, it has been shown that overexpression of three transcription factors (Gata4, Mef2C and Tbx5) in mouse fibroblasts or directly in mouse hearts can activate many characteristics of cardiomyocytes, including beating, in non-cardiac cells [80, 81]. However attempts to repeat this work using tail fibroblasts showed only inefficient reprogramming as well as the absence of spontaneous action potentials and contractile phenotype [80, 82]. In addition, this combination of transcription factors did not induce full reprogramming in human fibroblasts [83]. It may be that a different, or expanded set of transcription factors will be

required to accomplish full reprogramming in human fibroblasts. In addition to finding the reprogramming factors, the efficiency of this approach will also have to be improved, given that the average infarct in humans may involve injury to as many as a billion cells [4]. In addition, the current route of delivery of these reprogramming factors *in vivo* has been genetic modification of cells with viruses. This approach may therefore present some regulatory barriers.

Until recently, it has been assumed that reprogramming approaches would involve the conversion of a generic cell type, such as a fibroblast, to desired cell types, however, it may be possible (and more straight forward) to use transcription factors to convert cells from one fate to another closely related fate. For example, Kapoor et al. reported that they were able to convert neonatal rat ventricular cardiomyocytes to a pacemaker-like fate by transfection of the transcription factor Tbx18 [84].

These early studies are encouraging but await improvements in efficiency as well as studies to determine the extent to which reprogrammed cells recapitulate normal cardiac mechanics and electrophysiologies.

Engineering cardiovascular tissues

Although we have made tremendous progress there are still many challenges for cardiac regenerative medicine there are still many challenges that must be solved. Bone fide cardiac cells grafted into a non-human primate appeared to be functionally linked to the host myocardium, as demonstrated by synchronized calcium transient however the caused arrhythmias and did not statistically improve overall ventricular contractility [66].

These findings are possibly due to a failure of these cells to mature in place. In addition, thinning of the ventricular was after MI often results in remodel that affects overall heart function. Although this was not assessed in Chong et al. remodeling could also contribute to the poor recovery of contractile function.

Solutions for the unmet challenges for cardiovascular regenerative medicine may involve the use of engineered materials to enhance cardiac differentiation, electrophysiological maturation and/or to preserve or replicate the three dimensional (3D) structure of the heart following MI. Here we will specifically focus on the potential of hydrogels and the combination of hydrogels with cells in the context of 3-Dimensional (3-D) printing to meet some of these challenges.

Using bio-inks or other types of scaffolds, bioengineers are attempting to create microenvironments conducive to cardiac differentiation or maturation and/or that maintain the 3-D structure of cardiac tissue after MI. Hydrogel scaffolds have also been shown to facilitate the growth and expansion of vascular tissues within myocardial grafts. In addition to this, by varying the mechanical and chemical properties of hydrogel scaffolds, they can be designed in ways that allow researchers to test the roles of mechanical stress [85] or electrical pacing (reviewed in: [86]).

A. Hydrogels

A number of research groups are now exploring the feasibility of using hydrogel/cell combinations as patches or injectable/printable bio-inks. Natural hydrogels include Matrigel (a commercially available combination of laminin, TypeIV collagen and heparin sulfate) [87], collagen [88], fibrin [89] and alginates [90]. Each of these separately

been shown to enhance the retention and integration of injected cells and to preserve the normal morphology of the ventricular wall after MI [87]. In addition, a number of synthetic hydrogels are being explored [91], however the cytotoxic and immune potential of these various synthetic compounds is largely unknown but should be explored. For example injection of a non-degradable synthetic polyethylene glycol (PEG) hydrogel into the infarct zone of a rat MI model resulted in significant infiltration of macrophages suggesting an immune response [92].

The precise physical properties of hydrogels will likely vary somewhat depending on the experimental and therapeutic context, however there are some general characteristics that may be highly desirable for use in cardiac regenerative therapies.

1) The ability to vary the viscosity of a hydrogel would be highly desirable. Lower viscosity hydrogels could be injected the wall of a damaged heart with lower injection pressure so as to not create further damage to the wall of the heart during injection or cause damage to the cells being injected. This would include hydrogels that could be injected in a liquid or semi-liquid state but which would become more rigid at body temperature. Alternatively, slightly more viscose hydrogels would be useful for 3D printing of organs or patches.

2) For hydrogels that would be injected into heart tissue, it would be desirable to have gels with sufficient flexibility so as to not interfere with the contractility of cardiac cells within or near the site of the graft.

3) Temporary hydrogels that could degrade over time could be highly desirable. In the short run the gel itself could be used to maintain the geometry of the ventricular wall

of the heart during repair. This would give cells encapsulated within the gel time to expand and integrate into the host myocardium or provide a scaffold for endogenous stem cells to migrate into the infarct zone.

4) Hydrogels that could be linked through ionic or covalent bonds to peptides or proteins that enhance growth, differentiation or physiological function would be tremendously useful. Similarly attachment of nano-particles could be used for the delivery of drugs in a spatially and temporally controlled fashion. For example, Paul et al. recently demonstrated the feasibility of using a hydrogel for localized delivery of the angiogenic factor Vegf that was complexed with a functionalized graphene oxide nanosheet[93].

B. Hydrogels and Cardiac Repair

Jonathan Butcher and colleagues recently reported the development of bio-inks with high viscosity and low stiffness that were practical for 3D printing of structures that encapsulated human aortic valvular interstitial cells (HAVICs). This was accomplished by manipulating the relative amounts of methacrylated hyaluronic acid and methacrylated gelatin. Increased relative methacrylated gelatin resulted in improved cell spreading and maintained fibroblastic phenotype. Using 3D bio-printing they produced 3D tri-leaflet valve conduits with hybrid hydrogel encapsulating HAVICs.

After 7-day of culture, the encapsulated HAVICs showed high cell viability, cell-type appropriate cell morphologies and expressed all target genes that they tested, including αSMA, vimentin, periostin and collagen I [94].

Pathological remodeling of the ventricular wall is a common and deleterious effect of MI. Not only is there thinning of the site of the infarct but the intact wall nearby is also

susceptible to dilation that can ultimately lead to heart failure (Fig 1.2). Several groups have tested the ability of hydrogels to maintain the geometry of the left ventricular wall post-MI. Dobner and colleagues injected 100ul PEG hydrogel or saline into infarct areas within 2 minutes of coronary artery ligation. At 2 and 4 weeks after MI, PEG-injected hearts had less ventricular wall thinning and significant reduction in end-diastolic diameter (EDD) increase. However, after 13 weeks, there was no difference of EDD increase between PEG-treated groups with saline-treated [92], suggesting that the impact of this hydrogel alone was relatively short lived. Alginates [95, 96], fibrin [97] and collagen [97] have also been tested for their ability to moderate ventricular remodeling after infarct with similarly positive effects. More recently, hydrogels derived, at least in part from decellularized ventricular wall ECM have been used either in sheets as patches [98] or as fully injectable fillers to infarct zones [99, 100]. Increasing the percentage of native ventricular wall ECM in the injected region facilitated the differentiation of encapsulated hESCs-derived cardiac progenitors into differentiated cardiomyocytes, as evaluated by the expression of cardiac specific transcription factors, such as cTnT, Cx43 and cTnI. The addition of growth factors to hydrogels did not further increase cardiac differentiation suggesting the ECM was sufficient to support cardiac differentiation from a progenitor population [100]. However, in a similar hybrid hydrogel of ventricular ECM and fibrin, the addition of a low dose of TGFβ increased the vascular differentiation of mesenchymal progenitor cells [98]. A likely next step would be the use of hydrogel that would include both cardiac and vascular progenitor cells with or without the addition of growth factors (Fig 1.3).

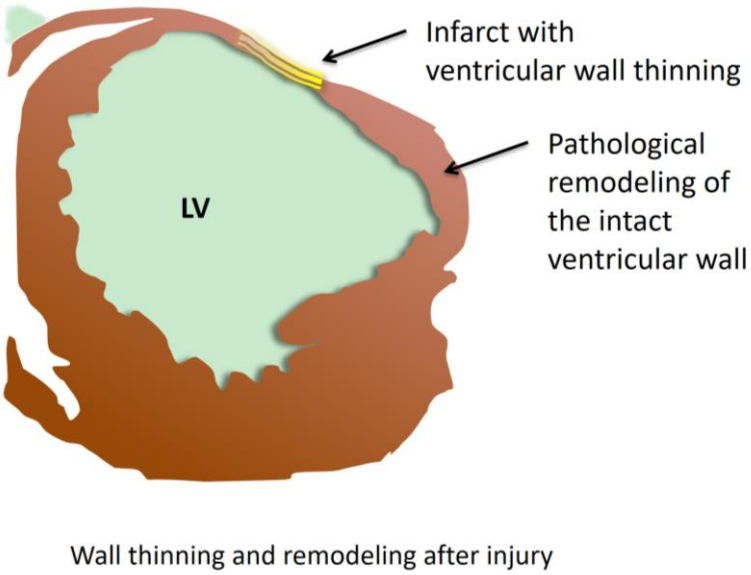

Fig 1.2. A graphical representation of a typical infarcted left ventricle (LV), showing wall thinning in the damaged area (yellow). Note that while not thinned, the wall adjacent can undergo pathological remodeling that can interfere with normal functioning.

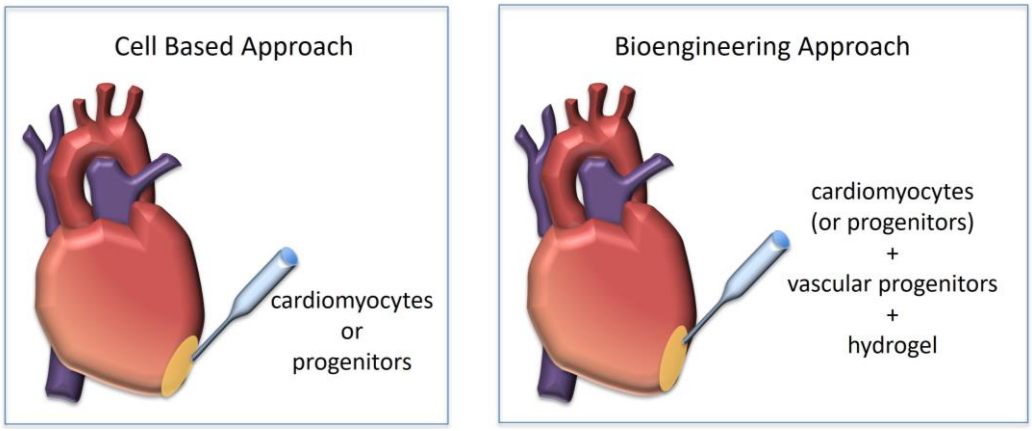

Fig 1.3. A comparison of cell-based therapies for heart repair with a hypothetical bioengineering approach. In cell-based therapies cells are injected directly into the infarct (yellow). Bioengineering approaches involve injecting cells (or progenitors) of both the cardiac and vascular lineages that have been encapsulated or coated on hydrogels. Hydrogels have been show to effectively preserve the 3-dimensional structure of the ventricular wall after myocardial infarction. They have also been shown to facilitate engraftment of donor cells and promote the physiological maturation of engrafted cells. Finally, hydrogels can be used for localized delivery of growth factors and drugs.

Other approaches used specifically to increase vascular formation within cardiac grafts include work by Cui and colleagues who used inkjet printer technology for 2-dimensional printing of a fibrin scaffold that allows for the growth of vascular structures with only minor deformation. After 21 days of culture, the proliferated cells formed a tubular microvasculature within the fibrin channels suggesting that thermal inkjet printing technology could be used for the bio-fabrication of human microvasculature with high resolution [101].

On the other hand, Vollert and colleagues, hand fabricated 3D structures with micro-channels that served as artificial vessels for the perfusion of engineered heart tissues (EHT). To accomplish this, thin alginate fibers were embedded in a matrix of cells, fibrin and thrombin. After polymerization the fibers were removed using alginate lyase or sodium citrate. These artificial vessels improved the oxygen concentration in the center of the EHT and were ultimately populated by endothelial cells [102].

By combining approaches similar to those described above, Vukadinovic-Nikolic et al., recently generated a large sample of EHT. This cardiac construct consisted of three separate layers. The bottom layer was decellularized porcine small intestinal submucosa. The middle layer was a monolayer of rat neonatal cardiomyocytes and the top layer was comprised of rat heart endothelial cells. With this approach, the authors were able to engineer an artificial tissue about 11cm2 in size and with an average beat rate of 208±78 beats/minute on day 3, and 154±48 beats/minute on day 10 as compared to 43±27 beats/minute only in cardiac cells grown without the other tissues, suggesting that this approach may improve the physiological or electrophysiological maturation of cardiac

cells. Rat endothelial cells seeded in the top layer cells migrated through the cardiac compartment within 7 days and co-localized with the vessel bed of the submucosal layer[103]. These studies demonstrate that effects seen by cell engraftment alone can be greatly enhanced by using engineering approaches.

The most ambitious projects in cardiac bioengineering are efforts to completely rebuild hearts either by 3D printing or by using decellularized hearts as a scaffold for repopulation by cardiac progenitor cells. In 2008, Doris Taylor's lab developed a technique to efficiently decellularize rat hearts and subsequently used them as a natural platform to fabricate a beating bio-artificial heart. At first, they carried out coronary perfusion with SDS over 12h to generate a decellularized construct with a perfusable vascular tree, patent valves and intact extracellular matrix (ECM). Then, they reseeded the construct with rat neonatal cardiac cells. By day 8, these repopulated structures beat and were able to generate a constant albeit weak contractile force (about 2% of the adult heart function)[104]. While far from clinical usefulness, this study showed proof of principle that scaffolds of ECM could be used to create bio-artificial heart tissue. More recently, Lu and colleagues reseeded decellularized mouse hearts with human iPSC-derived cardiovascular progenitors. After 26 days of culture, including the addition of growth factors to promote the differentiation of cardiac tissue and blood vessel formation, the repopulated hearts showed a spontaneous beat rate of 40-50 beats per minute. The beating rate was accelerated to 90 beats per minute by perfusing isoproterenol. Subsequent studies showed that the perfused multipotent cardiac progenitors had differentiated into cardiomyocytes, smooth muscle cells and endothelial cells. [105].

Heart Conduction System

The heart functions to supply the embryo with oxygen and nutrition as early as embryogenesis [106]. From initial heart formation, the heart generates an electrical impulse and propagates this impulse to efficiently pump blood with well-coordinated contractions throughout the entire body. In the developing heart, the cardiac conduction system (CCS) is made up of several components, each performing a specific function related to regulation of heart rate. For instance, SAN generates electrical impulses, which propagates through the atrium and reaches the atrioventricular node (AVN). At the AVN the electrical impulse is forced to slow down. This delay allows the atria to contract and give rise to filling ventricles before the ventricles are activated and contract themselves. Connective tissue formed by the annulus fibrosus isolates electrical signals between the atrial and ventricular myocardial tissues. The electric impulse passes from the atrium to the ventricle through the atrioventricular bundle (AVB/ bundle of His). The signal runs through the ventricular septal crest, later through the left and right bundle branches (BBs) and the Purkinje fibre network. Ventricular conduction system (VCS), activating the ventricular myocardium, consists of AVB/His bundle, the BBs and the Purkinje fiber network [106].

Developmental Origin of the Sinoatrial Node

Vincent Christofells' lab elucidated the transcriptional program involved in sinoatrial node (SAN) differentiation from mesodermal precursors in the mouse embryo [106, 107] (Fig 1.4). Tbx5 is at the top of a cascade of transcription factors that direct SAN

formation. Tbx5 is expressed in the sinus venosus (SV) and atria throughout cardiac development and interacts with Nkx2.5 to regulate several downstream transcription factor, including Shox2, Isl1 and Tbx3, key regulators of SAN programming [108, 109]. Dominant mutations in Nkx2.5 and TBX5 (Holt–Oram syndrome) cause congenital heart defects and AV conduction defects (AV block) [110-112]. Shox2, specifically expressed in SV, has an expression pattern complementary to that of Nkx2.5, the TF that activates cardiac chamber formation [113]. As a repressor of the Nkx2.5 gene, Shox2 prevents the formation of contractile myocardium characteristic of the atrium and ventricle, while allowing SAN-specific genes, such as Tbx3 and HCN4 to be expressed [114]. Deletion of Shox2 leads to a hypoplastic SV, upregulation of Nkx2.5 and, consequently downregulation of HCN4 and Tbx3 in both the SAN primordium of mouse hearts, and in ESC-derived cardiac cells [114-116]. With the help of transgenic mice and the advancement of lineage tracing techniques, the progenitors of the SAN cells have been well established [117]. Mommersteeg and colleagues have demonstrated that around E8, the SV develops from $Tbx18^{+}/Nkx2.5^{-}/Isl1^{-}$ progenitors, apart from the rest of the cardiac mesoderm. At E8.5, some cells begin to express Isl1, and later at E9.5, a subset within the SV starts to express Tbx3, a TF that represses chamber development [118]. Genetic lineage tracing has demonstrated that $Tbx3^{+}$ SAN primordium forms along with the SV between E9-9.5 and E11.5-12.5 by adding $Tbx18^{+}/Nkx.2.5^{-}/Isl1^{+}$ cells to venous pole of the heart tube [55, 117, 119, 120]. By E10, the SV and SAN has separated from $Nppa^{+}$ embryonic atrial cells and HCN4 has become restricted to this Tbx3+ domain [121]. Tbx3 is continuously expressed during cardiac development, forming the mature heart conduction

system, from the SAN to the bundle branches of the ventricular conduction system. Tbx3 also prevents atrialization by actively repressing genes associated with the working myocardium, including αMHC, βMHC, Cx40, Cx43, Scn5a and Nppa/b, (Fig 1.4). Ectopic Tbx3 expression leads to the formation of bona fide functional pacemaker cells within these atria [121, 122]. Thus Tbx3 directs a pacemaker phenotype in SAN, while Nkx2.5, acting in adjacent cells represses Tbx3 and HCN4 allowing development of the atrial myocardium. HCN4, hyperpolarization-activated cyclic nucleotide-gated cation channel, is initially expressed in the first-formed myocytes and immediately activated in $Tbx18^{+}/Nkx2.5^{-}$ SV domain and downregulated in $Nkx2.5^{+}$ myocardium, transferring its expression domain to newly-formed SV and the major pacemaker domain [51, 123, 124]. These data suggest that pacemaker cells derive from the activation of a particular genetic pathway in cardiac progenitors during cardiogenesis.

Tbx18 is expressed in all SV, including SAN, progenitor cells and in the later-formed sinus horns and head of the SAN; Tbx18 deficient mice result in a malformed and strongly hypoplastic SAN and SV [119, 125]. Tbx18 is required for correct morphogenesis and deployment of SV and SAN progenitor cells.

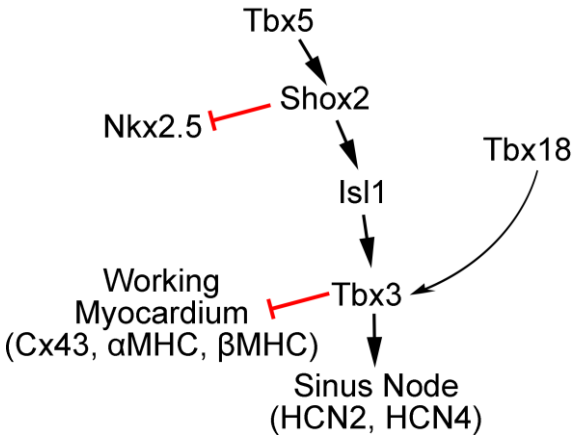

Fig 1.4. Proposed model of TF interactions during SAN differentiation.

The transcriptional program that directs formation of the AVC and Purkinje system

The AVC adopts its phenotype through a gene regulatory network, which inhibits chamber differentiation, facilitates nodal development, and delimits the strict border between the AVC and chamber myocardium [126]. Tbx2 and Tbx3 both play important roles in this process. Both Tbx2 and Tbx3 repress the chamber myocardium gene regulatory network, such as Nppa, Cx40 and Scn5a. [127-130]. Furthermore, Tbx2 and Tbx3 form a positive feedback loop with Bone morphogenetic protein 2 (Bmp2), which controls the AVC-restricted expression of Tbx2 and Tbx3 [130]. These T-box factors interact with muscle-segment homeobox transcription factor Msx2, suppressing Cx43 expression directly in the AVC [131, 132]. They also compete with Tbx5 for binding to T-box elements in target genes including Nppa and Cx40 [133], and for interaction with Nkx2.5 to inhibit Nppa in the AVC [134].

The Purkinje fiber network is found only in mammals and birds, which arises from the trabecular myocardium. The embryonic ventricles are mainly composed of trabecular myocardium during embryogenesis, acting as both the functional and cellular precursor of the Purkinje fiber network [135]. Elegant clonal and lineage analyses showed the spatiotemporal expression pattern of Cx40 [136, 137]. When Cx40+ cells were irreversibly labeled at E10.5, labeled descendants were observed both in the Purkinje fibers and in the Cx40- negative compact wall. However, when Cx40+ cells were labeled at E16.5, the Cx40+ trabecular zone had become a relative small population and labeled Cx40 descendants were only found in Purkinje network, indicating the lineages of Purkinje fibers and ventricular myocardium separated between E10.5 and E16.5.

Sinoatrial Node arrhythmias

In the adult human heart, the sinoatrial node (SAN) is crescent-shaped structure 1 to 2 cm long and 0.5 cm wide, that lies at the junction of the superior vena cava with right atrium and locates along the sulcus terminalis. The SAN itself consists of clusters of pacemaker cells organized in parallel rows with thin digitations. The SAN arrhythmias is referred to a clinical syndrome including SAN dysfunction, frequently depressed escape pacemaker, and atrioventricular nodal conduction disturbance. SAN arrhythmias describes a series of abnormalities, leading to complicated sinus bradycardia, sinus arrest, sinus pauses, SAN exit block, which is defined as inefficient and inappropriate response to physiological demands during exercise [138].

Conclusions

Work by Chong et al. [66] highlights the advances that have been made in cardiac regenerative medicines based on cell-based therapies alone. However these studies also highlight the unique challenges presented by this field. Here we highlight several recent studies that demonstrate the potential power of combining cells with engineered materials (Fig 1.3). These studies suggest that encapsulating cardiac or cardiac progenitor cells within hydrogels may greatly enhance their regenerative capacities. This is accomplished by providing scaffolds that facilitate migration and differentiation, mechanically protect cells and preserve the 3D structure of the damaged heart tissue during repair and recovery.

CHAPTER TWO

SPECIFIC AIMS

Abstract:

The overall goal of this research is to understand the mechanisms underlying the differentiation of the SAN. To study this I have used mouse embryonic stem cells, differentiated as EBs. Vincent Christofells' lab has identified a number of transcription factors that are necessary for differentiation of the SAN in mouse embryos. It is not yet clear if these factors are sufficient for SAN differentiation. To test this I mad lentiviruses to conditional overexpress these genes. At the top of this transcriptional cascade is the transcription factor Tbx5. Tbx5 has been shown to activate expression of Shox2, Tbx3 and Islet1. I made viruses to express all of these factors and also carried out detailed analysis of Tbx5. In addition to this, the Foley identified TAK1/Map3k7 as an important factor that can activate Tbx5 and this entire transcription pathway. I also made a virus to conditionally overexpress TAK1 and analyzed gene expression in a previous isolated TAK1 overexpressing cell line. Finally, I found that gene expression analysis within a EBs was complicated and that overall changes in genes sometimes masked gene changes specifically in cardiomyocytes, so I began to develop a technique to examine gene changes specifically in cardiac lineages. To accomplish these goals I carried the following specific aims.

Specific Aims:

Specific Aim 1: To study the role of Tbx5 overexpression in mouse embryonic stem cells-derived cardiomyocytes and determine if it is sufficient to drive SAN differentiation.

The goal of Specific Aim 1 is to test if overexpression of Tbx5 during EB differentiation is sufficient for SAN fate. In chapter 4, we will examine the role of Tbx5 in differentiation of the sinoatrial node (SAN) from mouse embryonic stem cells. The SAN of the mouse embryo arises from the wall of the right atrium near the border of the sinus venosus. Early in development this region expresses the transcription factor Tbx5. Because of this, Tbx5 is thought to sit at the apex of a transcriptional cascade leading to SAN differentiation. To test this we produced a mouse embryonic stem cell line B1 (pTripZ-mTbx5; αMHC::GFP) that conditionally overexpresses Tbx5 under the control of a Doxycycline inducible promoter.

We differentiated mESCs into EBs at Day 0 (D0) by using hanging drop method (around 300 cells per 20 μL drop) described in [139, 140]. After 24 hours (D1), EBs were washed off and plated on gelatin-coated plates for EB differentiation. We treated these EBs with 200ng/ml Dox from D4. By D15, D17 and D21, we recorded the 20-seconds-long videos with beating area (identified based on the expression of αMHC::GFP) to measure beat frequencies. Changes in mean intensity within regions of interests in phase contrast image sequences serve to detect motion indicative of cellular contractions, and beat frequencies are extracted using a MATLAB algorithm that first performs a non-linear

normalization (to account for non-specific large scale movements), followed by a fast fourier transformation of the data, which corrects for pausing of beating during imaging.

Differentiated EBs were treated with 200ng/ml Dox from D4. Then at D19 and D21, EBs were dissociated into single cell suspension by trypsin digestion and replated onto chamber slides. Immunocytochemistry staining was used to distinguish the cardiac subtype among all cardiomyocytes, such as HCN4, Shox2 for pacemaker-like myocytes; Cx43 for ventricular-like myocytes; GFP, DsRed and CT3 for marking all cardiomyocytes. The percentage of HCN4, Shox2 and Cx43 positive myocytes were measured to display the overall subtype characteristic of myocytes.

Activation of the SAN transcriptional program will be assayed by qRT-PCR. Differentiated pacemaker cells are expected to express high levels of genes involved in SAN development (Tbx3, Tbx5, Shox2, Isl1, HCN4) and low levels of ventricular genes (Cx43, Nkx2.5). At the meantime, MAP3K7/TAK1 mRNA level was measured between R1, B1 untreated and B1 Dox-treated EBs.

Specific Aim 2: To determine the effect of MAP3K7/TAK1 overexpression during EB differentitation on early lineage differentiation.

The goal of Specific Aim 2 is to determine how MAP3K7/TAK1 kinase affects SAN differentiation but also how it impacts the formation of early endodermal and neural markers. In chapter 5, I analyzed MAP3K7/TAK1 overexpressing EBs using qRT-PCR analyses and FACS data, comparing wild type EBs to MAP3K7-overexpressing EBs. I analyzed both pacemaker genes and genes expressed in other lineages relevant to heart

induction, specifically visceral endoderm (VE), anterior visceral endoderm (AVE) and definitive endoderm (DE). In addition I examined expression of genes related to Sonic Hedgehog (Shh) signaling and early neural induction.

Specific Aim 3: To develop a protocol for the single cell analysis of gene expression during myocardial differentiation

The goal of Specific Aim 3 is to figure out gene expression by single cell analysis during cardiac differentiation. In chapter 6, I will examine the expression of SAN and other cardiac markers specifically in cardiomyocytes. In all of these studies we are examining gene expression in whole EBs and examining markers that are expressed in the heart and endoderm but are also often expressed in other non-cardiac, non-endoderm lineages. Therefore it is sometimes difficult to know whether observed changes are due only changes in the cardiac (or endodermal lineage). To address this we have begun to develop a technique that will allow us to examine gene expression in just the cardiac lineage. Briefly, ES cells harboring the αMHC::GFP promoter reporter are differentiated until day 21 and cardiomyocytes isolated by flow cytometry. From these cells we isolated RNA and then carried out real time PCR for genes expected to be expressed in cardiomyocytes. A number of technical challenges remain to be addressed with this protocol. These data represent promising preliminary data for a new, more accurate assessment of cardiac differentiation in our assay system.

Specific Aim 4: Design and verify cell lines overexpressing SAN genes

The goal of Specific Aim 4 is to test the effect of overexpression of SAN specific genes other than Tbx5 during EB differentiation. In Chapter 7, I will show data verifying gene overexpression in both the Tbx5 and other overexpression cell lines. Vincent Christofells has described a transcriptional hierarchy that directs the differentiation if sinoatrial node cells in the mouse embryo. The major transcription factors involved are: Tbx3, Isl1, Shox2, Tbx18 and MAP3K7/TAK1 [107, 141]. To study their function in directing SAN differentiation I made ES cell lines that will allow me to conditionally overexpress these factors. One of these lines (B1, which overexpressed Tbx5) is described in Chapter 4. Detailed information of each individual mESC that I produced is discussed here

CHAPTER THREE

MATERIAL AND METHODS

Cell Culture

Mouse embryonic stem cells (mESCs) were cultured in 10 cm tissue culture dishes, covered with 10 ml high glucose Dulbecco's Modified Eagles Medium (DMEM) with 10% ES-Qualified Fetal Bovine Serum (FBS), 1% penicillin-streptomycin, 1% L-glutamine, 1% non-essential amino acids, 1% sodium pyruvate, 0.1 mM 2-mercaptoethanol and 1000 U per ml LIF.

293T cells were culture in 10 cm tissue culture dish, covered with 10ml DMEM with 10% FBS, 1% penicillin-streptomycin, 1% L-glutamine and 1% Sodium pyruvate.

Plasmid transfection and Lentivirus production

Before plasmid transfection, cell medium of 293T (60-80% confluent) were removed and replaced with 11 ml standard culture medium supplemented with 20% FBS. Virus were produced using the second generation lentiviral system according to the protocol [142]. Plasmids were combined as follows: 30 µg (30 µl) transfer vector, 20 µg (20µl) p8.74, 10 µg (10µl) pVSV-g and 1290 µl H20 (total volume 1350µl). Note: from this point on, consider this to be "live virus" in terms of safety precautions, for example, wear double gloves, lab coat and disposable sleeve protectors. Do not aspirate solutions but pipet them into bleach so that the final concentration is at least 10%. All pipets and other plastic ware should also be washed in bleach for 10 minutes before discarding. Hood

and all equipment should be “UV” irradiated for 10 minutes after you are done. Any drops of viral-containing solutions should be wiped up immediately. Additional 150 µl CaCl2-dropwise was added using a 200 µl pipetman very slowly and gently with constant vortexing (1800rpm, medium strength), following 1500 µl of Hank's balanced salt solution (HBSS) dropwise slowly. The mixed solution will form complexes in about 20 minutes. Cultures should not be disturbed at this time. The mix solution was added to the 293T cells dropwise using a 2ml pipetman. Try not to disturb the plates when transferring them back to the incubator. Next day cell medium were switched to 25 ml Lonza Ultraculture Medium, plus 1% penicillin-streptomycin and 2% L-glutamine. Ultraculture medium were collected every day for three days. On the last day, these medium were ultracentrifuged in swing bucket rotor SW28 at 20,000 rpm for 2 1/2 hours (These would take a total of 4 hours almost to complete run). Finally, supernatant was carefully removed and the virus pellets were resuspended within 400-600 µl remaining medium. Then the viruses were aliquoted and stored at -80C.

Lentivirus Transduction and establishment of clonal cell lines.

Multiplicity of Infection (MOI): Multiplicity of Infection is the number of transducing lentiviral particles per cell. Typically, 5000 cells are used for infection and MOI rate are set up at 10, 20, 40; this needs lentivirus package for 50000, 100000 and 200000, respectively. At first, dissociated mESCs were mixed with lentivirus packages at MOI 10, 20 and 40, plus 10 µg/ml polybrene and incubated at 37C for an hour with gentle re-suspension every 15 minutes. Mix solution was replated onto 24 well pre-coated plate.

Fresh medium was added after 24 hours and 1 μg/ml puromycin selection media was added after 48 hour. After 2-3 days of puromycin selection, cells were trypsinized and replated onto 96 well plate for one cell per well. Continuous monitor for a couple of days, potential mouse embryonic stem cell colonies grown from single cell clone were expanded and then analyzed for doxycycline treatment later.

Embryoid Body (EB) Differentiation

mESCs were differentiated in standard differentiation medium, which contains Iscove's Modified Dulbecco's Medium (IMDM) supplemented with 10% differentiation-tested FBS, 5% protein-free Hybridoma Media (PFHM-II), 1% penicillin-streptomycin, 0.5 mM L-ascorbic acid, 0.45 mM monothioglycerol and 200 μg/ml apo-Transferrin. Embryoid Bodies (EBs) were formed into 20 μl hanging drop, which consists of 300 cells and then incubated at 37C for 24 hours. After 24 hours, EBs were gently washed with petri dish pre-coated with 0.1% gelation, as marked as "Day 1".

Construct of pTripZ Vector, doxycycline-inducible-Gene of Interest (GOI)-overexpression Vector

The open reading frame of different GOI, including mTbx5, mTbx3, hIsl1, hShox2, hTbx18 and mouse MAP3K7 was amplified by PCR and directly cloned into downstream of TurboRFP motif into the pTripZ vector (purchased from Add gene), which drives expression of TurboRFP and the insert GOI with administration of Doxycycline.

Lentiviruses were produced using the second-generation lentiviral expression system (Table 3.1).

Construct of pTET-ON Vector, doxycycline-inducible-GOI-overexpression Vector

The open reading frame of different GOI, including mTbx5, mTbx3, hIsl1, hShox2, hTbx18 and mouse MAP3K7 was amplified by PCR and directly cloned into downstream of pTight TET-Responnsive promoter into the pTET-ON vector (purchased from Add gene), which drives expression of the insert GOI with administration of Doxycycline. Transfection of target vector into mESCs was used to generate GOI-overexpression mouse ES cell line (Table 3.2).

pTripZ	Forward Primer	Reverse Primer
mTbx5	CCCATCGATATGGCCGATACAGATGAGGGC	CGACGCGTTTAGCTATTCTCACTCCACTC
mTbx3	CCCATCGATATGAGCCTCTCCATGAGAGAT	CGACGCGTTTAAGGGGACCCGCTGCAAG
hIsl1	CCCATCGATTTACTCCCTCTTACAGATATG	CGACGCGTTCATGCCTCAATAGGACTGGC
hShox2	CCCATCGATATGGAAGAACTTACGGCGTTC	CGACGCGTTCACAGACCCAGGGCTG
hTbx18	CCATCGATATGGCCGAGAAGCGAAGG	CGACGCGTTCAGACCATATGTGCAGATAC
MAP3K7	CCCATCGATTCGACAGCCTCCGCCGCC	CGACGCGTTCATGAAGTGCCTTGTCGTTTCTGCT

Table 3.1. GOI Primer was used to clone into downstream of TurboRFP motif into the pTripZ vector.

pTET-ON	Forward Primer	Reverse Primer
mTbx5	CGACGCGTATGGCCGATACAGATGAGGGC	CCATCGATTTAGCTATTCTCACTCCACTC
mTbx3	CGACGCGTATGAGCCTCTCCATGAGAGAT	CCATCGATTTAAGGGGACCCGCTGCAAGA
hIsl1	CGACGCGTTTACTCCCTCTTACAGATATG	CCATCGATTCATGCCTCAATAGGACTGGC
hShox2	CGACGCGTATGGAAGAACTTACGGCG	CCATCGATGTTGGCGTCACAGACCCA
hTbx18	CGACGCGTATGGCCGAGAAGCGAAGG	CCATCGATTCAGACCATATGTGCAGATAC
MAP3K7	CGACGCGTTCGACAGCCTCCGCCG	CCATCGATGGTCATGAAGTGCCTTGTCGTTTCTGCT

Table 3.2. GOI Primer was used to clone into downstream of pTight TET-Responnsive promoter into the pTET-ON vector.

List of vectors and mESCs line made

Here is the detailed list of all vectors and mESCs made in Foley lab (Table 3.3).

No	Vector	Insert Gene	mESCs
1	pTripZ	mTbx5	B1, B5, B10, B12
2	pTripZ	mTbx3	X1, X6, X13
3	pTripZ	hIsl1	I4
4	pTripZ	hShox2	S2
5	pTripZ	hTbx18	T2
6	pTripZ	MAP3K7	M8
7	pTET-ON	mTbx5	DB4, DB6
8	pTET-ON	mTbx3	DX5, DX9
9	pTET-ON	hIsl1	DI1, DI2, DI3, DI7
10	pTET-ON	hShox2	DS13, DS14
11	pTET-ON	hTbx18	DT2, DT5
12	pTET-ON	MAP3K7	DM11

Table 3.3 The detailed list of all vectors and mESCs made in Foley lab.

Real-time PCR

EBs were collected on specific days of differentiation, such as D5, D7 and so on. Total RNA was extracted with RNeasy Mini Kit (Qiagen, cat#74106), and 1 μg was used to synthesize the first strand cDNA using QuantiTect Reverse Transcritption Kit (Qiagen, cat#205313). Quantitative PCRs were performed with SybrGreen Master Mix (Roche, cat# 3752186001), using 40 ng template/reaction on a Roche LightCycler® 480 Real-Time PCR Instrument, and analyzed with the LightCycler 480 software package (version 1.5.0 SP1). Crossing point data were first adjusted to reflect the efficiency of primer pairs by comparison to standard curves (based on dilution series over a total dynamic range of 1:1,000 or 1:10,000 for positive control cDNAs) and subsequently normalized to the ubiquitously expressed transcript GAPDH. Data represent averages ± standard error of 3 independent experiments. Further analyses were using GraphPad Prism (version 7.0). Primers used in this study are as follows:

Primer	Forward	Reverse
Cx30.2	TGATCATGCTGATCTTCCGCATCC	GCTGCAACGTGTTACACACGAACT
Cx43	GACTGCGGATCTCCAAAATA	AAATCAAACGGCTGGGCGTGG
GAPDH	AATGGATACGGCTACAGC	GTGCAGCGAACTTTATTG
HCN4	ACC TGA CGA TGC TGT TGC TG	CTC TGC GGG TCA AGG ATG AT
m/h Isl1	GGTTGTACGGGATCAAAT	GAGCGGGCACGCATCACG
m/h Shox2	ACC AAT TTT ACC CTG GAA CAA C	TCG ATT TTG AAA CCA AAC CTG
m/h Tbx18	CACAACCGTCACTGCCTATCAG	CCGTAGTGATGGTCGCCAGAAT
MAP3K7	CGTAGATCCATCCAAGACTTGAC	GAGGTTGGTCCTGAGGTAGTGAT
Tbx3	GTT TTG TCT GGG AGG GAG CA	CTT CAG CCC CGA CTT CCA TA
Tbx5	CCA GCT CGG CGA AGG GAT GTT T	CCG ACG CCG TGT ACC GAG TGA T
mCXCR4	CCGCCTTTACCCCGATAGC	ACCCCCAAAAGGATGAAGGAG
mGPC1	TGGTGCTCATCACTGACAAGTTC	GGATGACCTTAGCTGTGAGTGTGT
mTm4sf2	CCAGTTGCTGCATGAACGAA	CACCAGATCATAACAGCCCTTCT
mSox17	GCTAGGCAAGTCTTGGAAGG	CTTGTAGTTGGGGTGGTCCT
mSox2	GAGGGCTGGACTGCGAACT	TTTGCACCCCTCCCAATTC

mDkk1	ATCTGTCTGGCTTGCCGAAAGC	GAGGAAAATGGCTGTGGTCAGAG
mHhex	CGGTCAAGTGAGGTTCTCCAAC	CTCGGCGATTCTGAAACCAGGT
mCer1	ATCCTGCCCATCAAAAGCCACG	CGAATGGAACTGCATTTGCCAAAG
Shh	AATGCCTTGGCCATCTCTGT	GCTCGACCCTCATAGTGTAGAGAC
Gli1	GGAAGTCCTATTCACGCCTTGA	CAACCTTCTTGCTCACACATGTAAG
Gli2	TACCTCAACCCTGTGGATGC	CTACCAGCGAGTTGGGAGAG
Gli3	ATTCCCGTAGCAGCTCTTCA	TTGCTGTCGGCTTAGGATCT

Table 3.4. qRT-PCR primers of Cx30.2, Cx43, GAPDH, HCN4, m/h Isl1, m/h Shox2, m/h Tbx18, MAP3K7, Tbx3, Tbx5, mCXCR4, mGPC1, mTm4sf2, mSox17, mSox2, mDkk1, mHhex, mCer1, Shh and Gli1-3.

Flow Cytometry

EBs were treated with 0.25% Trypsin/EDTA at 37C for 30 minutes and then neutralized with regular differentiation medium. Cells were centrifuged at 2000 rpm for 5 minutes and resuspended with fluorescence-activated cell sorter (FACS) buffer (PBS plus 1% BSA and 10 ng/ml DNAse). Then cells were centrifuged again and resuspended with FACS buffer. Cells were filtered through a 100 μm sieve and cell numbers were counted using a haemocytometer, checking single cell suspension at the same time. Flow cytometry was performed with the Beckman Coulter MoFlo Astrios EQ cell sorter and data was analyzed using FlowJo VX software.

Immunocytochemistry

EB dissociation was performed as decribed above for Flow Cytometry. Around 55000 cells with the property of single cell suspension were replated onto 4 well Lab-Tek II chamber slide (Nunc, cat#154526), pre-coated with 0.1% gelation and then incubated within standard differentiation medium at 37C overnight to allow dissociated cells to attach and spread. Cells were fixed at 4% PFA for 15 minutes and gently washed with PBS 3 times for 5 minutes. Then cells were block with either cytosol antibody staining buffer (CASB) or nuclear antibody staining buffer (NASB) for an hour, depending on subcellular location of target protein expression. CASB is consist of PBS, 1% FBS, 0.1% BSA and 0.1% Triton-X-100; while NASB contains PBS supplemented with 1% FBS, 0.2% BSA and 0.25% Triton-X-100 for nuclear membrane penetration. Cells were incubated with primary antibody diluted within either CASB or NASB overnight. Cells were washed with

PBS 3 times for 5 minutes and then incubated with Alexa Fluor-labelled secondary antibody for an hour. Additional PBS wash was performed and at the last wash DAPI was added into PBS buffer for 5 minutes incubation. Finally, chamber slides were mounted with special fluorescence mounting media and sealed with clear nail polish. Later, images were taken on Zeiss AxioImager microscopy. The primary antibodies were used as follow: Cx43 (Sigma, cat#C6219, 1:1000), CT3 (DSHB, cat#CT3, 1:250), DsRed (Clontech, cat#632392, 1:500), GFP (Thermo, cat#A11122, 1:500), HCN4 (Sigma, cat#SAB520035, 1:250), Shox2 (abcam, cat#ab55740, 1:1000), Tbx5 (Thermo, cat#42-6500, 1:500).

Beat Rate data

During EB differentiation, we will use live cell imaging of beating cardiomyocytes (identified based on the expression of αMHC::GFP) to measure beat frequencies. Changes in mean intensity within regions of interests (ROI) in phase contrast image sequences serve to detect motion indicative of cellular contractions, and beat frequencies are extracted using a MATLAB algorithm that first performs a non-linear normalization (to account for non-specific large scale movements), followed by a fast fourier transformation of the data, which corrects for pausing of beating during imaging.[143]

CHAPTER FOUR

TBX5 OVEREXPRESSION ENHANCES CARDIAC DIFFERENTIATION AND INCREASES BEAT RATE BUT DOES NOT INCREASE THE FORMATION OF FULLY DIFFERENTIATED SINOATRIAL NODE CELLS

Introduction

The Sinoatrial Node (SAN), as the primary pacemaker of the mammalian heart and controls heart rate throughout the life of all mammals. Failure of SAN function leads to slow heart rate (bradycardia) and inefficient circulation of blood flow. Bradycardia may be due to congenital disease or heart attack. Currently, the sole treatment for bradycardia is implantation of electronic pacemakers and there are several complications including, surgical complication, battery life issues and lead displacement. That's the reason why we need a biological pacemaker. Producing a biological pacemaker in vitro would result in an alternative pacemaker therapy in which replacing the failing SAN with a new biological one would become practical through cell transplantation. My project is to determine whether a biological pacemaker can be produced by direct reprogramming of cells to the SAN fate. Specifically I will address whether forced overexpression of the SAN specific gene, Tbx5. can accomplish this.

Four independent clonal lines that conditionally overexpress Tbx5 were established.

To test the role of Tbx5 in SAN development, mouse embryonic stem cell (mESC) lines were generated to conditionally overexpress Tbx5. To do this, the open reading frame

of Tbx5 was cloned downstream of the TurboRFP motif into the pTripZ vector. This was used to generate lentivirus in which genes of interest (GOI) can be overexpressed by the administration of doxycycline (Fig 4.1A).

These vectors can be used to conditionally overexpress all of the key transcriptional regulators of SAN differentiation. At the top of this cascade is Tbx5. Genetic studies in mouse have revealed an essential role for Tbx5 in establishing the SAN however, it has not been shown whether Tbx5 is sufficient for SAN differentiation. To study its role we established four independent, clonal ESC lines (B1, B5, B10 and B12), all of which showed stable, inducible, upregulation of Tbx5 transcripts, as confirmed by qRT-PCR at 24, 48 and 72 hours after addition of 1 μg /mL doxycycline (Fig 4.1B).

Immunocytochemistry using the anti-Tbx5 antibody was performed to confirm that doxycycline also activated Tbx5 protein formation (Fig 4.1C). We found within colonies of ES cells Tbx5 expression in nuclei.

Together these data confirm that four separate ES cell lines were generated that overexpressed Tbx5 in both transcripts and protein level in response to doxycycline.

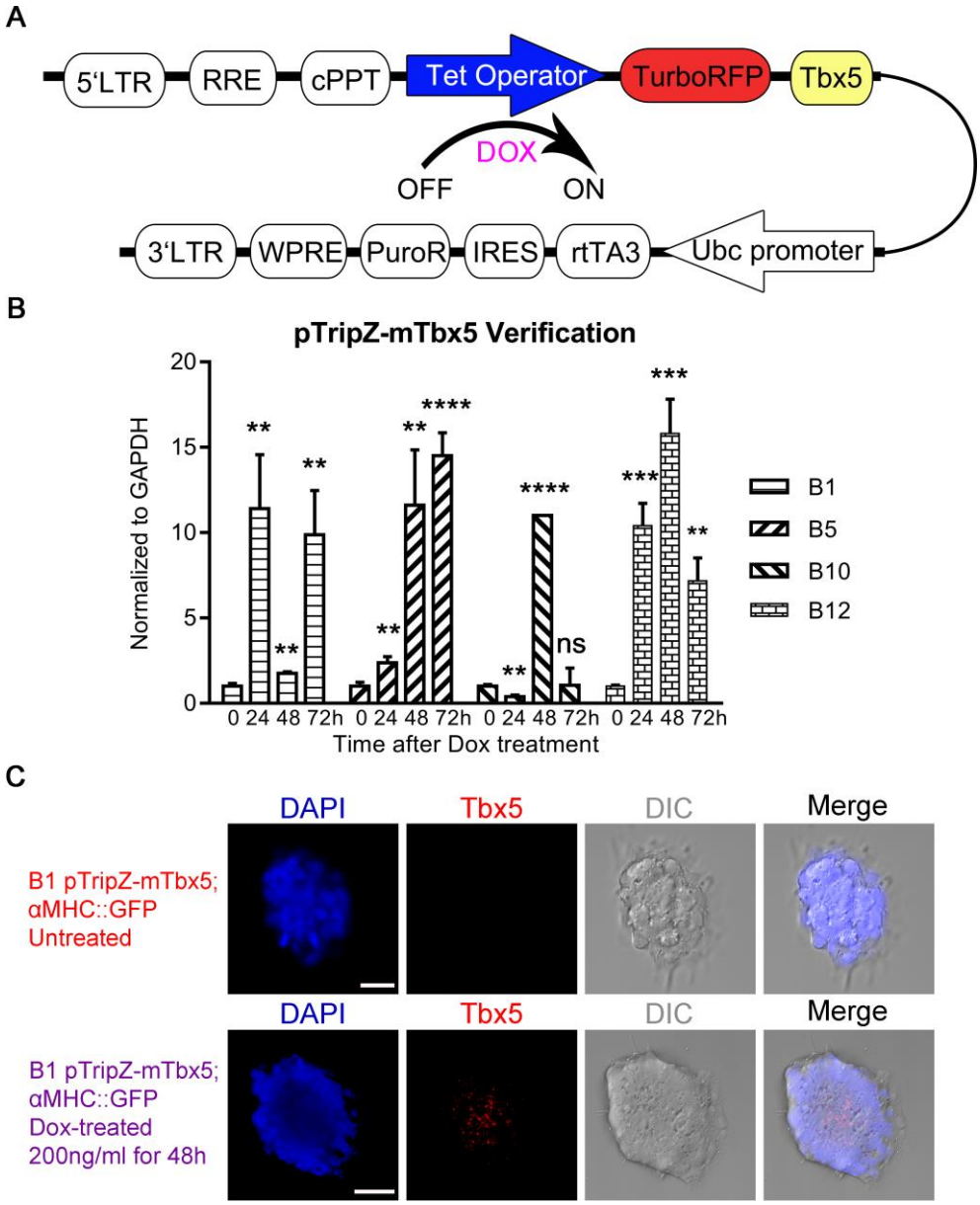

Fig 4.1. Verification of B1 pTripZ-mTbx5; αMHC::GFP mouse embryonic stem cell line. Fig 4.1A. Schematic design of pTripZ-mTbx5 Vector, doxycycline-inducible-Tbx5-overexpression backbone. Fig 4.1B. B1, B5, B10, B12 mESCs were treated with doxycycline at 1000ng/ml and then collected after 0, 24, 48, 72h. Later qRT-PCR was performed to detect relative expression of Tbx5. Fig 4.1C. B1 mESCs were treated with doxycyline at 200ng/ml for 48h or untreated, and then immunostained the anti-Tbx5 antibody to detect nuclear expression of this protein. Scale bar, 20 μm. Data represent means ± standard error of 3 independent experiments. Statistical significance was determined by unpaired, two-tailed t-test. **p<0.01, ***p<0.001

Addition of Doxycycline increased beat rate

One indication that cardiac cells have adopted the SAN identity, is an increased rate of beating. To determine if our mESCs differentiate as SAN cells in response to increased expression of Tbx5, mESCs were differentiated as EBs and doxycycline added from Day 2 until either day 15 or Day 20 at which point beat rate was assessed. B1, B5 and B10 EBs were tested for increased beat rate with working dose curve of doxycycline. Beating areas were identified based on visual inspection and confirmed by expression of αMHC::GFP which we previously showed was a faithful reporter of cardiac differentiation [141]. Beat was manually calculated but visual inspection, counting beats/minute.

Lines B5 and B10 showed a modest increase in beat rate at 100 ng/ml. Line B1 showed significant increase in beat rate at 100ng/ml, 200ng/ml and 500ng/ml. However the greatest increase in beat rate was observed at 200ng/mL (Fig 4.2A). For this reason, line B1 and a dose of 200 mg/ml doxycycline were used for all subsequent evaluation.

We previously showed that MAP3K7 overexpressing cells that later adopted a sinoatrial node fate began to beat quickly around Day 15 of EB differentiation [141]. To test this, beat rate was also collected and analyzed at Day 15. We found that beat rate was also significantly increased at day 15 at 100ng/ml, 200 ng/ml and 500ng/ml.

Manual counting of beat rates is subject to interpretation and cannot always account for pausing of EBs; in addition, beats greater than 100 beats per minute are very difficult to count manually with great accuracy. We previously developed a MATLAB automation to calculate cardiac beats from movie clips based on changes of pixel density at the edges of beating areas [143]. To determine how well this software compares to manual count,

beating data were recalculated for the B1 line at Day 15, 17 and 21 using the automation. This also allowed us to check all beating areas accurately (Fig 4.2B). At Day 15, both B1 and B1 dox showed increasing rate of beating as compared to cardiomyocytes from EBs differentiated from the parent cell line R1 αMHC::GFP (R1). However, B1 treated with doxycycline did not beat faster than untreated B1 cells until Day 17 in this assay (Fig 4.2C). At D21, B1 Dox-treated beat faster than both B1 and R1 cells, while B1 and R1 had no significant difference.

All these beat data confirms that administration of dox to B1 does increase beat rate of cardiac cells but also confirms that manual counting may not be as accurate as our automation.

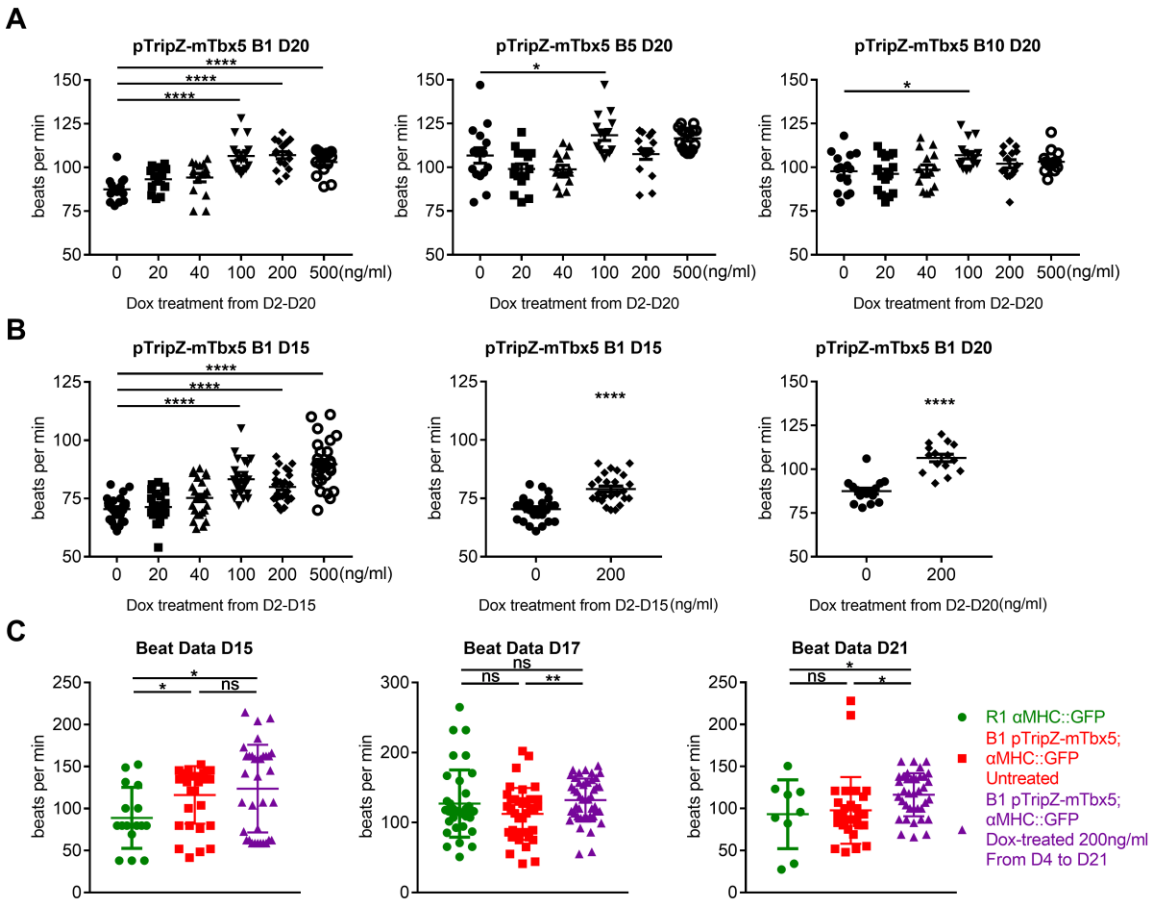

Fig 4.2. Manual beat data and automatic beat data. Fig 4.2A. Manual beat data counting of B1, B5 and B10 EBs at Day 20 with Doxycycline dose of 0ng/ml, 20ng/ml, 40ng/ml, 100ng/ml, 200ng/ml and 500ng/ml. Fig 4.2B. Manual beat data counting of B1 EBs at Day 15 with indicated dose of doxycycline treatment. Fig 4.2C. Using MATLAB automation to calculate cardiac beats of R1, B1 and B1 Dox-treated EBs at Day 15, Day 17 and Day 21. Data represent means ± standard error of 3 independent experiments. Statistical significance was determined by one-way ANOVA (Fig 3.2A&3.2B) or unpaired, two-tailed t-test (Fig 3.2C). *p<0.05, **p<0.01, ***p<0.001, ****p<0.0001

Relative Tbx5 RNA Expression during EB differentiation

Although addition of Dox worked well in B1 mESCs, yet regulation of gene expression within differentiating EBs is much more complicated. To test whether addition of Dox also upregulated Tbx5 transcripts during EB differentiation, EBs were collected from Day 5 to Day 21 and assessed Tbx5 transcription by qRT-PCR (Fig 4.3). Interestingly, both B1 and B1 dox showed higher levels of Tbx5 than the parent cell line R1. Doxycycline treatment did also result in statistically significant increases of Tbx5 at Day 15 and Day19, but not at all days of differentiation. In fact, by Day 21, when we saw increased beat rates, dox-treated cells had lower levels of Tbx5 transcripts. This suggests: 1) regulation of transcriptions within EBs is highly complex and dox-inducible transcripts may not be able to activate sufficiently high levels of expression to overcome normal changes in gene expression that occur during EB differentiation; 2) The B1 line either due to leakiness of the construct or due to gene insertion effects has naturally higher levels of Tbx5 expression as compared to the parent cell line (R1); 3) at Day 21 increased beat rate cannot be due to active transcription of Tbx5. Besides B1, B5 and B10 EBs treated with Dox compared to untreated EBs were tested for regulation of Tbx5 (Fig 4.4). EBs were treated with Dox from Day 2 to Day 11 and collected for later qRT-PCR analysis. As shown in Fig 4.4, both B5 and B10 EBs treated with Dox did not increase Tbx5 transcripts.

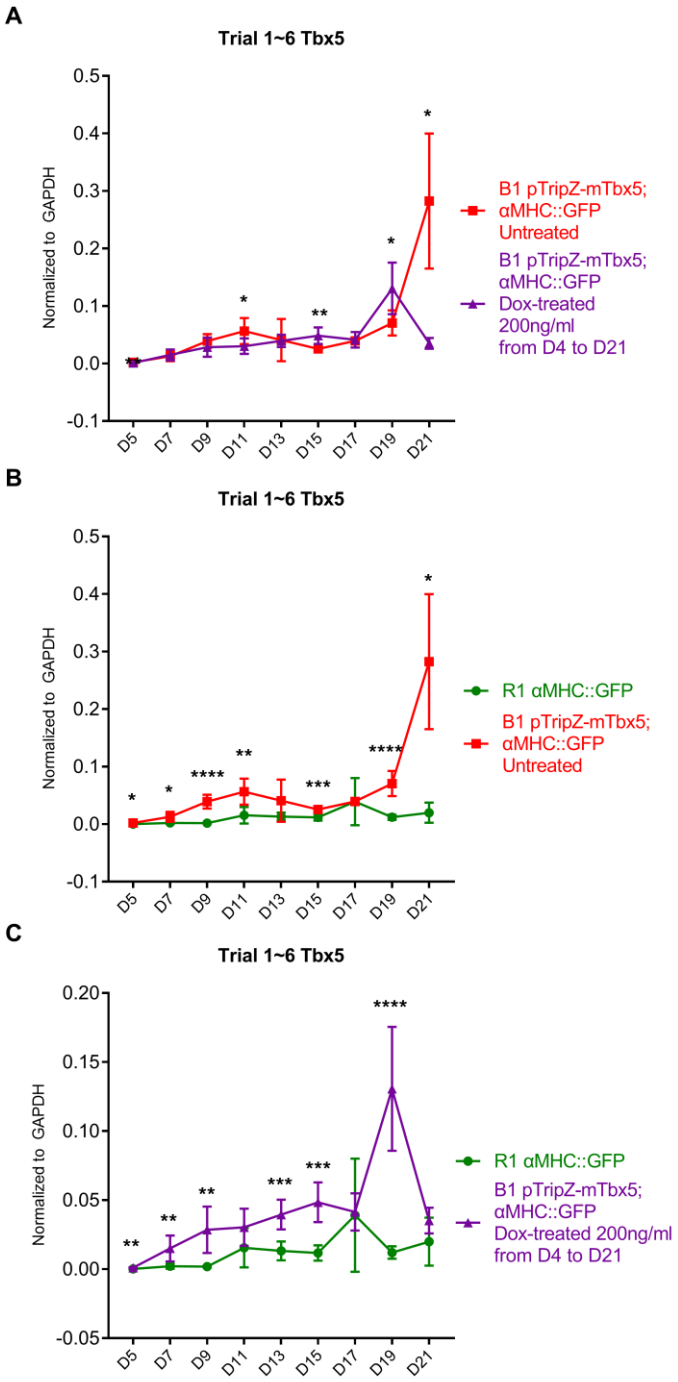

Fig 4.3. Relative Tbx5 expression during EB differetiation. EBs were collected from Day 5 to Day 21 and assessed Tbx5 transcription by qRT-PCR between B1 and B1 Dox-treated EBs (Fig 4.3A), R1 and B1 EBs (Fig 4.3B) or R1 and B1 Dox EBs (Fig 4.3C). Data represent means ±standard error of 3 independent experiments. Statistical significance was determined by unpaired, two-tailed t-test. *p<0.05, **p<0.01, ***p<0.001, ****p<0.0001

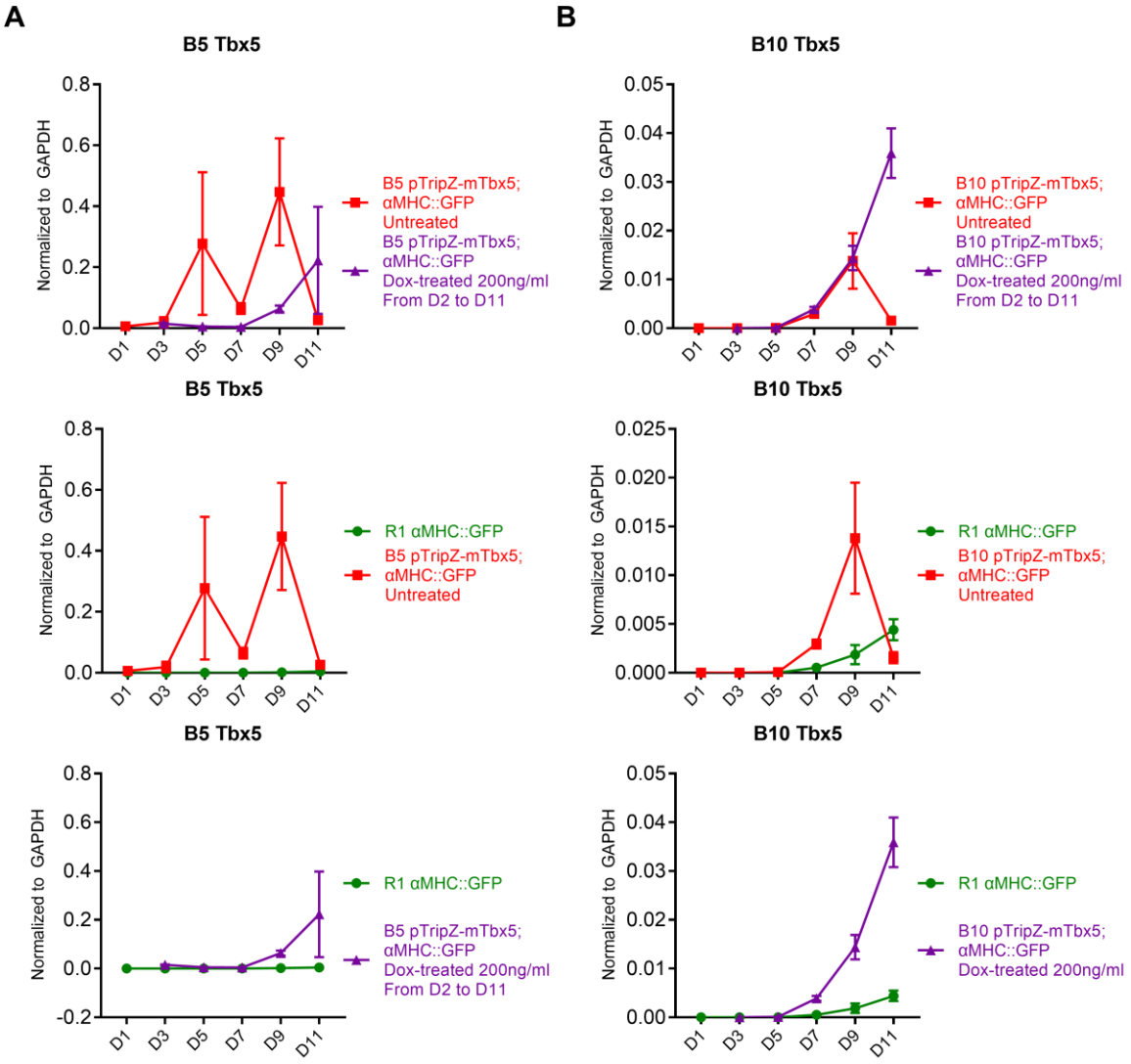

Fig 4.4. Relative Tbx5 expression during B5 and B10 EB differetiation. EBs were collected from Day 1 to Day 11 and assessed Tbx5 transcription by qRT-PCR among R1, B5 and B5 Dox-treated EBs (Fig 4.4A) or among R1, B10 and B10 Dox-treated EBs (Fig 4.4B). Data represent means ± standard error of one independent experiment.

One possible explanation for increased expression of Tbx5 in the absence of dox would be the presence of tetracycline (TET) in the serum (FBS #A87F82H). To test this, one experiment was repeated with EBs grown in TET-free medium (TET-free FBS #AC10251184). Tbx5 expression in B1 EBs was not decreased when cells were grown in Tet-free media (Fig 4.5A). Next, another experiment was repeated again with R1 EBs grown in TET-free medium versus normal medium. The relative Tbx5 expression of R1 αMHC::GFP EBs grown in TET-free media only increased at Day 9 compared to normal medium (Fig 4.5B). Then two more analysis were done with between R1 and B1 EBs either with TET-free medium or normal medium (Fig 4.5C&D). In Fig 4.5D, increased Tbx5 expression was observed with the same pattern as Fig 4.5A. As concerned, we decided to use FBS #A87F82H for all subsequent experiments.

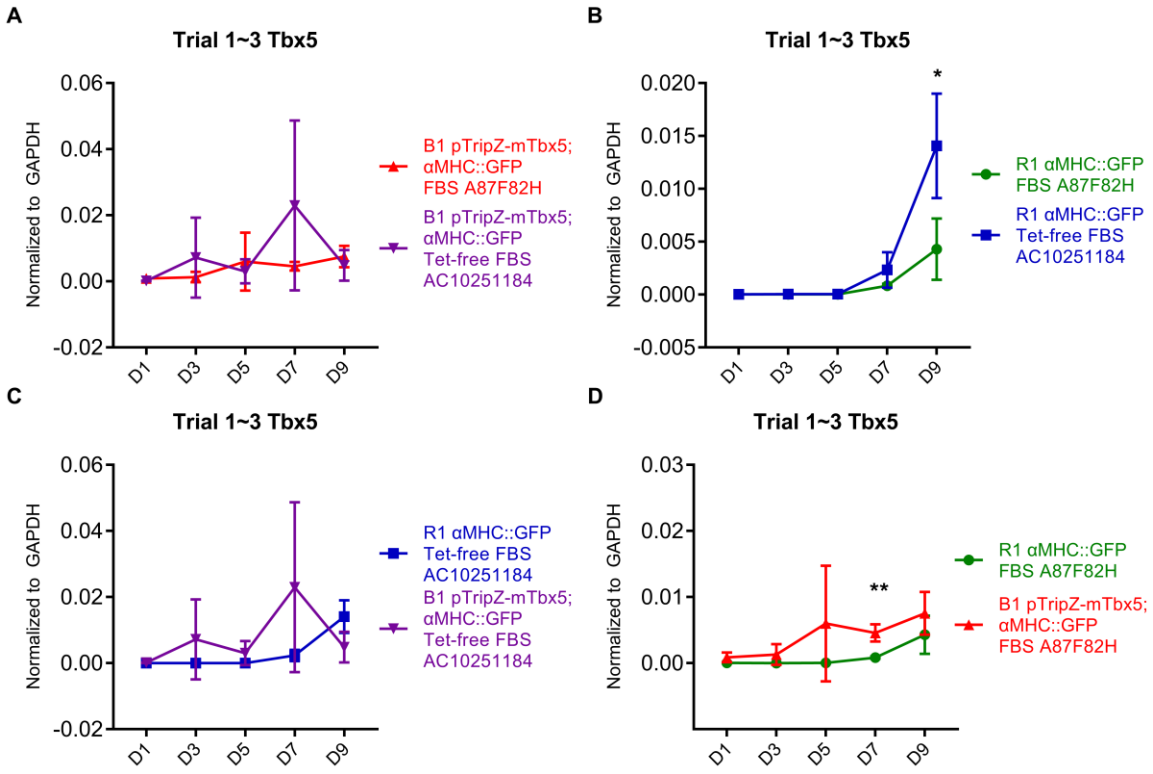

Fig 4.5. B1 or R1 EBs were cultured in standard differentiation medium with either FBS #A87F82H or TET-free FBS #AC10251184. EBs from D1 to D9 were collected and relative Tbx5 level was analyzed by qRT-PCR. Data represent means ± standard error of 3 independent experiments. Statistical significance was determined by unpaired, two-tailed t-test. *$p<0.05$, **$p<0.01$.

Tbx5 overexpression increases overall cardiac formation

Tbx5 is a key player in cardiac development. Since B1 naturally expresses higher levels of Tbx5, it should also be more active in cardiogenesis. To test this, EBs were differentiated with or without the addition of dox from Day 2 to Day 21 (Fig 4.6A) or from Day 4 to Day 21 (Fig 4.6B). Cells were isolated at Days 17, 19 and 21. The percentage of cardiac differentiation was assessed based on expression of GFP by flow cytometry. In all cases, more cardiac cells formed from B1 cells but addition of Dox never enhanced cardiac differentiation further.

In another study, the goal is to figure out whether administration of doxycycline increases R1 parent cell line's cardiac differentiation. EBs were differentiated with or without the addition of dox from Day 4 to Day 21 (Fig 4.7). Dissociated EBs were analyzed by flow cytometry at Day 19 and Day 21. Expression of GFP recognized the percentage of cardiac differentiation by flow cytometry. At Day 19 and Day 21, addition of doxycycline did not increase the cardiac cells formed from R1 αMHC::GFP cells, while B1 treated with doxycycline did not also increase cardiogenesis further more.

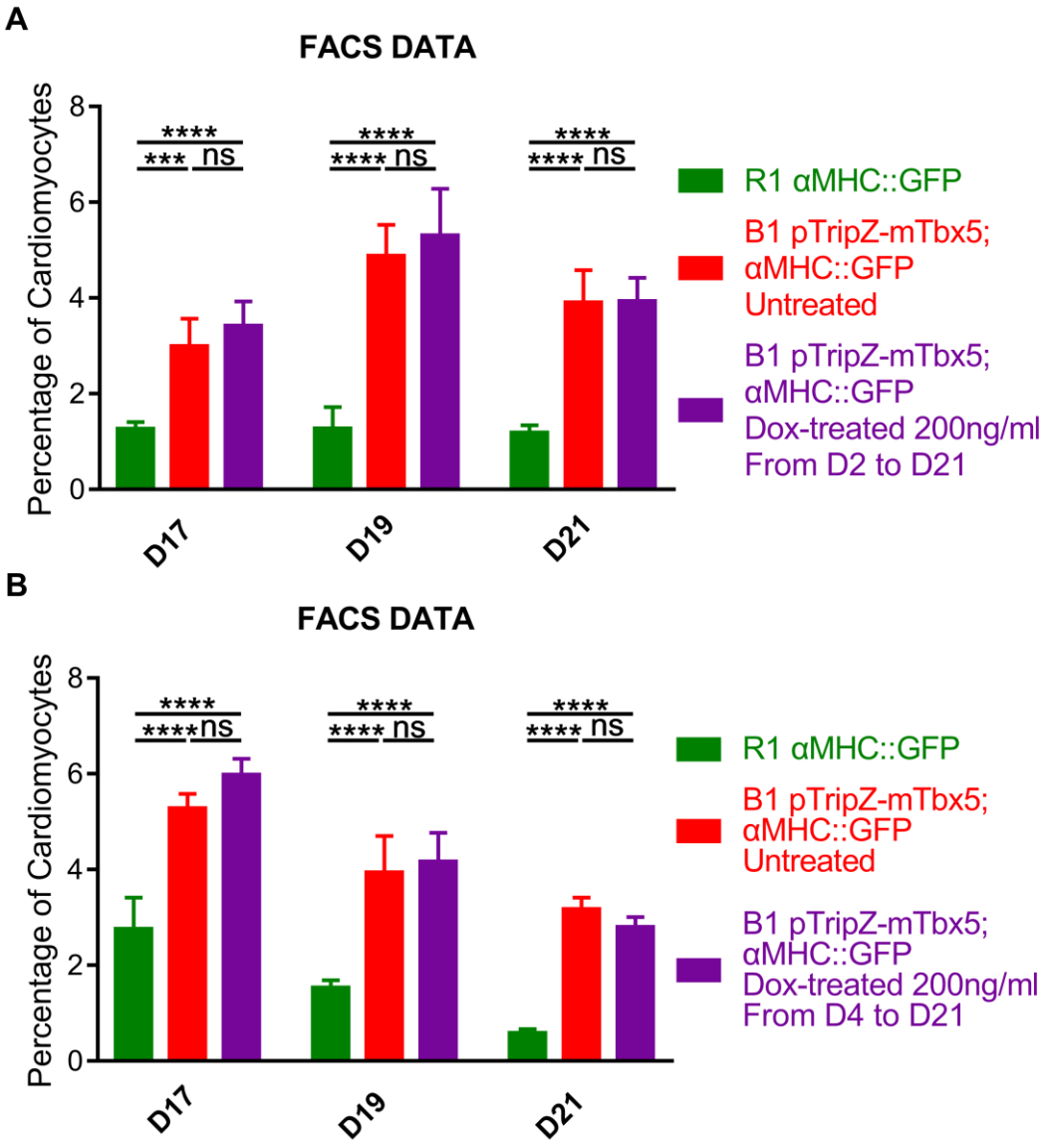

Fig 4.6. Cardiac differentiation analyzed by Flow Cytometry. EBs were differentiated with or without the addition of Doxycycline from Day 2 to Day 21 (Fig 4.6A) and from Day 4 to Day 21 (Fig 4.6B). The percentage of cardiomyocytes was determined by Flow Cytometry Data represent means ±standard error of 3 independent experiments. Statistical significance was determined by unpaired, two-tailed t-test. ***p<0.001, ****p<0.0001

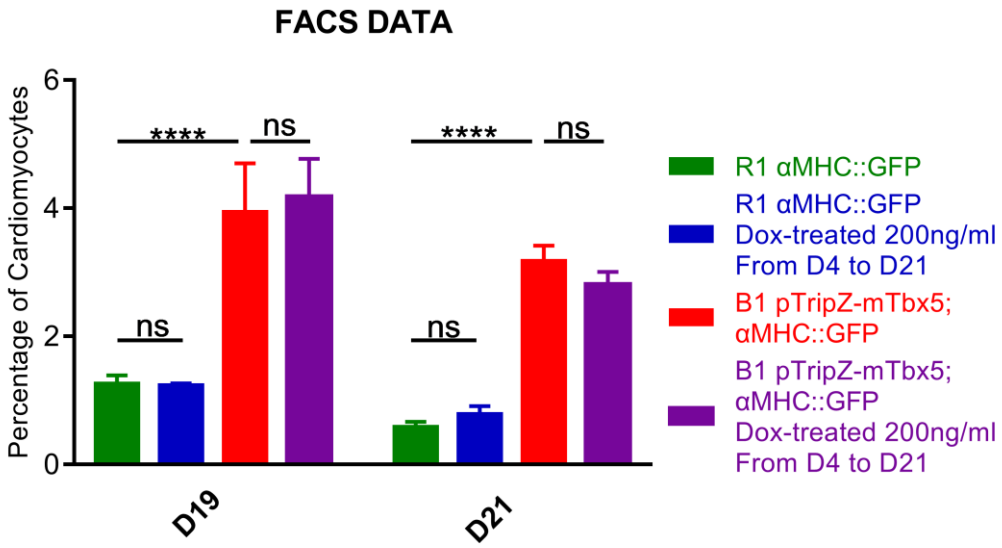

Fig 4.7. Cardiac differentiation analyzed by Flow Cytometry at Day 19 and Day 21. EBs were differentiated with or without the addition of Doxycycline from Day 21. The percentage of cardiomyocytes was determined by Flow Cytometry Data represent means ± standard error of 3 independent experiments. Statistical significance was determined by unpaired, two-tailed t-test. ****p<0.0001

Subtype of Differentiated Cardiomyocytes

Immunocytochemistry (ICC) staining is current standard to figure out cardiac subtype based on protein expression, such as HCN4 and Shox2 for pacemaker marker or Cx43 for ventricular marker. Here four different EBs including R1, MAP3K7/TAK1-overexpressing EBs (pgk:MAP3K7/TAK1; αMHC:mCherry) [141], B1 untreated, B1 Dox-treated were analyzed for HCN4, Shox2 and Cx43 positive cardiomyocytes (Fig 4.8A). MAP3K7/TAK1-overexpressing EBs had more HCH4 and Shox2 positive cardiomyocytes than R1 EBs, however there was no significant difference either between R1 and B1, or between B1 and B1 dox-treated EBs. Meanwhile, MAP3K7/TAK1-overexpressing EBs had less Cx43 positive cardiomyocytes than R1, while B1 and B1 dox-treated EBs also had less Cx43 positive cardiac cells than R1 EBs. B1 Dox-treated EBs had less Cx43 positive cardiomyocytes compared to B1 untreated EBs.

At the same time, whole EBs from R1, B1 and B1 dox-treated group were collected and later assessed by qRT-PCR at Day 21 (Fig 4.8B). All transcripts data were normalized to B1 untreated EBs, each trials normalized. MAP3K7/TAK1 transcripts did not change among three groups. Tbx5 as previous described, B1 dox-treated EBs and R1 EBs had significant less Tbx5 transcripts. Compared to R1 EBs, B1 EBs had more Shox2, Tbx3, Tbx18, HCN4 and Isl1, theses downstream pacemaker marker of Vincent Christofells models. There was no significant difference between B1 and B1 Dox-treated EBs, while B1 Dox-treated showed the similar expression pattern. However, B1 EBs activated Nkx2.5 expression compared to R1 EBs.

In parallel, the same experiments described above were performed again to figure out the subtype of cardiomyocytes at Day 19 (Fig 4.9). MAP3K7/TAK1-overexpressing EBs had more HCN4 and Shox2 positive cardiomyocytes than R1 EBs, however there was no significant difference either between R1 and B1, or between B1 and B1 dox-treated EBs. Meanwhile, MAP3K7/TAK1-overexpressing EBs had less Cx43 positive cardiomyocytes than R1, while B1 and B1 dox-treated EBs also had the similar level of Cx43 positive cardiac cells compared to R1 EBs (Fig 4.9A). For all markers at Day 19, there was no significant difference among R1, B1 and B1 dox-treated EBs (Fig 4.9B).

Taken together, activation of Tbx5 transcription in B1 EBs did not drive the cardiac progenitor cells into pacemaker fate.

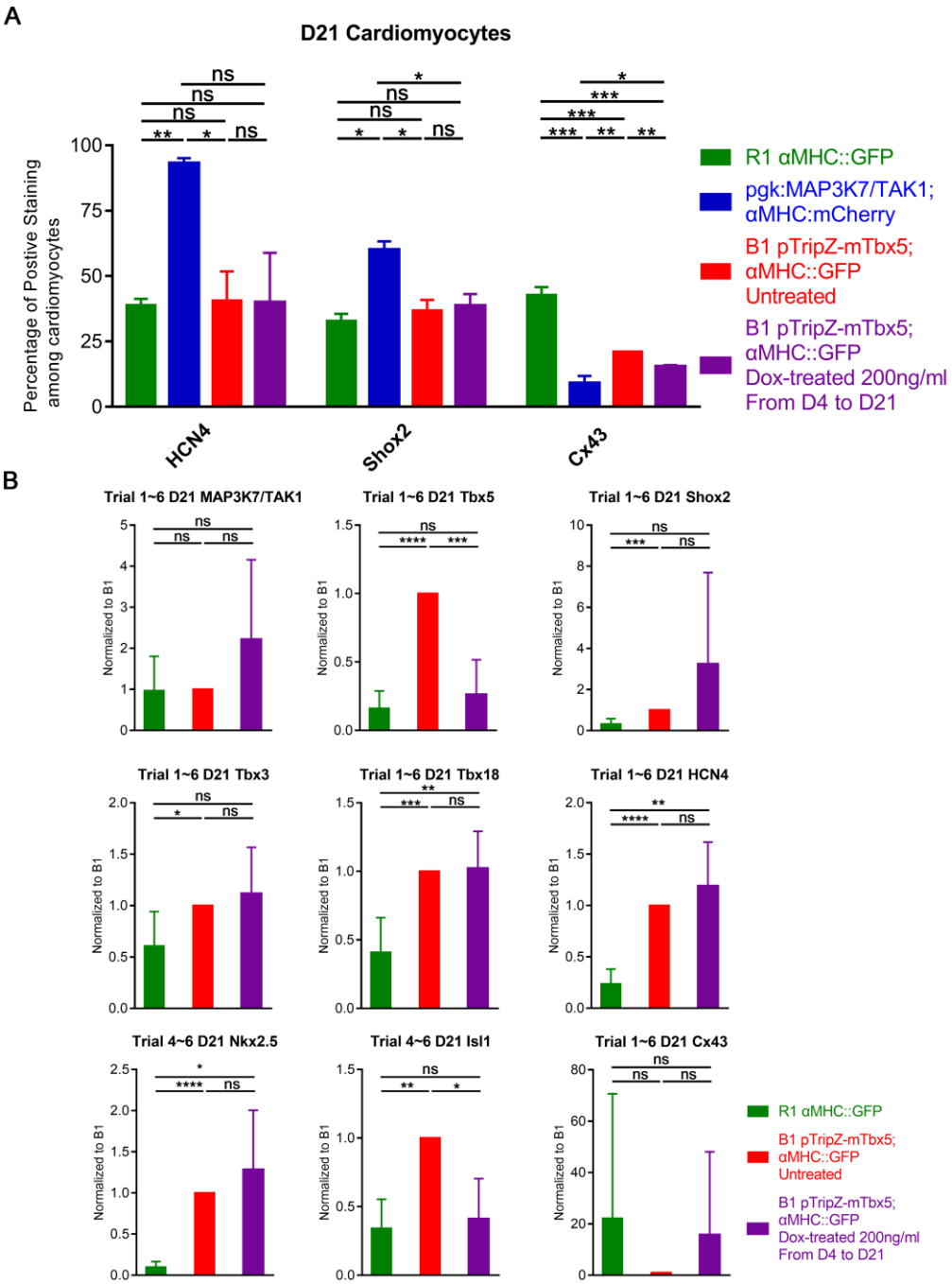

Fig 4.8. The subtype of cardiomyocytes and relative transcripts of R1, B1, B1 Dox-treated EBs at Day 21. Fig 4.8A. The percentage of HCN4, Shox2 and Cx43 positive cells were analyzed by ICC. Fig 4.8B. MAP3K7/TAK1, Tbx5, Shox2, Tbx3, Tbx18, HCN4, Nkx2.5, Isl1 and Cx43 transcription were assessed by qRT-PCR. Data represent means ± standard error of 6 independent experiments, normalized to B1. Statistical significance was determined by unpaired, two-tailed t-test. *p<0.05, **p<0.01, ***p<0.001, ****p<0.0001.

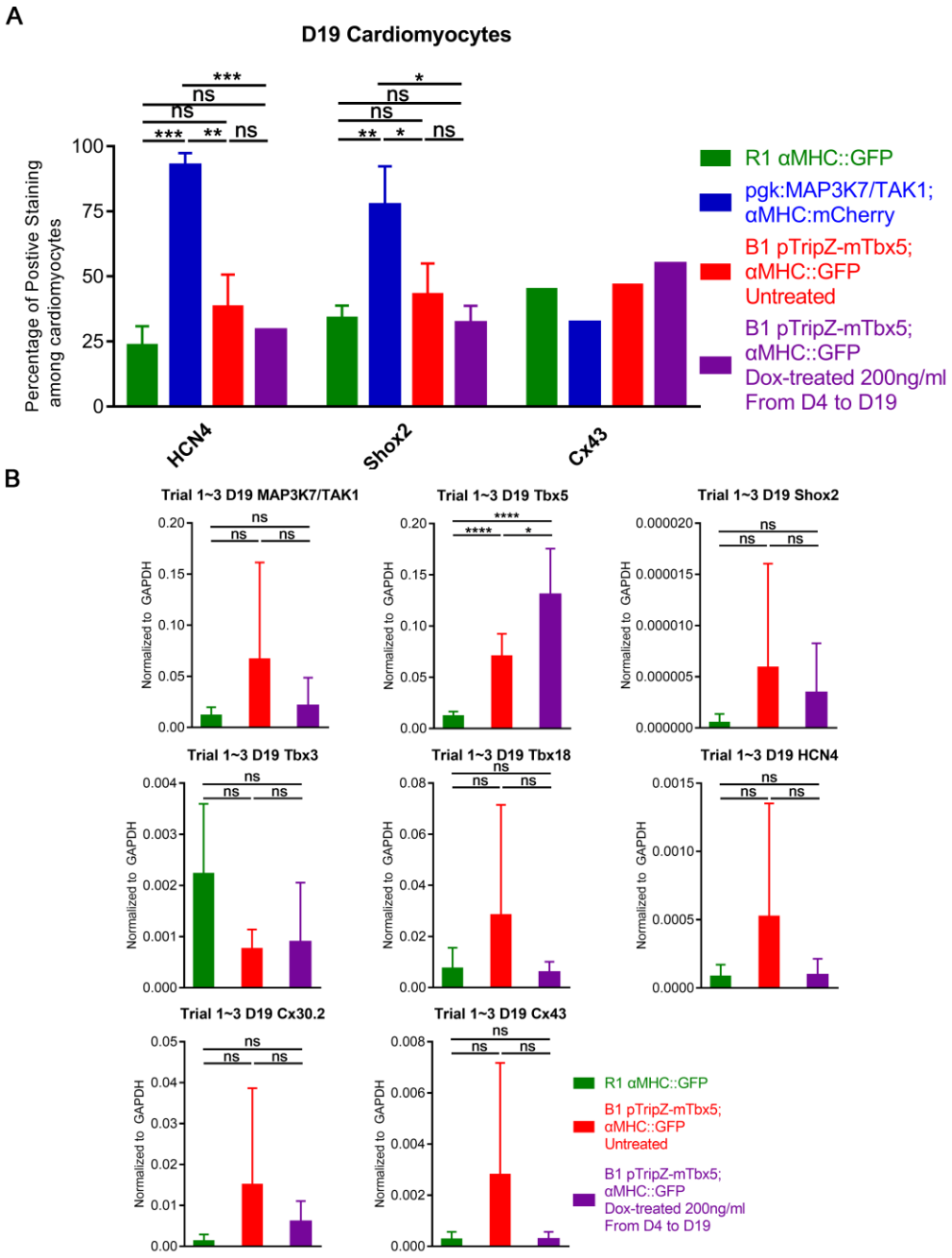

Fig 4.9. The subtype of cardiomyocytes and relative transcripts of R1, B1, B1 Dox-treated EBs at Day 19. Fig 4.9A. The percentage of HCN4, Shox2 and Cx43 positive cells were analyzed by ICC. Fig 4.9B. MAP3K7/TAK1, Tbx5, Shox2, Tbx3, Tbx18, HCN4, Cx30.2 and Cx43 transcription were assessed by qRT-PCR. Data represent means ±standard error of 3 independent experiments. Statistical significance was determined by unpaired, two-tailed t-test. *p<0.05, **p<0.01, ***p<0.001.

Representative Image of ICC staining

The golden standard for subtype of cardiomyocytes is to figure out the protein expression of cardiac cells: HCN4 and Shox2 for pacemaker marker; Cx43 for ventricular marker. Representative images of HCN4 staining of Day 21 (Fig 4.10) and Day 19 (Fig 4.11) show that HCN4 expressing cells at these time points show morphologies charatcteristic of SAN cells. Cardiomyocytes of R1, MAP3K7-Overexpressing, B1, B1 Dox-treated EBs. At first, GFP positive cardiomyocytes were found under the microscopy to confirm its location, and then switch to HCN4 signaling, which expressed in the cell cytosol and imaged with DAPI nuclear staining at the same time. Here only GFP and HCN4 double positive cardiac cells were shown.

Representative Image of Shox2 staining of Day 21 (Fig 4.12) and Day 19 (Fig 4.13) Cardiomyocytes of R1, MAP3K7/TAK1-Overexpressing, B1, B1 Dox-treated EBs. At first, GFP positive cardiomyocytes were found under the microscopy to confirm its location, and then switch to Shox2 signaling, which expressed in the nuclear sublocation and imaged with DAPI nuclear staining at the same time. Here only GFP and Shox2 double positive cardiac cells were shown. Surprisingly, in MAP3K7/TAK1-overexpressing EBs at Day 21, cardiomyocyte with multiple Shox2 positive nucleus was observed and it was not found in other cell type.

Representative Image of Cx43 staining of Day 21 (Fig 4.14) and Day 19 (Fig 4.15) Cardiomyocytes of R1, MAP3K7/TAK1-Overexpressing, B1, B1 Dox-treated EBs. At first, GFP positive cardiomyocytes were found under the microscopy to confirm its location, and then switch to Cx43 signaling, which expressed in the cell membrane and imaged with

DAPI nuclear staining at the same time. Here only GFP and Cx43 double positive cardiac cells were shown. At the edge of each cardiomyocyte, Cx43/Gap Junction was lined up as dash line to contour the shape of individual cells and most expressed between two cells next to each other.

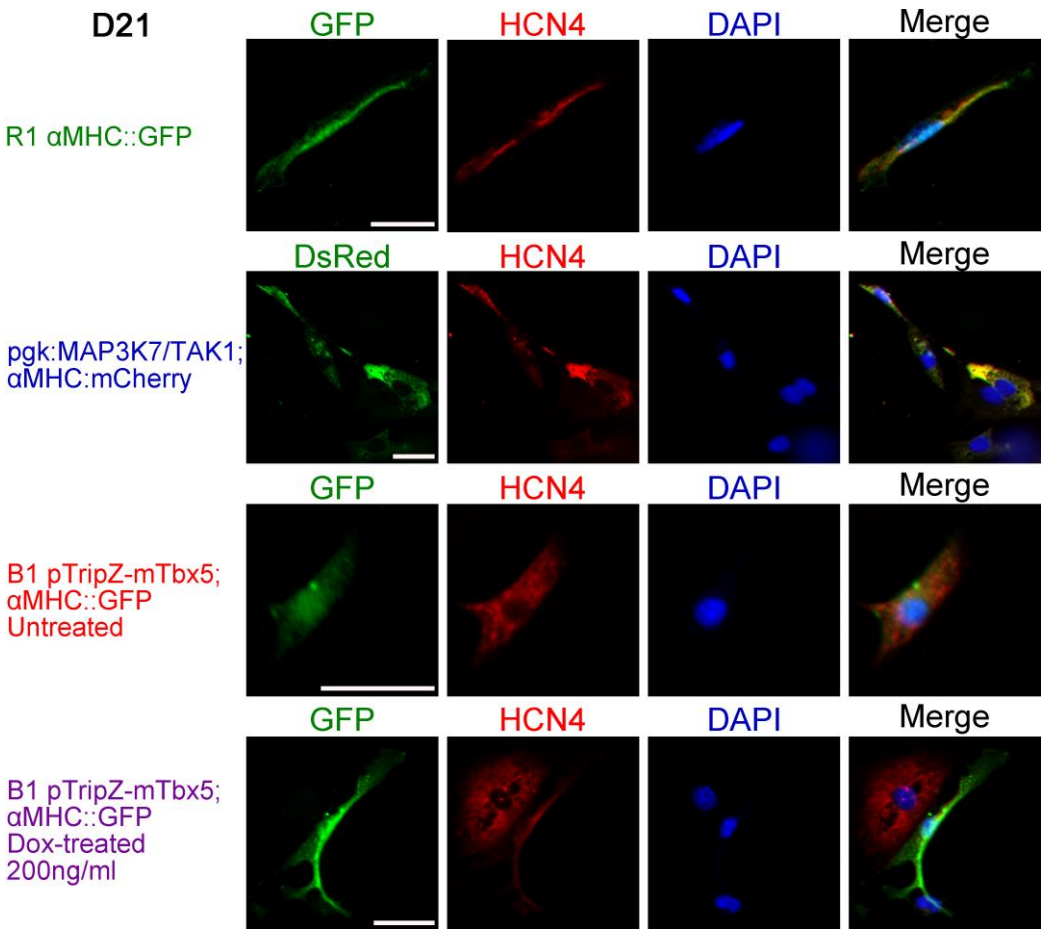

Fig 4.10. Representative Image of Immnuocytochemistry (ICC) staining of Day 21 Cardiomyocytes of R1, MAP3K7/TAK1-overexpressing, B1, B1 Dox-treated EBs. EBs were dissociated into single cell suspension and replated onto chamber slide. Then these cells were stained with GFP or DsRed antibody to determine cardiomyocytes based on expression of αMHC:GFP or αMHC:mCherry, while HCN4 antibody to figure out the subtype of cardiac cells. Scale bar, 30 μm.

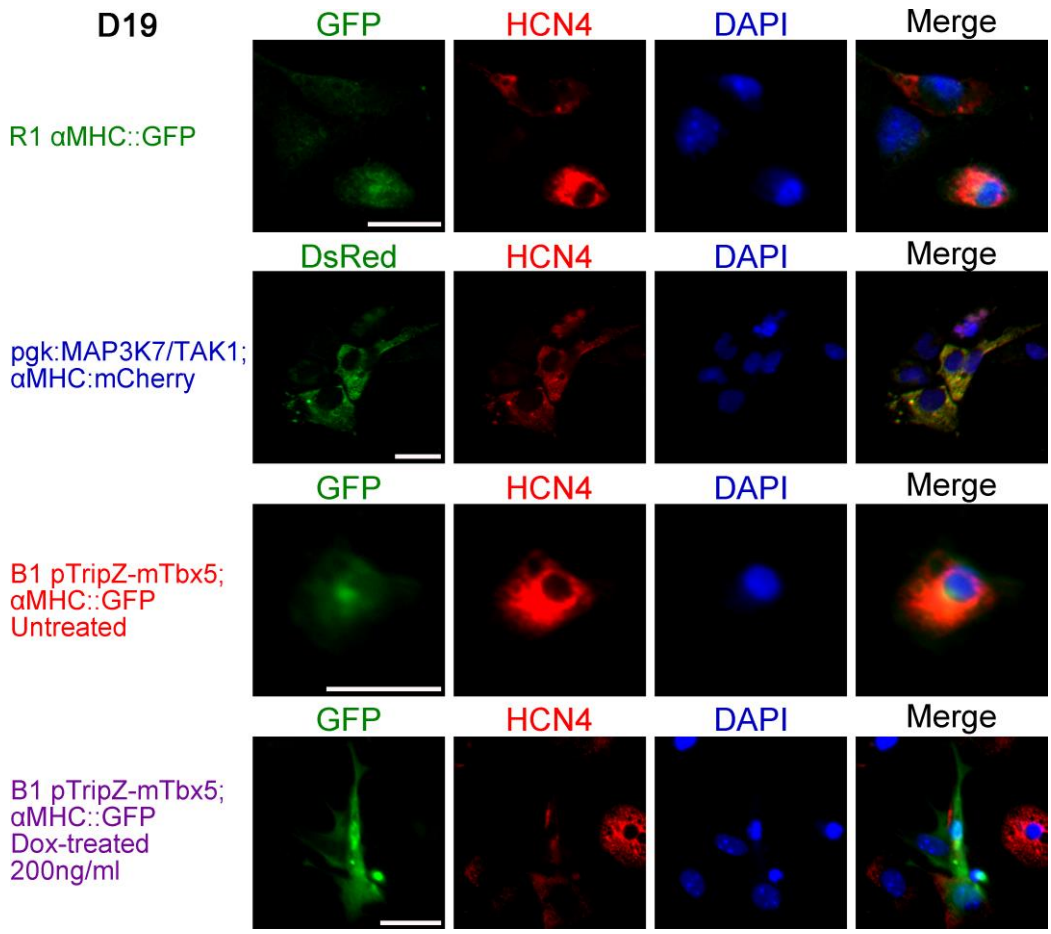

Fig 4.11. Representative Image of Immnuocytochemistry (ICC) staining of Day 19 Cardiomyocytes of R1, MAP3K7/TAK1-overexpressing, B1, B1 Dox-treated EBs. EBs were dissociated into single cell suspension and replated onto chamber slide. Then these cells were stained with GFP or DsRed antibody to determine cardiomyocytes based on expression of αMHC:GFP or αMHC:mCherry, while HCN4 antibody to figure out the subtype of cardiac cells. Scale bar, 30 μm.

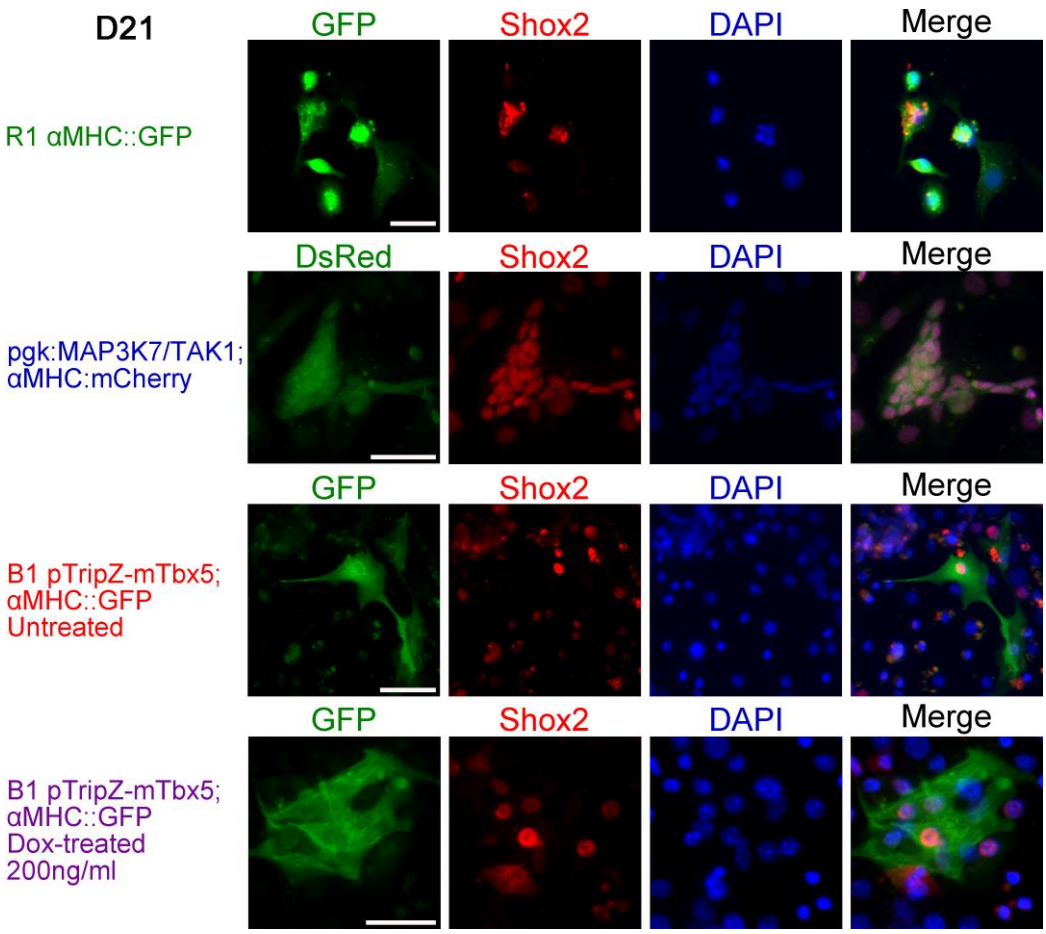

Fig 4.12. Representative Image of ICC staining of Day 21 Cardiomyocytes of R1, MAP3K7/TAK1-overexpressing, B1, B1 Dox-treated EBs. EBs were dissociated into single cell suspension and replated onto chamber slide. Then these cells were stained with GFP or DsRed antibody to determine cardiomyocytes based on expression of αMHC:GFP or αMHC:mCherry, while Shox2 antibody to figure out the subtype of cardiac cells. Scale bar, 30 μm.

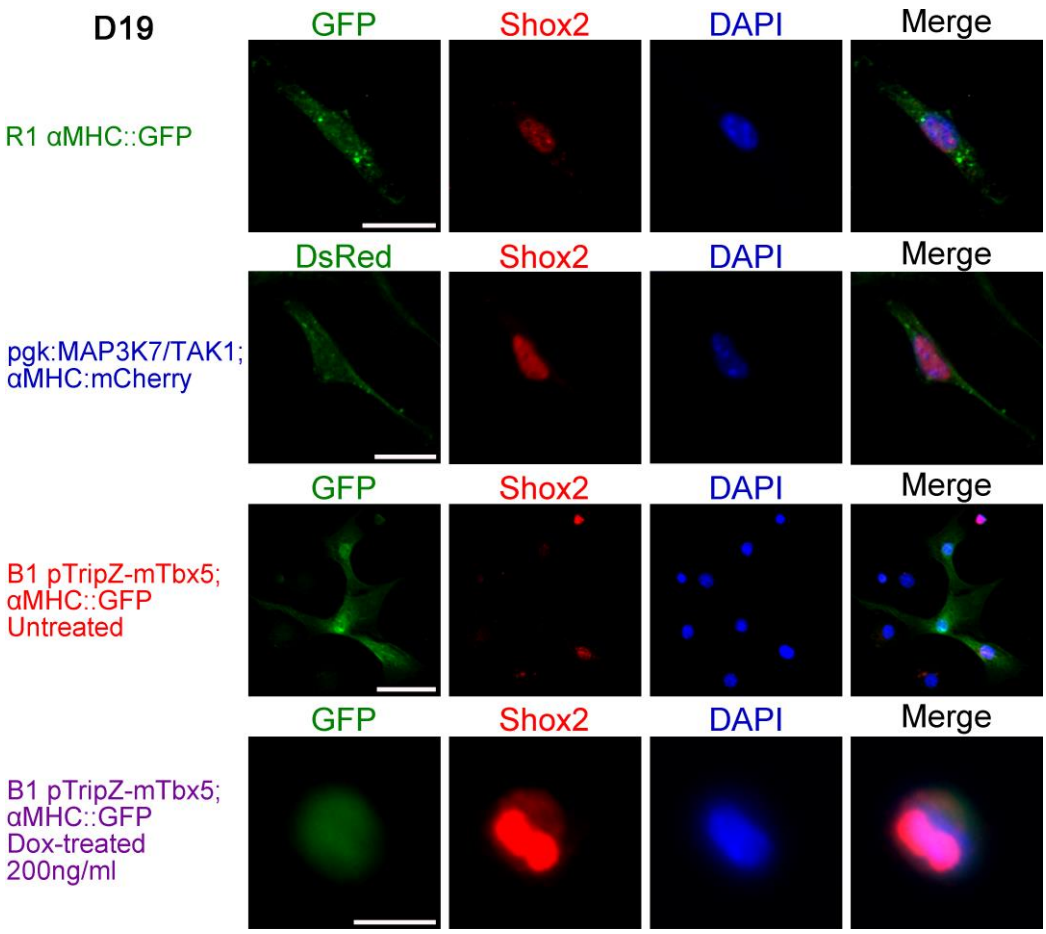

Fig 4.13. Representative Image of ICC staining of Day 19 Cardiomyocytes of R1, MAP3K7/TAK1-overexpressing, B1, B1 Dox-treated EBs. EBs were dissociated into single cell suspension and replated onto chamber slide. Then these cells were stained with GFP or DsRed antibody to determine cardiomyocytes based on expression of αMHC:GFP or αMHC:mCherry, while Shox2 antibody to figure out the subtype of cardiac cells. Scale bar, 30 μm.

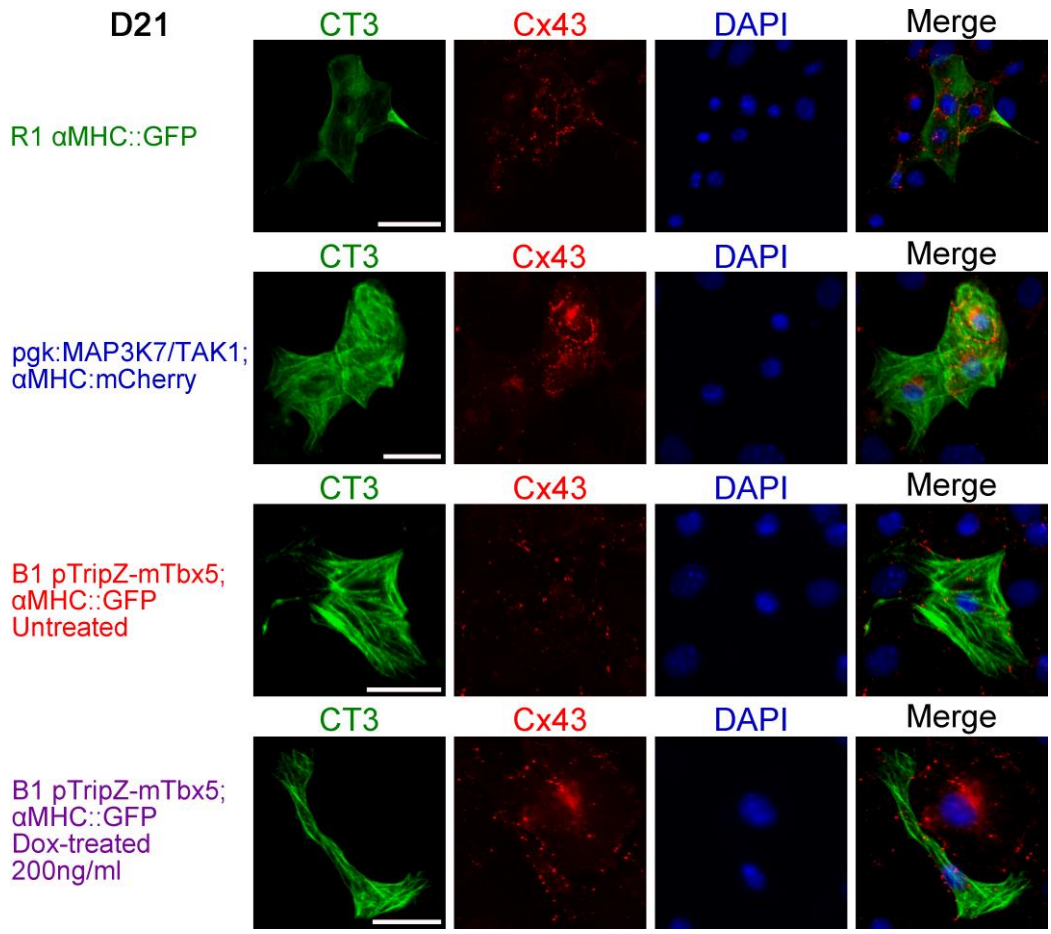

Fig 4.14. Representative Image of ICC staining of Day 21 Cardiomyocytes of R1, MAP3K7/TAK1-overexpressing, B1, B1 Dox-treated EBs. EBs were dissociated into single cell suspension and replated onto chamber slide. Then these cells were stained with CT3 antibody to determine cardiomyocytes based on expression of αMHC:GFP or αMHC:mCherry, while Cx43 antibody to figure out the subtype of cardiac cells. Scale bar, 30 μm.

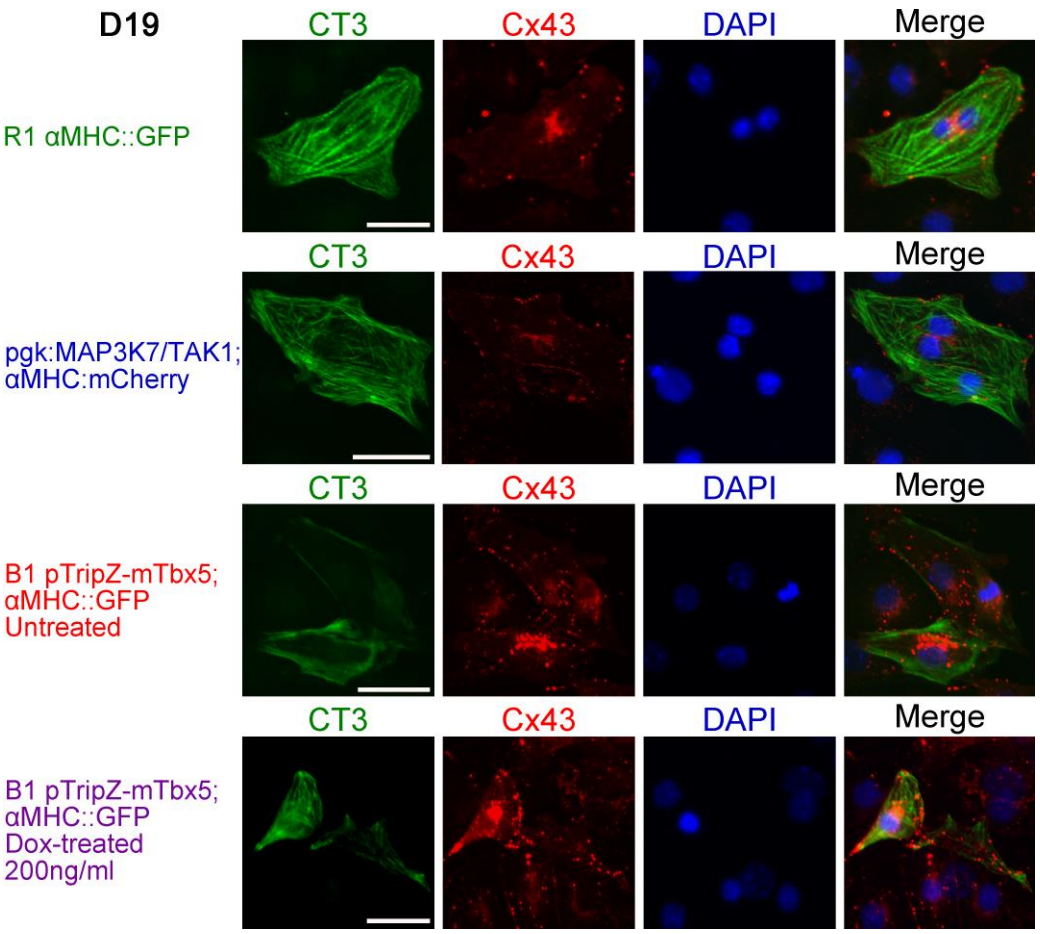

Fig 4.15. Representative Image of ICC staining of Day 19 Cardiomyocytes of R1, MAP3K7/TAK1-overexpressing, B1, B1 Dox-treated EBs. EBs were dissociated into single cell suspension and replated onto chamber slide. Then these cells were stained with CT3 antibody to determine cardiomyocytes based on expression of αMHC:GFP or αMHC:mCherry, while Cx43 antibody to figure out the subtype of cardiac cells. Scale bar, 30 μm.

Summary

Here, we produced a mouse embryonic stem cell line B1 (pTripZ-mTbx5; αMHC::GFP) that conditionally overexpresses Tbx5. We found that B1 ES cells overexpressing Tbx5 showed enhanced overall cardiac differentiation and that cardiac cells showed increased beat rates as compared control embryos. Besides, key genes associated with SAN differentiation including HCN4 and Shox2 were increased in cells overexpressing Tbx5 while other gene associated with early SAN lineage were impacted. Despite this, faster beating cells showed a decreased expression of the chamber specific marker Cx43 and did not alert in HCN4 or Shox2 positive cardiac cells. These data suggest that Tbx5 overexpression is not sufficient for SAN differentiation, although it does activate some of early steps in the SAN cascade.

CHAPTER FIVE

THE ROLE OF MAP3K7/TAK1 OVEREXPRESSION DURING EB DIFFERNTIATION

Introduction:

In this chapter, I analyzed the effect of the MAP3K7/TAK1 overexpression on SAN differentiation. Using qRT-PCR analyses and FACS data I analyzed gene expression comparing wild type EBs to MAP3K7-Overexpressing EBs. I analyzed both pacemaker genes and genes expressed in other lineages relevant to heart induction, specifically visceral endoderm (VE), anterior visceral endoderm (AVE) anddefinitive endoderm (DE). In addition I examined expression of genes related to Sonic Hedgehog (Shh) signaling.

Cardiomyocytes derived from MAP3K7/TAK1-overexpressing EBs display molecular characteristics of the SAN

To determine if MAP3K7/TAK1-overexpressing EBs influences the cardiac differentiation into the SAN fate, qRT-PCR analyses were performed to examine pacemaker-specific markers that are already known to direct SAN fate in vivo (reviewed in [107]). MAP3K7-overexpressing ES cells were differentiated as EBs and then assessed by qRT-PCR for cardiac marker expression from Day 1 to Day 16. During EB differentiation, continuous overexpression of MAP3K7 had a profound impact on the transcriptional expression of the cardiac progenitor markers like Nkx2.5 and Tbx5 [141]. By Day 5, decreased Nkx2.5 transcription in MAP3K7 cells was observed and two days

later, by day 7, dramatic increase of Tbx5 transcripts were found in MAP3K7-overexpressing EBs.

Within approximately the same differentiation window, mRNAs encoding the SAN-specific transcription factors Shox2 and Tbx3 were upregulated, and meanwhile cardiac contractile proteins, αMHC, βMHC, were markedly decreased. Other SAN-specific markers were either unchanged as compared to wild-type R1 EBs (HCN2) or upregulated (HCN4). HCN1, which is not expressed in the SAN of the mouse embryo was expressed at similar levels as compared to wild-type R1 EBs, yet the timing of expression was very different.

Isl1 expression was found in cardiac precursors and went down in most differentiated myocardial cells. However, Sinus Node cells continued to express Isl1 during later differentiation [55]. In MAP3K7-overexpressing cells, three pulses of Isl1 expression were observed, while only one of these pulses was observed in wild type R1 cells, the other two missing; however, the overall expression pattern was similar between R1 and MAP3K7-overexpressing cells. Due to Isl1's role, non-specific for the sinus node, another marker of SAN precursor, Tbx18, was examined. In addition, we showed that when TAK1 cells are co-cultured with wild type cells that the wild type cells respond by increasing cardiac differentiation, suggesting that TAK1 overexpression leads to the formation of cardiogenic tissues. The lab had also previously shown that gut endoderm markers are upregulated in these cells (Hunter, A; Dai, Y. et al, 2019, in revision). To address this possibility I carried out an extensive marker analysis comparing gene expression in the TAK1 over-expressing cells to that in wild type cells.

Unlike Isl1, Tbx18 (Fig 5.1) was not significantly different between the two populations. This data suggests that MAP3K7 acts on established SAN precursors but does not determine the size of the precursor population.

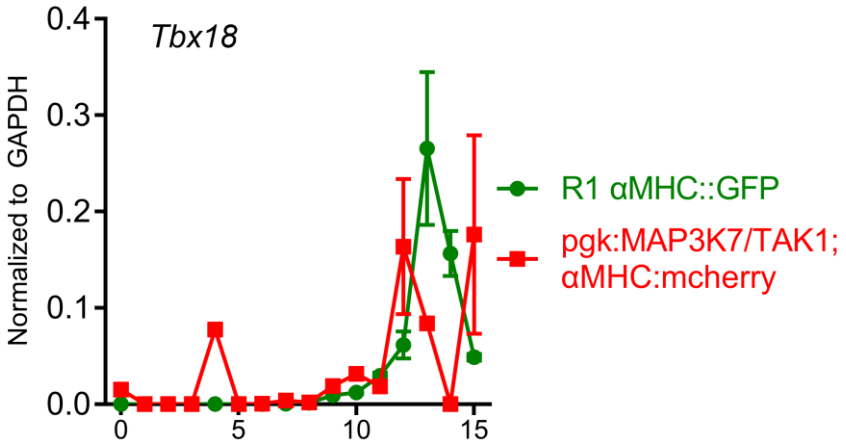

Fig 5.1. Relative Tbx18 expression during EB differetiation. EBs were collected from Day 1 to Day 16 and assessed Tbx18 transcription by qRT-PCR between wild-type R1 and MAP3K7-overexpressing. Data represent means ± standard error of 3 independent experiments. Statistical significance was determined by unpaired, two-tailed t-test.

MAP3K7/TAK1 specifically upregulates the expression of markers for the cardiogenic endoderm.

Transthyretin, α-feto-protein, Hnf4 and Gata4 are all expressed in both the visceral endoderm (VE), which surrounds mouse embryos prior to gastrulation, and in the gut endoderm which is made up of both VE and streak-derived definitive endoderm (DE) [144, 145]. We previously published that TAK1 overexpressing cells also upregulate these markers. To clarify if this up regulation of endodermal markers is the result of expansion of the VE or DE, or both, specific markers for each of these lineages were assessed.

First, markers for the AVE were assessed, as this is the source of cardiogenic signals in the embryo. Both Cerberus and hHex were significantly upregulated suggesting that a MAP3K7 overexpressing EBs do show a general expansion of AVE (Fig 5.2A). Interestingly, Dkk1 was not upregulated, suggesting that its expression in the AVE may be controlled by another pathway (Fig 5.2A). Sox17, a marker for all early endodermal lineages, including the VE and DE was also upregulated but only transiently (Fig 5.2A). Markers that are specifically expressed in the DE but not in the VE, including mCXCR4, mTM4sf2 and GPC, were not changed in these EBs as compared to wild type controls (Fig 5.2B). Finally, we assessed the early neural marker Sox2. This was also not significantly different than in control EBs (Fig 5.2B). From this we conclude that MAP3K7 dramatically and consistently causes an increase in markers for the VE and AVE, but does not affect the formation of streak-derived DE. To confirm the role MAP3K7 on endoderm formation, we differentiated EBs harboring an endoderm specific promoter reporter, Afp::GFP [146]. These were treated with the MAP3K7/TAK1 specific inhibitor 5z-7-oxozeaenol. EBs were

treated with the inhibitor from Day 1 to Day 4 of EB differentiation and assessed on Day 10 for expression of the endoderm reporter (Fig 5.3). Control EBs grown in the presence of the carrier DMSO showed robust endoderm differentiation, as assessed by the presence of cells expressing the GFP reporter. By contrast cells grown in the presence the MAP3K7 inhibitor showed almost no endoderm formation, even 6 days after the inhibitor was removed.

MAP3K7/TAK1 Overexpression leads to up regulation of Shh and Gli2

It has previously been observed that TGFbeta signaling regulates the expression of Sonic Hedgehog (Shh) during gastrulation in Hensen's node of avian embryos [147]. To examine whether SMAD-independent TGFbeta signaling might be involved in regulation of Shh, we examined the expression of Shh and several Gli genes by qRT_PCR during EB differentiation. Shh and Gli2, but not Gli1 or Gli3 showed robust overexpression in EBs overexpressing MAP3K7/TAK1 (Fig 5.4).

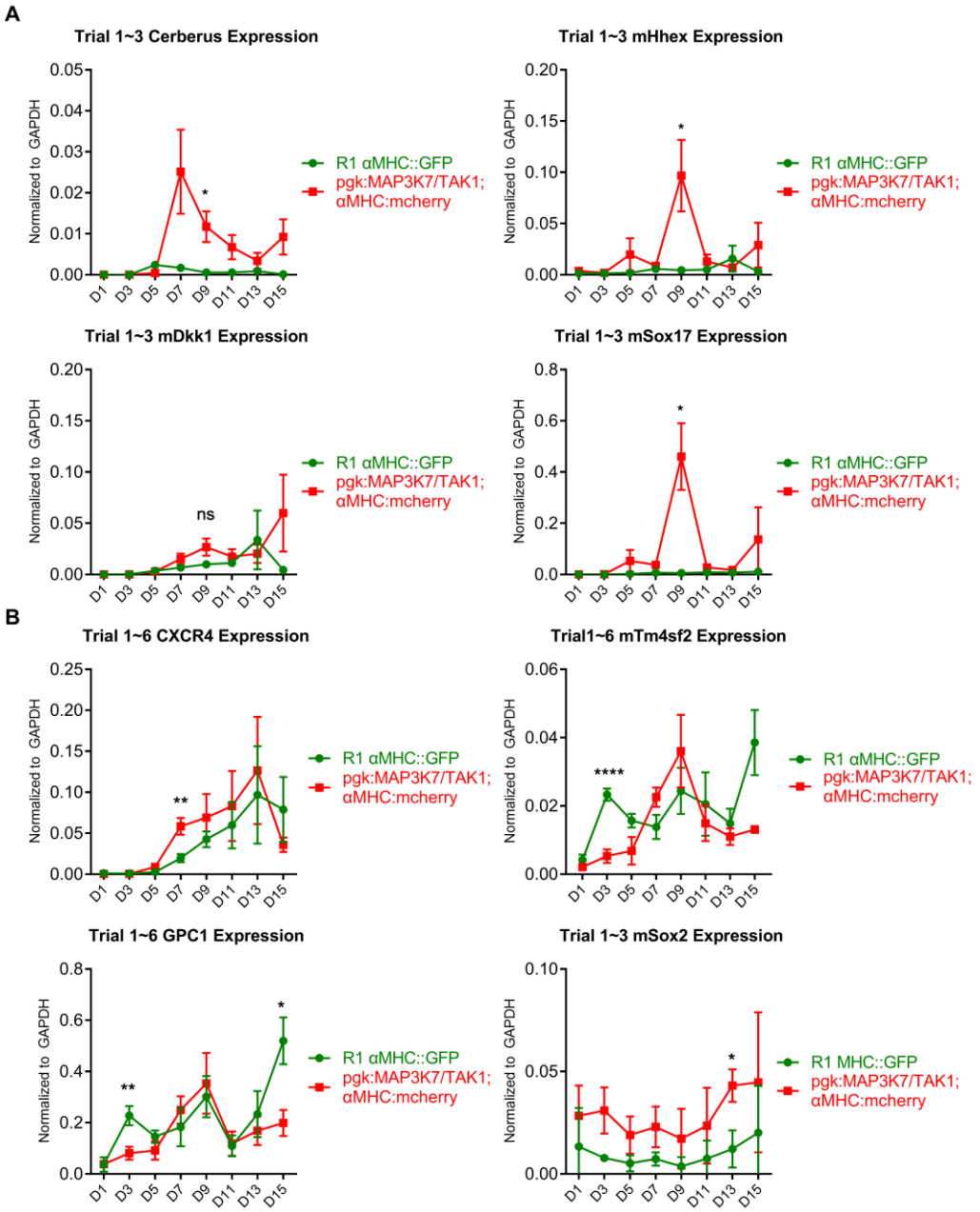

Fig 5.2. Quantitative Real-Time PCR data showing transient up regulation of the AVE markers Cerberus and hHex, as well as the pan-endodermal marker Sox17 (Fig 5.2A). By contrast the AVE Dkk1, which is regulated by Wnt signaling was not upregulated (Fig 5.2A). Markers for the definitive endoderm (CXCR4, mTm4sf2 and GPC1) and the early neural marker, mSox2 were unaffected in MAP3K7/TAK1 overexpressing EBs (red) as compared to control EBs (green line) (Fig 5.2B). Error bars represent standard error of mean. Statistical significance was determined by unpaired, two-tailed t-test. *p<0.05, **p<0.01, ****p<0.0001.

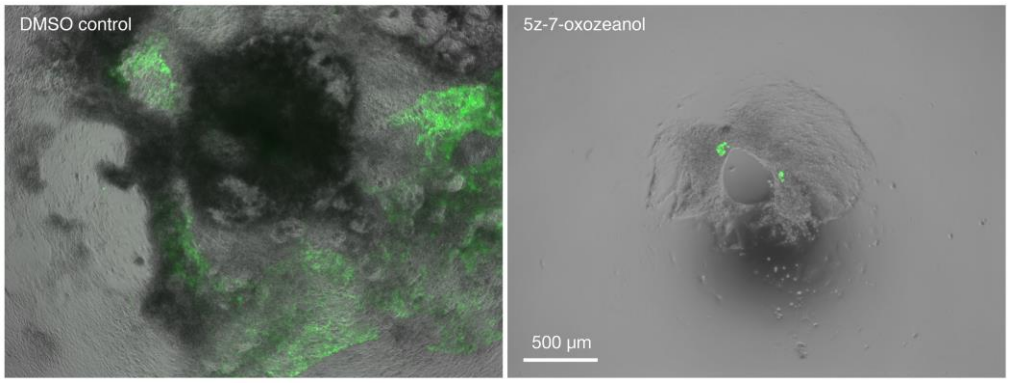

Fig 5.3. The effect of MAP3K7/TAK1 inhibitro 5z-7-oxozeaenol during EB differentiation. EBs harboring an endoderm specific promoter reporter AFP::GFP were grown in the presence of the MAP3K7 inhibitor 5z-7-oxozeaenol from Day 1 to Day 4 of EB differentiation showed a significant decrease in endoderm formation as assessed by the expression of green fluorescent protein, as compared DMSO-treated controls. (hunter, A.; Dai, Y et al 2019, in revision)

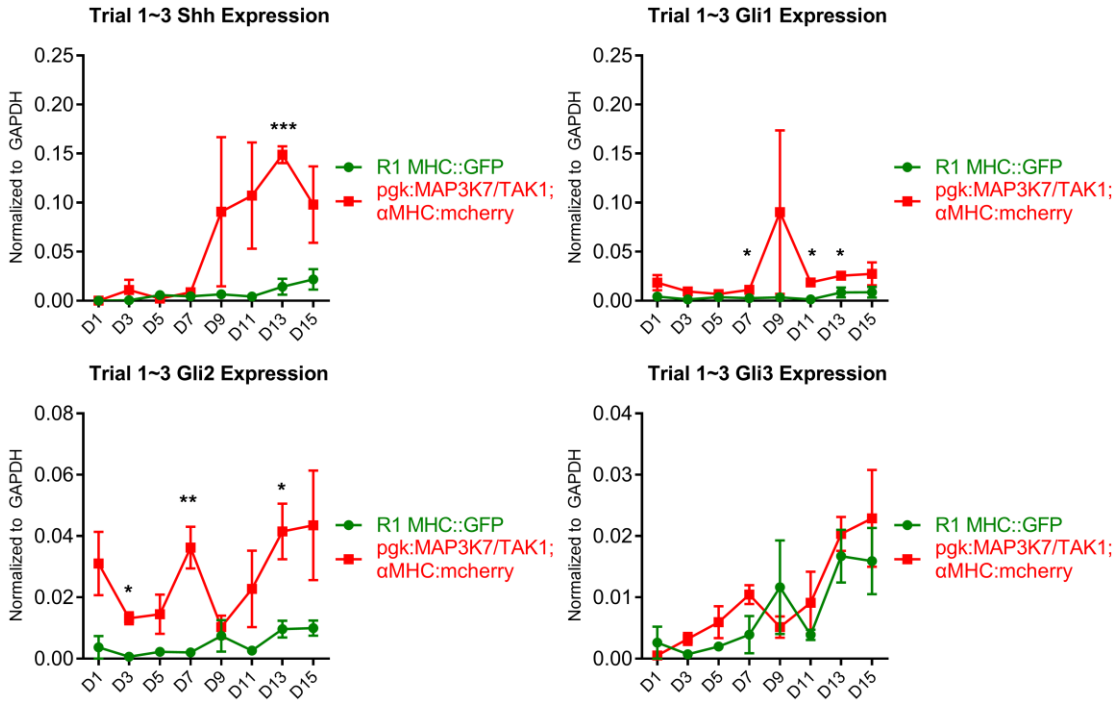

Fig 5.4 Quantitative Real-Time PCR data showing a strong, transient up regulation of Shh and Gli2. Gli1 showed a small but statistically significant up regulation in MAP3K7 overexpressing EBs (red) as compared to control EBs (green line) and Gli3 was not affected. Error bars represent standard error of mean from 3 replicates. Statistical significance was determined by unpaired, two-tailed t-test. *p<0.05, **p<0.01.

MAP3K7/TAK1 Overexpression does not affect early mesoderm formation

Given that MAP3K7 seems to specifically expand the VE and AVE in the endoderm it was hypothesized that MAP3K7 overexpressing EBs might also show an expansion of the cardiac mesoderm. We used qRT-PCR on differentiated EBs to determine if MAP3K7 impacted early mesoderm formation by assessing expression of the early mesoderm markers T/Brachyury and FGF8. There was a small but statistically significant difference between MAP3K7 overexpressing EBs and controls, suggesting that mesoderm formation in these cells may be slightly increased.

We also assessed total cardiac formation on Day 17 in these cells by flow cytometry, but found that there was no statistically significant difference between the percentages of cardiac cells that formed in the MAP3K7/TAK1-overexpressing EBs as compared to the parent (R1) cell line (Fig 5.5).

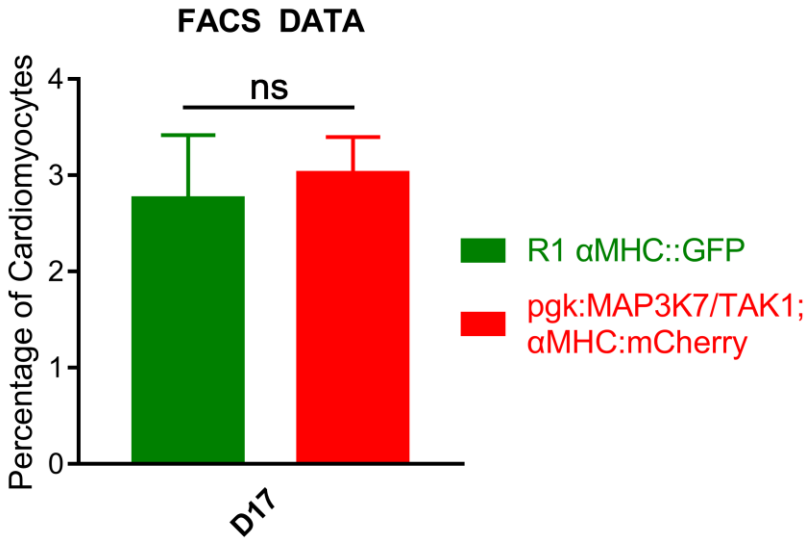

Fig 5.5. Summary of flow cytometry data. Flow cytometry data comparing cardiac differentiation in two separate expansions of MAP3K7/TAK1-overexpressing cells (red bar) and wild type cells (green bar) based on expression of the cardiac specific promoter reporter αMHC::GFP. Error bars in qRT-PCR data indicate standard error from three technical replicates. A change in gene expression between MAP3K7-overexpressing and wild type EBs is considered relevant if the same change was observed in each of a minimum of three biological replicates. Error bars in flow cytometry data represent standard deviation. Statistical significance was determined by unpaired, two-tailed t-test.

Discussion:

Here, MAP3K7-overexpression EBs did not affect overall cardiac formation. Meanwhile, pacemaker marker such as Tbx18, AVE marker (Cerberus, hHex and Dkk1), early endoderm marker (Sox17), DE marker (mCXCR4, mTM4sf2 and GPC), early neural marker Sox2, Sonic Hedgehog Signaling (Shh and Gli1~3), all these relative transcripts were examined during EB differentiation. From all these results, we concluded that MAP3K7 dramatically and consistently causes an increase in markers for the VE and AVE, but does not affect the formation of streak-derived DE.

CHAPTER SIX

SINGLE CELL ANALYSIS OF GENE EXPRESSION DURING MYOCARDIAL DIFFERENTIATION

Introduction:

In this chapter, I will specifically examine the expression of SAN and other cardiac markers in cardiomyocytes. In all of these studies we are examining gene expression in whole EBs and examining markers that are expressed in the heart and endoderm but are also often expressed in other non-cardiac, non-endoderm lineages. Therefore it is sometimes difficult to know whether observed changes are due only changes in the cardiac (or endodermal lineage). To address this we have begun to develop a technique that will allow us to examine gene expression in just the cardiac lineage. Briefly, ES cells harboring the αMHC::GFP promoter reporter are differentiated until day 21 and cardiomyocytes isolated by flow cytometry. From these cells we isolated RNA and then carried out real time PCR for genes expected to be expressed in cardiomyocytes. A number of technical challenges remain to be addressed with this protocol. These data represent promising preliminary data for a new, more accurate assessment of cardiac differentiation in our assay system.

FACS Protocol

EBs were treated with 0.25% Trypsin/EDTA at 37C for 30 minutes and then neutralized with regular differentiation medium. Cells were centrifuged at 2000 rpm for 5

minutes and resuspended with FACS buffer. Then cells were centrifuged again and resuspended with FACS buffer. Cells were filtered through a 100μm sieve and cell numbers were counted using a haemocytometer, checking single cell suspension at the same time. Flow cytometry was performed with the Beckman Coulter MoFlo Astrios EQ cell sorter and data was analyzed using FlowJo VX software (Fig 5.1). Here is the representative analysis of R1 FACS control, R1 and B1 cells. Using two different laser, GFP (488-513_26) and PE (488-576_21) laser, we are able to figure out the real GFP positive cells based on the gate of R1 FACS Control (0.29%), and will figure out R1 αMHC::GFP for 1.12% cardiomyocytes and B1 pTripZ-mTbx5; αMHC::GFP for 3.51% cardiomyocytes. Next, around 20,000 cells were sorted based on this gate.

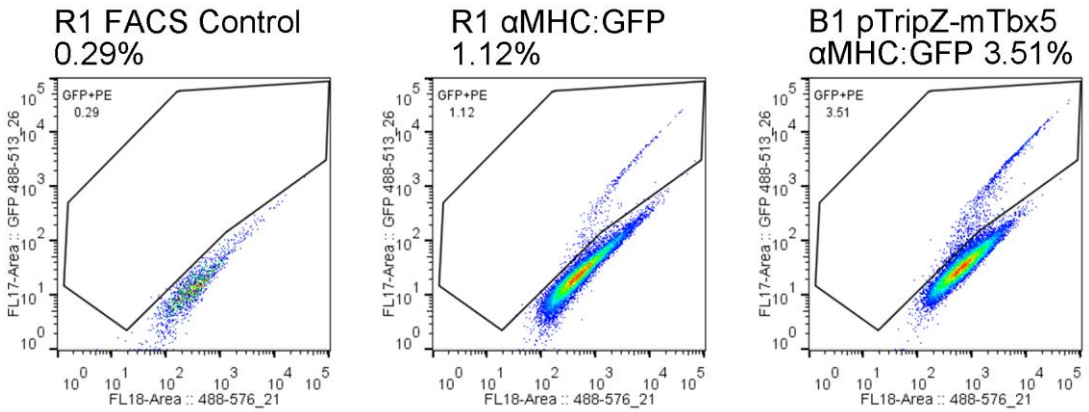

Fig 6.1. Representative Image of FACS analyze data of R1 FACS Control, R1 αMHC::GFP and B1 pTripZ-mTbx5; αMHC::GFP at Day 21.

RNA Isolation and Reverse Transcription

After sorting, 20, 000 (20K) cells from FACS-sorted samples were collected as a cell pellet. The RNeasy Plus Micro Kit (Qiagen, cat#74034) was used as manufacturer's instructions. The RNA concentration and quality was shown in Table 6.1. The ideal RNA A260/A280 is 1.7~2.0. The result of RNA quality was from 0.9~1.37, so the RNA was not in good quality. These data suggest that either the FACS protocol or our RNA isolation technique is not sufficient to generate high quality RNA.

Despite poor 260/280 ratios for isolated RNA we decided to perform reverse transcription of RNA samples to synthesis cDNA. Typically we use 800ng-1ug of RNA/reaction however because of low RNA yields, we decided to input 10 µl of all 8 samples regardless of RNA concentration and then adjust the concentrations of the all 8 cDNAs during the PCR reaction as shown in Table 6.2. Finally, 8.1ng cDNA per PCR reaction was added. (We typically add, 40ng of cDNA, for each PCR reaction.) As a result, the mean Cross Point (CP) and CP Error calculated automatically from PCR Machine were shown in Table 6.3.

Date	No	Name	260/280	ng/µl	Input	Water
FACS SORT 20K RNA	1	R1-2 D19#3	0.9	33.174	10.0	4.4
	2	R1-2 Dox D19#3	1.37	6.574	10.0	4.4
	3	B1 D19#3	1.02	72.39	10.0	4.4
	4	B1 Dox D19#3	1.1	96.71	10.0	4.4
	5	R1-2 D21#3	1.14	12.654	10.0	4.4
	6	R1-2 Dox D21#3	1.13	4.028	10.0	4.4
	7	B1 D21#3	1.01	105.26	10.0	4.4
	8	B1 Dox D21#3	1.35	-3.496	10.0	4.4

Table 6.1. RNA concentration of FACS-sorted samples.

	No	Name	260/280	ng/µL	Input	Water	ng/reaction
FACS SORT 20K cDNA	1	R1-2 D19#3	1.65	14.51524	13.4	10.6	8.1
	2	R1-2 Dox D19#3	1.77	11.86512	16.4	7.6	8.1
	3	B1 D19#3	1.72	16.54216	11.7	12.3	8.1
	4	B1 Dox D19#3	1.71	20.1818	9.6	14.4	8.1
	5	R1-2 D21#3	1.75	11.64244	16.7	7.3	8.1
	6	R1-2 Dox D21#3	1.68	16.46996	11.8	12.2	8.1
	7	B1 D21#3	1.76	8.58344	22.6	1.4	8.1
	8	B1 Dox D21#3	1.78	8.09096	24.0	0.0	8.1

Table 6.2. cDNA concentration of FACS-sorted samples.

No	Name	Mean CP	CP Error
1	R1-2 D19#3	26.104	0.112361
2	R1-2 Dox D19#3	25.454	0.149497
3	B1 D19#3	23.892	0.017546
4	B1 Dox D19#3	24.219	0.170053
5	R1-2 D21#3	23.448	0.305958
6	R1-2 Dox D21#3	22.026	0.109814
7	B1 D21#3	22.253	0.436087
8	B1 Dox D21#3	23.896	0.06666

Table 6.3. Mean CP and CP Error collected from PCR machine.

To test the relative transcripts of pacemaker marker like HCN4, Shox2, Tbx3, and Isl1, or ventricular marker such as Cx43, qRT-PCR experiments were performed to analysis the difference between R1 vs R1 Dox-treated cells , or R1 vs B1 cells , or R1 vs B1 Dox-treated cells or B1 vs B1 Dox-treated cells. As shown in Fig 6.2A and Fig 6.2B, the batch-to-batch variation between these three trials is so huge. From this, we conclude that our input cDNA is outside of the dynamic range of the Roche Lightcycler real time PCR machine. Each bar (Fig 6.2A and Fig 6.2B) represented a single independent trial from PCR data. At the same time, the range of error bars mean the challenges of artificial effect. All different markers were compared, however these was no significant difference among all five markers. As discussed, we decided to normalize the expression of each gene in a given trial to the value in R1 untreated cardiac cells to get an idea of overall changes of gene expression (Fig 6.3A and Fig 6.3B). The relative HCN4 expression of R1 cardiac cells is much more than B1 group at Day 19 and R1 had much more Isl1 expression than both B1 and B1 Dox-treated group. Meanwhile, at Day 21, B1 Dox-treated cardiac cells had more Shox2 and Tbx3 relative expression than R1 untreated group. Taken together, it is very hard to interpret the transcripts data.

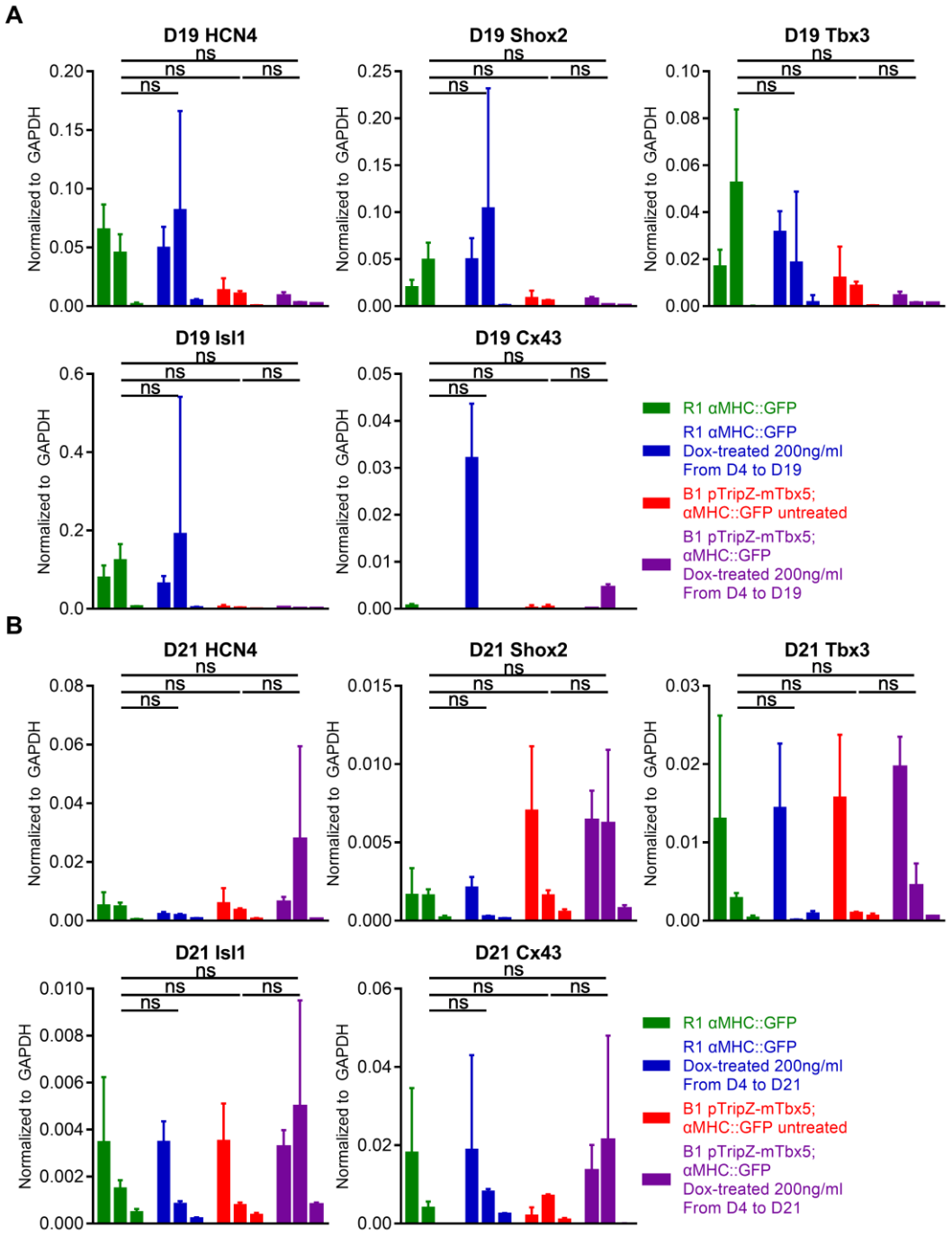

Fig 6.2 HCN4, Shox2, Tbx3, Isl1, Cx43 relative transcription were assessed by qRT-PCR for Day 19 cardiac cell (Fig 6.2A) and Day 21 cardiac cell (Fig 6.2B). Data represent means ± standard error of 3 independent experiments. Statistical significance was determined by unpaired, two-tailed t-test.

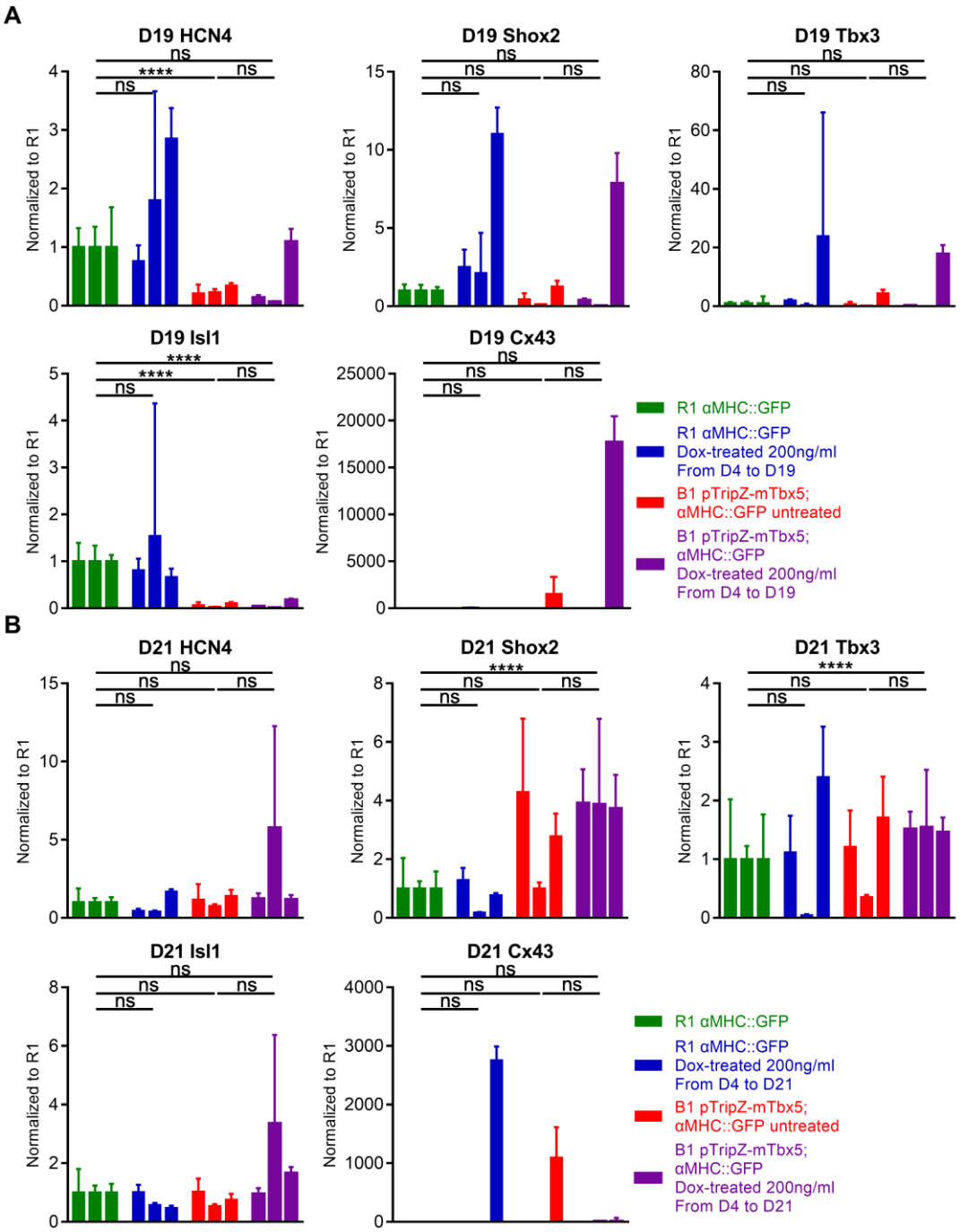

Fig 6.3 HCN4, Shox2, Tbx3, Isl1, Cx43 normalized transcription were assessed by qRT-PCR for Day 19 cardiac cell (Fig 6.3A) and Day 21 cardiac cell (Fig 6.3B). Data represent means ± standard error of 3 independent experiments. Each trial is normalized to R1 untreated cells. Statistical significance was determined by unpaired, two-tailed t-test. ***p<0.001, ****p<0.0001

Discussion

There are still a few challenges from this protocol, especially RNA quality from FACS sorted cells. Here are several improvements we will need: 1) Collect 30,000 cardiac cells instead of 20,000 cells; 2) Improve RNA Isolation Protocol to generate fairly well good RNA quality; 3) Strengthen the capability of PCR protocol to eliminate standard error of each individual trial.

CHAPTER SEVEN

DESIGN AND VERIFICATION OF OVEREXPRESSION LINES

Introduction:

In this chapter, I will show data verifying gene overexpression in both the Tbx5 and other overexpression cell lines. Vincent Christofells has described a transcriptional hierarchy that directs the differentiation if sinoatrial node cells in the mouse embryo. The major transcription factors involved are: Tbx3, Isl1, Shox2, Tbx18 and MAP3K7/TAK1 (Fig 7.1) [107, 141]. To study their function in directing SAN differentiation we made ES cell lines that will allow us to conditionally overexpress these factors. One of these lines (B1, which overexpressed Tbx5) is described in Chapter 4. Detailed information of each individual mESC that I produced is discussed here (Table 7.1).

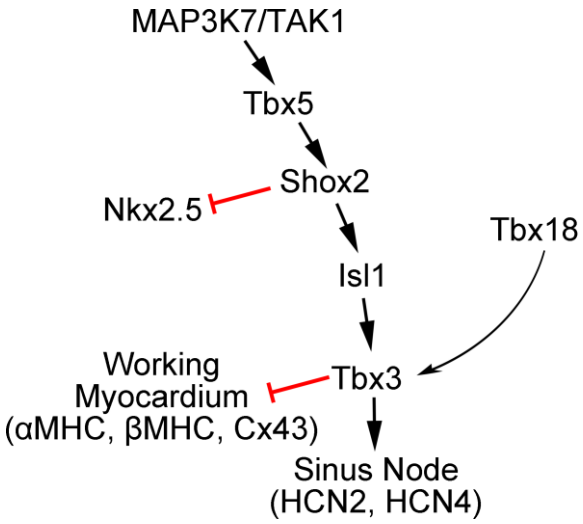

Fig 7.1. Proposed model of SAN differentiation in MAP3K7/TAK1 Paper.

No	Vector	Insert Gene	mESCs
1	pTripZ	mTbx3	X1, X6, X13
2	pTET-ON	mTbx3	DX5, DX9
3	pTripZ	hIsl1	I4
4	pTET-ON	hIsl1	DI1, DI2, DI3, DI7
5	pTripZ	hShox2	S2
6	pTET-ON	hShox2	DS13, DS14
7	pTripZ	hTbx18	T2
8	pTET-ON	hTbx18	DT2, DT5
9	pTripZ	MAP3K7	M8
10	pTET-ON	MAP3K7	DM11
11	pTET-ON	mTbx5	DB4, DB6

Table 7.1. List of cell lines discussed in this chapter.

Independent clonal lines that conditionally overexpress Tbx3 were established.

To test the role of Tbx3 in SAN development, mouse embryonic stem cell (mESC) lines were generated to conditionally overexpress it by addition of doxycycline. To do this, the open reading frame (ORF) of Tbx3 was cloned downstream of the TurboRFP motif into the pTripZ vector. This was used to generate lentivirus and used to transduce wild type ES cells. (Fig 7.2A). Another design is to clone Tbx3 ORF into downstream of pTight TET-Responsive promoter into the pTET-ON vector (Fig 7.3A), which drives expression of the insert GOI with administration of doxycycline.

These vectors can be used to conditionally overexpress all of the key transcriptional regulators of SAN differentiation. Genetic studies in mouse have revealed an essential role for Tbx3 in establishing the SAN [119, 148]. However, it has not been shown whether Tbx3 is sufficient for SAN differentiation. To study its role we established six independent, clonal ESC lines (X1, X6, X8, X9, X11, X13), three of these, X1, X6, X13, showed stable upregulation of Tbx3 transcripts in an inducible fashion, as assessed by qRT-PCR at 24, 48 and 72 hours after addition of doxycycline (1 µg /mL) (Fig 7.2B). Other clonal mESC lines (DX2, DX3, DX4, DX5, DX6, DX7, DX8 and DX9), two of these,DX5, DX9, showed stable upregulation of Tbx3 transcripts as described above (Fig 7.3B). To test the best GOI-inducible dose, DX5, DX9 mESCs were treated with doxycycline at 200ng/ml, 400ng/ml and 800ng/ml and then collected after 48 hours (Fig 7.3C). Later qRT-PCR was performed to detect relative expression of Tbx3. DX5 showed upregulation of Tbx3 expression at dose 400ng/ml, while DX9 showed downregulation of Tbx3 expression at dose 400ng/ml. DX5 will be used for future study.

A. Addition of Doxycycline increased beat rate in X1 X6 EBs

One indication that cardiac cells have adopted the SAN identity, is an increase rate of beating speed. To determine if any of our mESCs could differentiate towards SAN cells in response to increased expression of Tbx3. mESCs were differentiated as EBs and doxycycline added from Day 2 to Day 16 at which point beat rate data was collected and assessed. X1, X6 EBs were tested for increased beat rate with working dose curve of doxycycline (Fig 7.2C). Beating areas were identified based on visual inspection and confirmed by expression of αMHC::GFP. Beat was manually calculated but visual inspection counting beats/minute. Lines X1 showed a modest increase in beat rate at 200 ng/ml. Line X6 showed significant increase in beat rate at 100ng/ml, 200ng/ml and 500ng/ml. For this reason, line X1 and X6 were used for all subsequent evaluation.

B. Relative Tbx3 RNA Expression during EB differentiation

Although addition of Dox worked well in X1 and X6 mESCs, regulation of gene expression within differentiating EBs is much more complicated. To test whether addition of Dox also upregulated Tbx3 transcripts during EB differentiation, EBs were collected from Day 1 to Day 11 and assessed Tbx3 transcription by qRT-PCR (Fig 7.4).

Interestingly, X1 EBs showed a modest increase of Tbx3 transcripts without doxycycline compared to parent R1 cell line, while X6 EBs showed the similar level of Tbx3 expression. X1 Dox-treated EBs only showed increased Tbx3 expression at Day 3 and the same for Day 5 to D11 compared to X1 untreated EBs, while X6 Dox-treated EBs showed increased Tbx3 expression at Day 5, Day 7 and Day 9. For this reason, line X6 was used for future analysis.

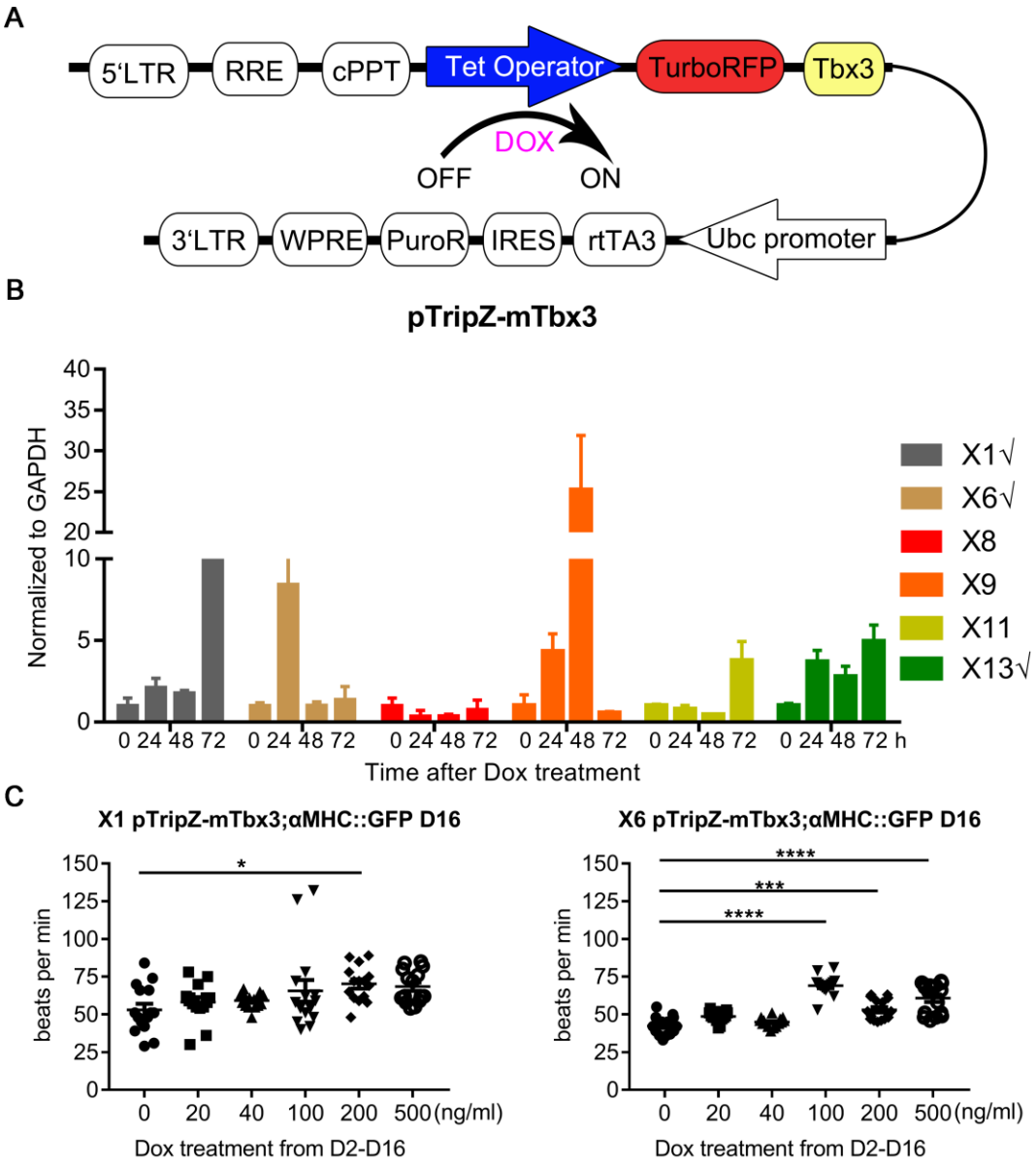

Fig 7.2. Verification of X1, X6 pTripZ-mTbx3; αMHC::GFP mouse embryonic stem cell line. Fig 7.2A. Schematic design of pTripZ-mTbx3 Vector, doxycycline-inducible-Tbx3-overexpression backbone. Fig 7.2B. X1, X6, X8, X9, X11, X13 mESCs were treated with doxycycline at 1 μg /mL and then collected after 0, 24, 48, 72h. Later qRT-PCR was performed to detect relative expression of Tbx3. Fig 7.2C. Manual beat data counting of X1, X6 EBs at Day 16 with Doxycycline dose of 0ng/ml, 20ng/ml, 40ng/ml, 100ng/ml, 200ng/ml and 500ng/ml. Data represent means ± standard error of 3 independent experiments. Statistical significance was determined by one-way ANOVA. *p<0.05, ***p<0.001, ****p<0.0001.

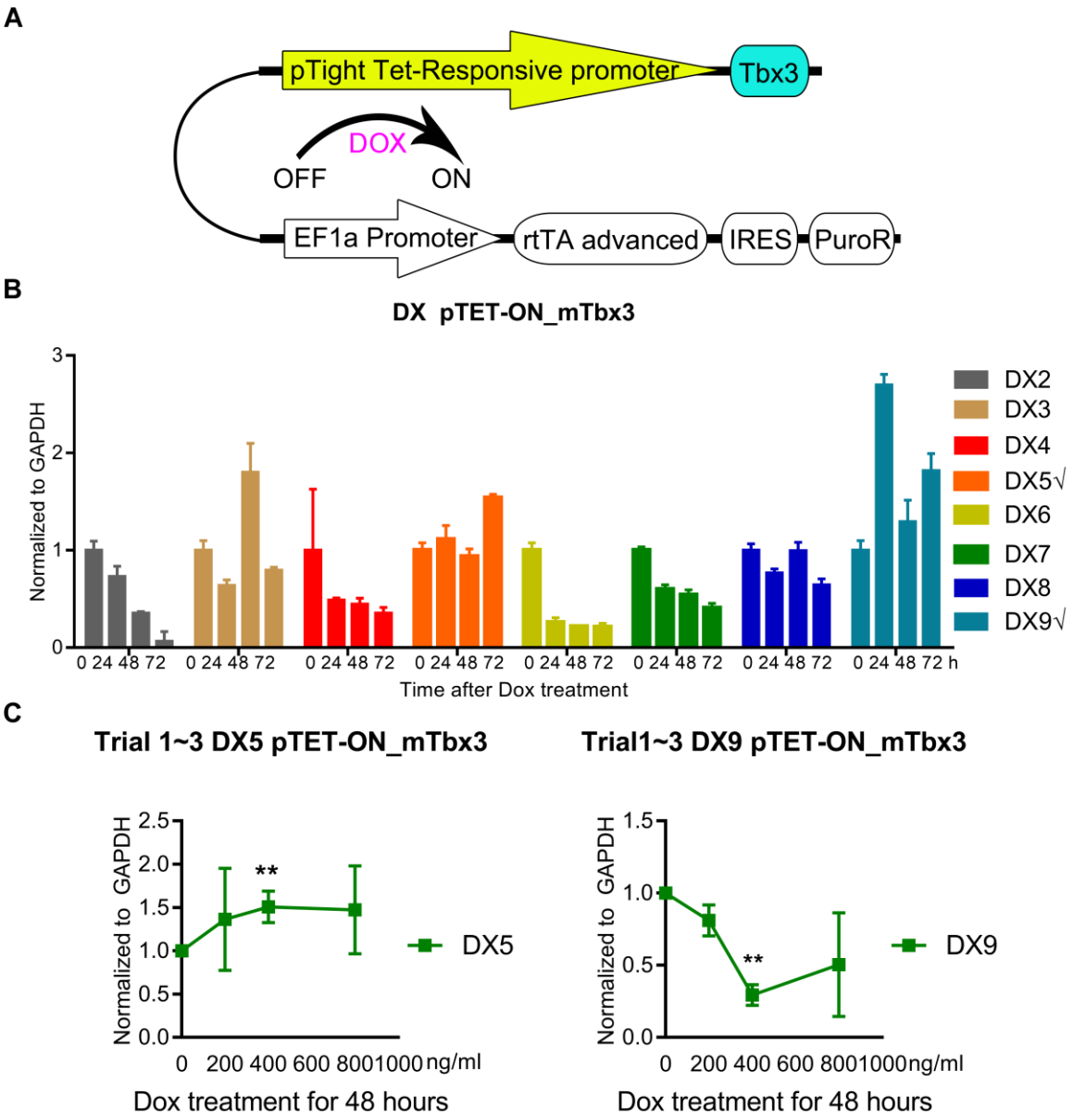

Fig 7.3. Verification of DX5, DX9 pTET-ON-mTbx3; αMHC::GFP mouse embryonic stem cell line. Fig 7.3A. Schematic design of pTET-ON-mTbx3 Vector, doxycycline-inducible-Tbx3-overexpression backbone. Fig 7.3B. DX2, DX3, DX4, DX5, DX6, DX7, DX8 and DX9 mESCs were treated with doxycycline at 1 μg /mL and then collected after 0, 24, 48, 72h. Later qRT-PCR was performed to detect relative expression of Tbx3. Fig 7.3C. DX5, DX9 mESCs were treated with doxycycline at 0ng/ml, 200ng/ml, 400ng/ml and 800ng/ml and then collected after 48 hours. Later qRT-PCR was performed to detect relative expression of Tbx3. Data represent means ± standard error of 3 independent experiments. Statistical significance was determined by unpaired, two-tailed t-test. **p<0.01.

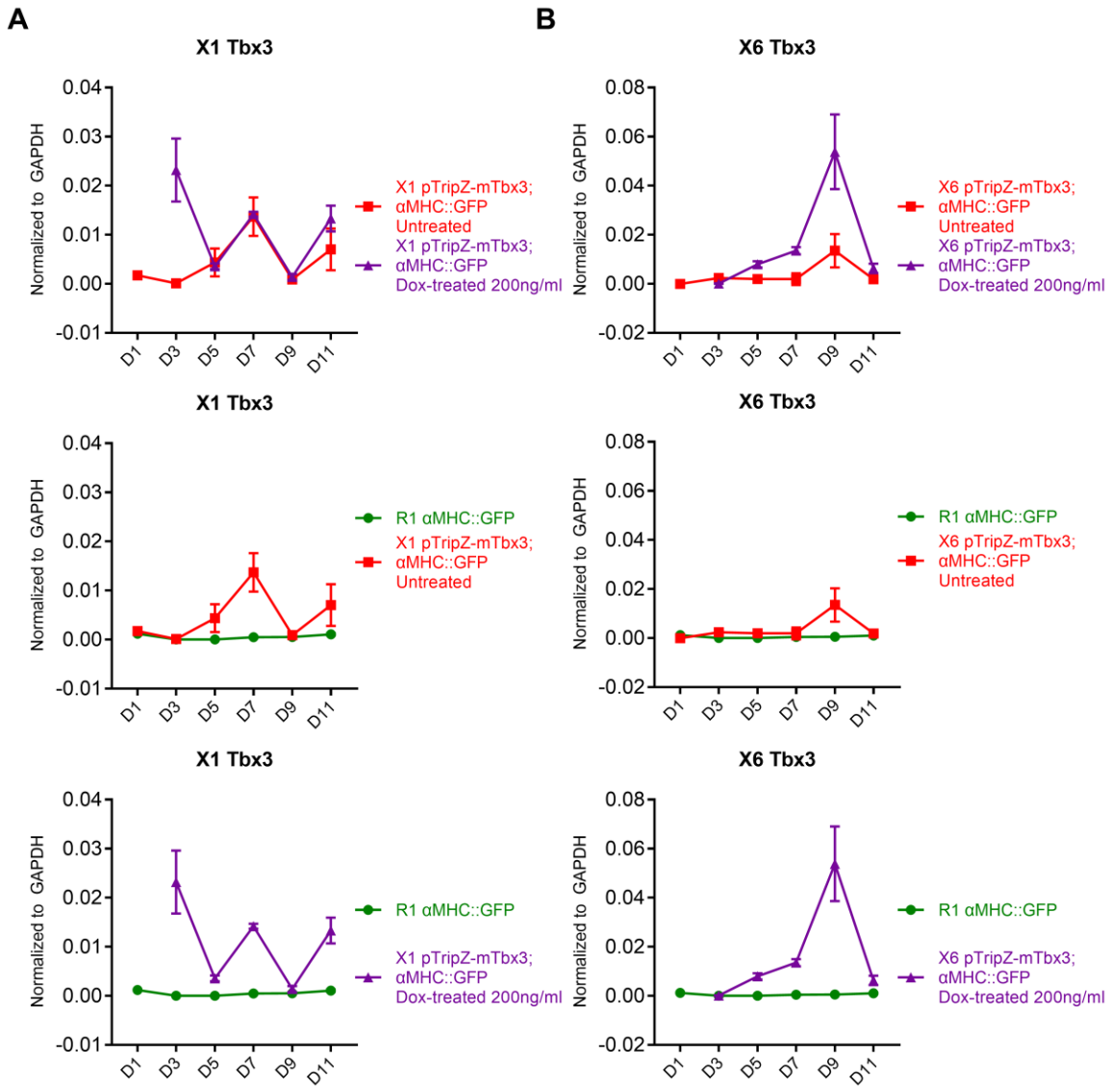

Fig 7.4. Relative Tbx3 expression during EB differetiation. EBs were collected from Day 1 to Day 11 and assessed Tbx3 transcription by qRT-PCR among X1 Dox-treated or untreated EBs and R1 EBs (Fig 7.4A) and among X6 Dox-treated or untreated EBs and R1 EBs (Fig 7.4B). Data represent means ± standard error of one independent experiment.

Independent clonal line that conditionally overexpress hIsl1 was established.

To test the role of Isl1 in SAN development, mESC lines were generated to conditionally overexpress hIsl1. To do this, the open reading frame of hIsl1 was cloned downstream of the TurboRFP motif into the pTripZ vector. This was used to generate lentivirus in which GOI can be overexpressed by the administration of Doxycycline (Fig 7.5A). Another design is to clone Isl1 ORF into downstream of pTight TET-Responsive promoter into the pTET-ON vector (Fig 7.6A), which drives expression of the insert GOI with administration of Doxycycline.

These vectors can be used to conditionally overexpress all of the key transcriptional regulators of SAN differentiation. Downstream of this cascade is Isl1. Genetic studies in mouse have revealed an essential role for Isl1 in establishing the SAN [149, 150]. However, it has not been shown whether Isl1 is sufficient for SAN differentiation. To study its role we established five independent, clonal ESC lines (I2, I3, I4, I5, I6), only I4 showed stable upregulation of Isl1 transcripts in an inducible fashion, as assessed by qRT-PCR at 24, 48 and 72 hours after addition of doxycycline (1 μg /mL) (Fig 7.5B). Other clonal mESC lines (DI1, DI2, DI3, DI4, DI6 and DI7), two of all DI1, DI3 showed stable upregulation of Isl1 transcripts as described above (Fig 7.6B). To test the best GOI-inducible dose, DI1, DI3 mESCs were treated with doxycycline at 0ng/ml, 50ng/ml, 100ng/ml and 200ng/ml and then collected after 48 hours (Fig 7.6C). Later qRT-PCR was performed to detect relative expression of Isl1. Both DI1 and DI3 did not show upregulation of Isl1. Other potential cell lines (DI2 and DI7) will be tested in the future study.

A. Addition of Doxycycline increased beat rate in I4 EBs

One indication that cardiac cells have adopted the SAN identity, is an increase rate of beating speed. To determine if any of our mESCs could differentiate towards SAN cells in response to increased expression of Isl1. mESCs were differentiated as EBs and doxycycline added from Day 2 to Day 16 at which point beat rate data was collected and assessed. I4 EBs were tested for increased beat rate with working dose curve of doxycycline (Fig 7.5C). Beating areas were identified based on visual inspection and confirmed by expression of αMHC::GFP. Beat was manually calculated but visual inspection counting beats/minute. Lines I4 showed a modest increase in beat rate at 500 ng/ml. For this reason, line I4 was used for all subsequent evaluation.

B. Relative Isl1, Tbx5, Tbx3, Nkx2.5 RNA Expression during EB differentiation

Although addition of Dox worked well in I4 mESCs, regulation of gene expression within differentiating EBs is much more complicated. To test whether addition of Dox also upregulated Isl1 transcripts during EB differentiation, EBs were collected from Day 1 to Day 16 and assessed Isl1, Tbx5, Tbx3, Nkx2.5 transcription by qRT-PCR (Fig 7.7). Interestingly, I4 Dox-treated EBs showed increase Isl1 expression at Day 2, Day 5, Day 6 and Day 8 compared to I4 untreated EBs. Then I4 Dox-treated EBs showed four pulses of Tbx5 upregulation at Day 6, 8, 10 and 13; one pulse of Tbx3 upregulation at Day 6; two pulses of Nkx2.5 upregulation at Day 8 and 13. For this experiment only one trial is included, further data will be collected and analyzed.

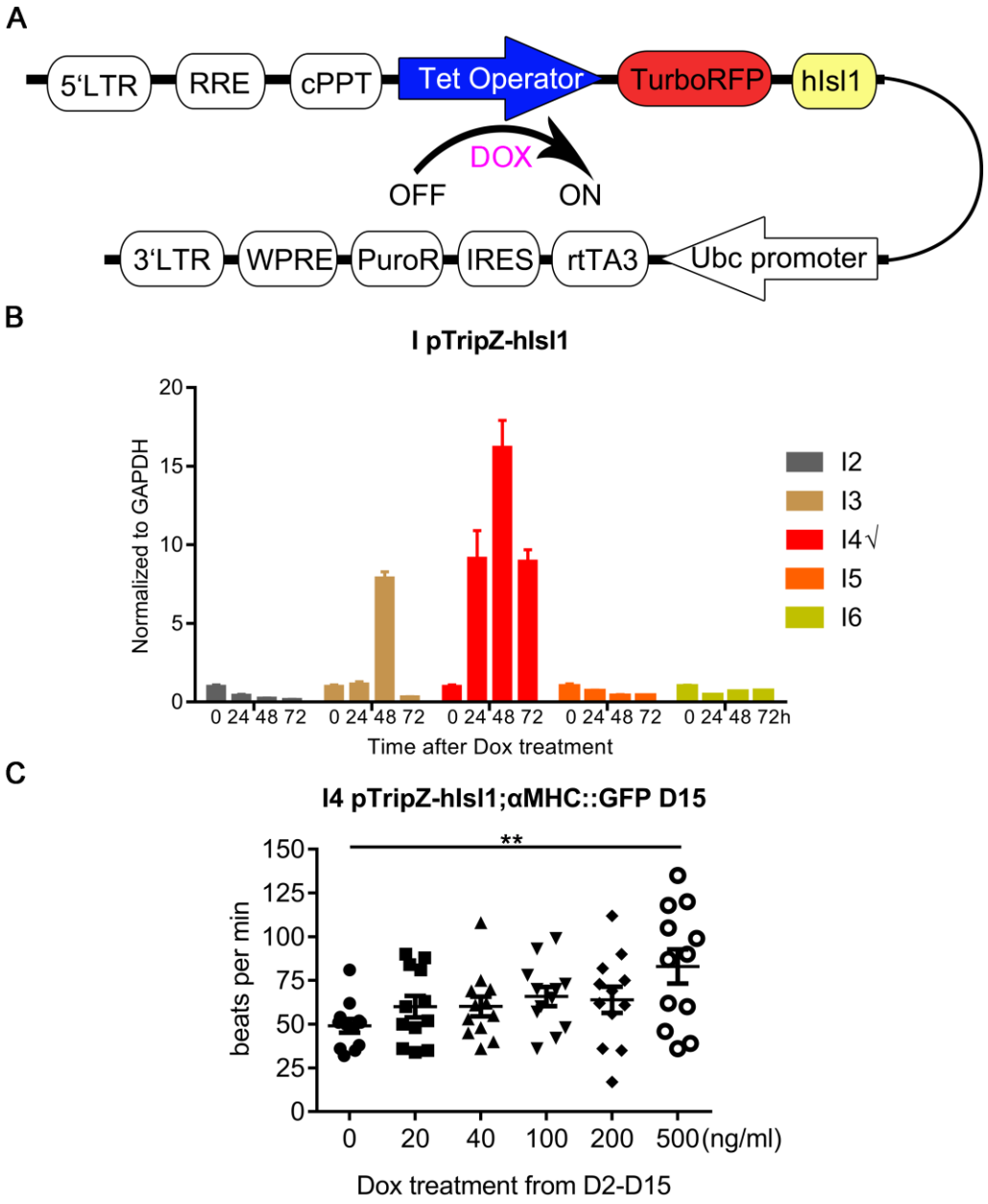

Fig 7.5. Verification of I4 pTripZ-hIsl1; αMHC::GFP mouse embryonic stem cell line. Fig 7.5A. Schematic design of pTripZ-hIsl1 Vector, doxycycline-inducible-Isl1-overexpression backbone. Fig 7.5B. I2, I3, I4, I5 and I6 mESCs were treated with doxycycline at 1 μg /mL and then collected after 0, 24, 48, 72h. Later qRT-PCR was performed to detect relative expression of Isl1. Fig 7.5C. Manual beat data counting of I4 EBs at Day 15 with Doxycycline dose of 0ng/ml, 20ng/ml, 40ng/ml, 100ng/ml, 200ng/ml and 500ng/ml. Data represent means ± standard error of 3 independent experiments. Statistical significance was determined by one-way ANOVA. **p<0.01.

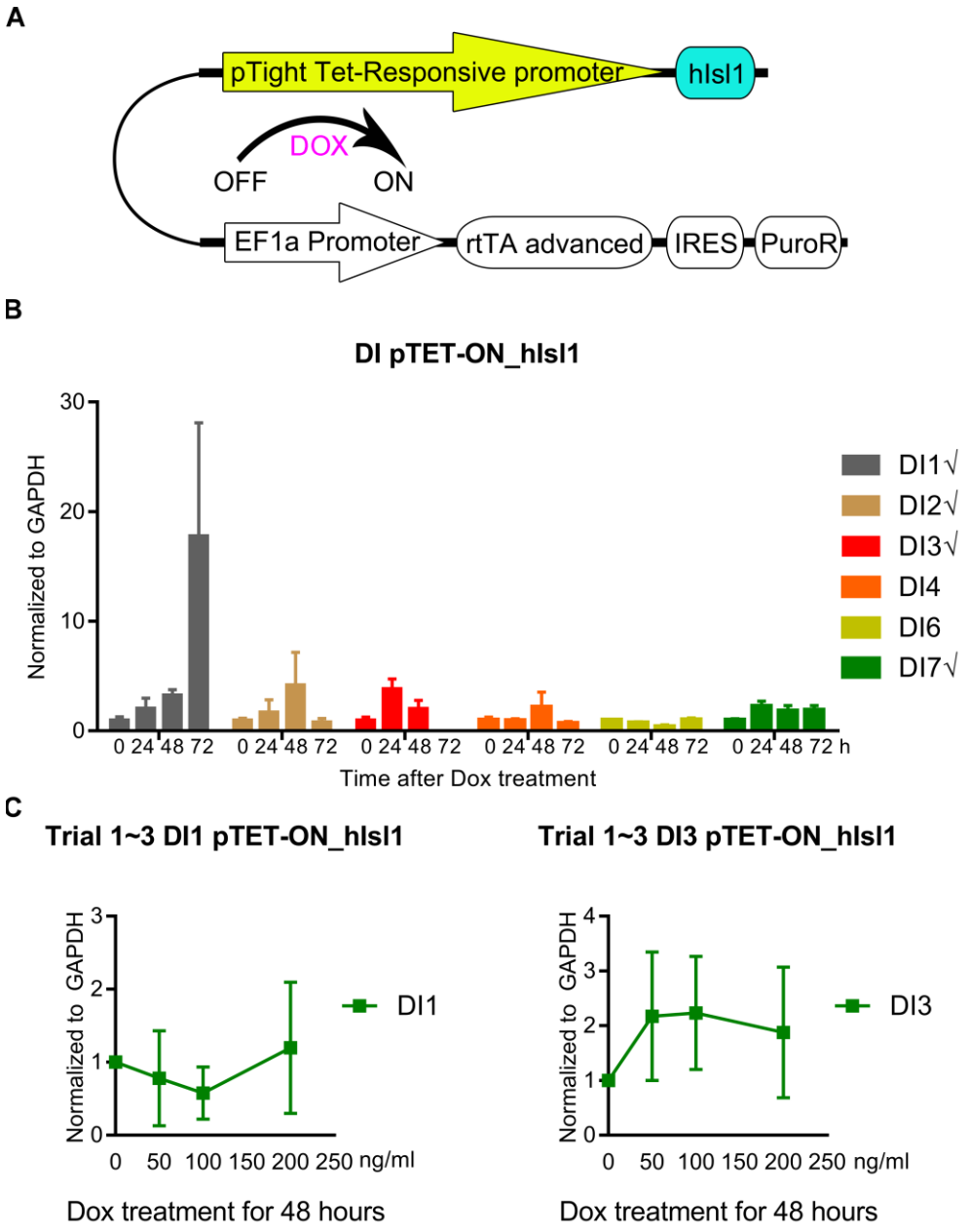

Fig 7.6. Verification of DI1, DI3 pTET-ON-hIs1; αMHC::GFP mouse embryonic stem cell line. Fig 7.6A. Schematic design of pTET-ON- hIs1 Vector, doxycycline-inducible-Is1-overexpression backbone. Fig 7.6B. DI1, DI2, DI3, DI4, DI6 and DI7 mESCs were treated with doxycycline at 1 µg /mL and then collected after 0, 24, 48, 72h. Later qRT-PCR was performed to detect relative expression of Is1. Fig 7.6C. DI1, DI3 mESCs were treated with doxycycline at 0ng/ml, 50ng/ml, 100ng/ml and 200ng/ml and then collected after 48 hours. Later qRT-PCR was performed to detect relative expression of Is1. Data represent means ± standard error of 3 independent experiments. Statistical significance was determined by unpaired, two-tailed t-test.

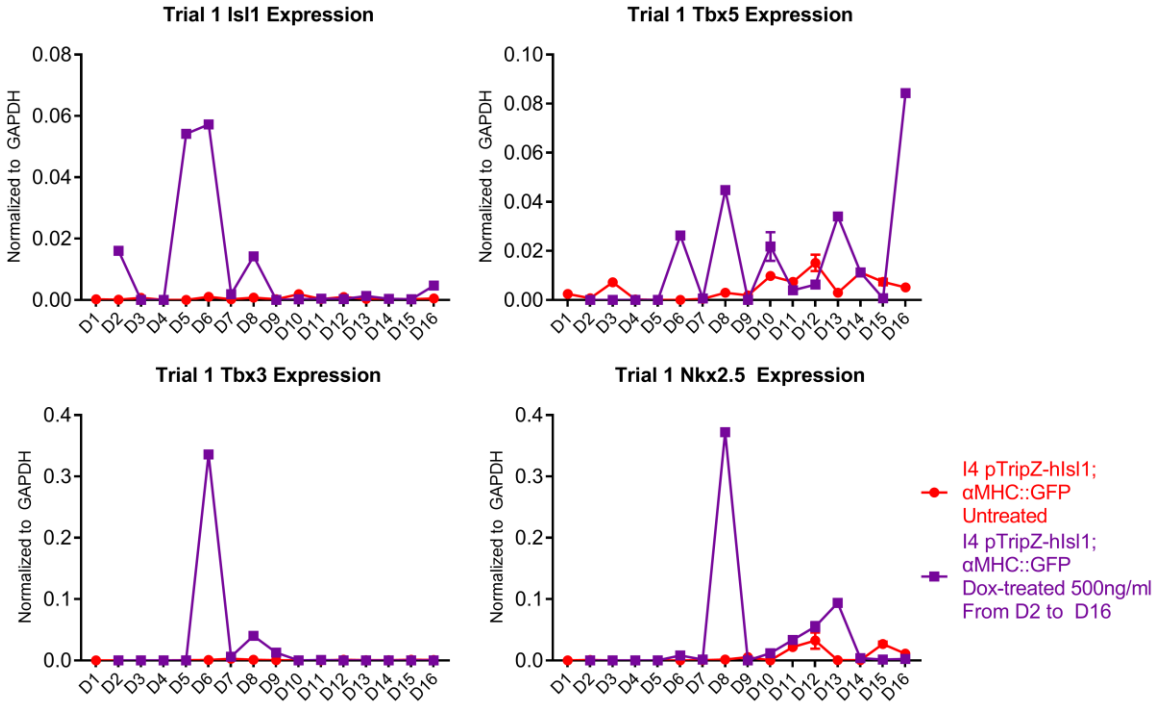

Fig 7.7. Relative Isl1, Tbx5, Tbx3, Nkx2.5 expression during EB differetiation. EBs were collected from Day 1 to Day 16 and assessed Tbx3 transcription by qRT-PCR between I4 Dox-treated or I4 untreated EBs (Fig 7.7). Data represent means ± standard error of one independent experiments.

Independent clonal line that conditionally overexpress hShox2 was established.

To test the role of Shox2 in SAN development, mESC lines were generated to conditionally overexpress hShox2. To do this, the open reading frame of hShox2 was cloned downstream of the TurboRFP motif into the pTripZ vector. This was used to generate lentivirus in which GOI can be overexpressed by the administration of Doxycycline (Fig 7.8A). Another design is to clone Shox2 ORF into downstream of pTight TET-Responnsive promoter into the pTET-ON vector (Fig 7.9A), which drives expression of the insert GOI with administration of Doxycycline.

Genetic studies in mouse have revealed an essential role for Shox2 in establishing the SAN [113, 151, 152]. However, it has not been shown whether Shox2 is sufficient for SAN differentiation. To study its role we established six independent, clonal ESC lines (S1, S2, S7, S10, S14 and S16), only S2 showed stable upregulation of Shox2 transcripts in an inducible fashion, as assessed by qRT-PCR at 24, 48 and 72 hours after addition of doxycycline (1 μg /mL) (Fig 7.8B). Other clonal mESC lines (DS13, DS14), both showed stable upregulation of Shox2 transcripts as described above (Fig 7.9B). To test the best GOI-inducible dose, DS13 and DS14 mESCs were treated with doxycycline at 0ng/ml, 50ng/ml, 100ng/ml and 200ng/ml and then collected after 48 hours (Fig 7.9C). Later qRT-PCR was performed to detect relative expression of Shox2. DS13 showed downregulation of Shox2 at dose 200ng/ml, while DS14 showed upregulation of Shox2 at dose 50ng/ml. DS14 will be used in the future study.

A. Addition of Doxycycline did not increase beat rate in S2 EBs

One indication that cardiac cells have adopted the SAN identity is an increase rate of beating speed. To determine if any of our mESCs could differentiate towards SAN cells in response to increased expression of Shox2. mESCs were differentiated as EBs and doxycycline added from Day 2 to Day 16 at which point beat rate data was collected and assessed. S2 EBs were tested for increased beat rate with working dose curve of doxycycline (Fig 7.8C). Beating areas were identified based on visual inspection and confirmed by expression of αMHC::GFP. Beat was manually calculated but visual inspection counting beats/minute. Line S2 with administration of Dox did not increase beat rate at either Day 15 or Day 16. In our model, S2 may not be the best choice for future study.

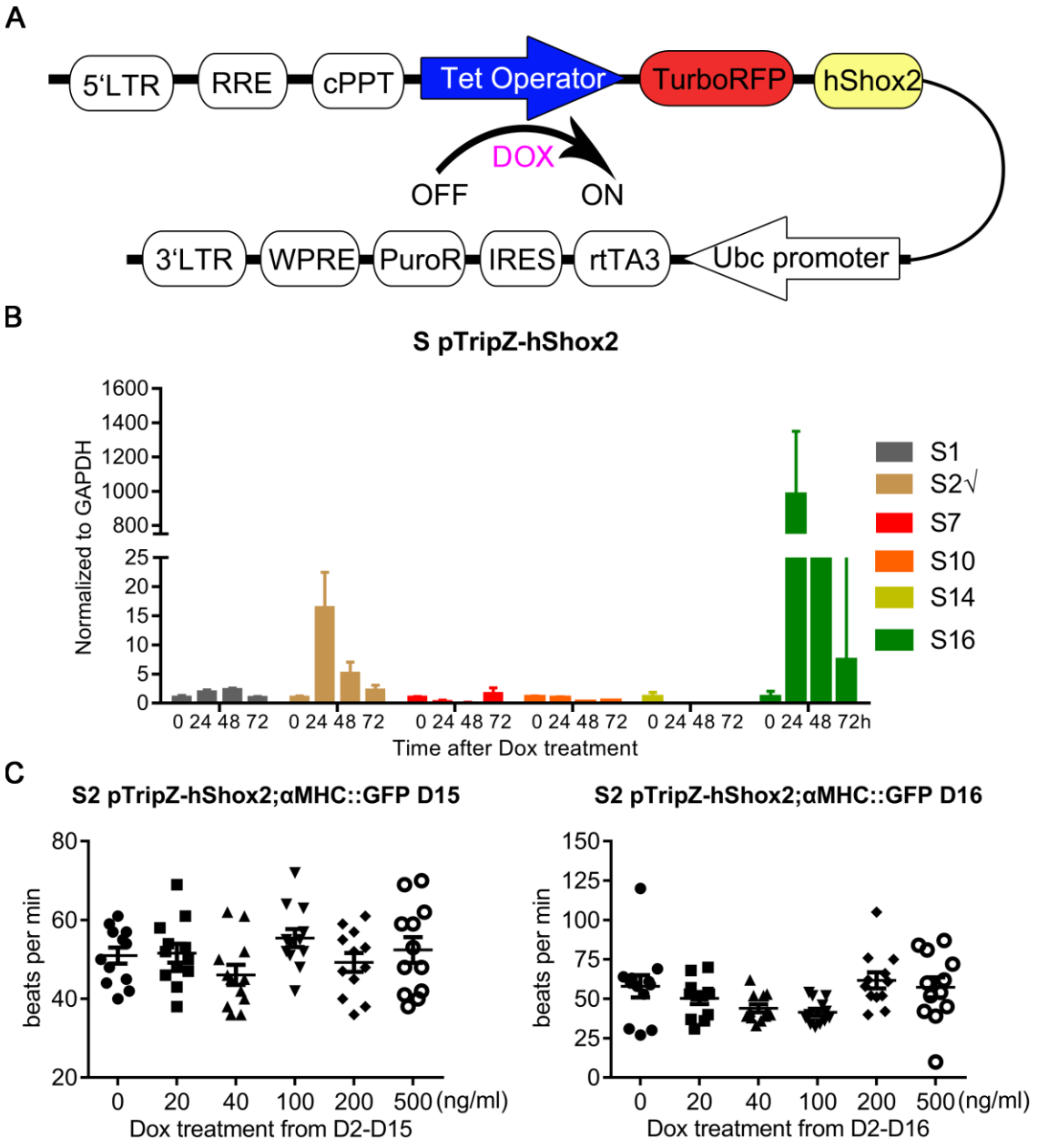

Fig 7.8. Verification of S2 pTripZ-hShox2; αMHC::GFP mouse embryonic stem cell line. Fig 7.8A. Schematic design of pTripZ-hShox2 Vector, doxycycline-inducible-Shox2-overexpression backbone. Fig 7.8B. S1, S2, S7, S10, S14 and S16 mESCs were treated with doxycycline at 1 μg /mL and then collected after 0, 24, 48, 72h. Later qRT-PCR was performed to detect relative expression of Isl1. Fig 7.8C. Manual beat data counting of S2 EBs at Day 15 or Day 16 with Doxycycline dose of 0ng/ml, 20ng/ml, 40ng/ml, 100ng/ml, 200ng/ml and 500ng/ml. Data represent means ± standard error of 3 independent experiments. Statistical significance was determined by one-way ANOVA.

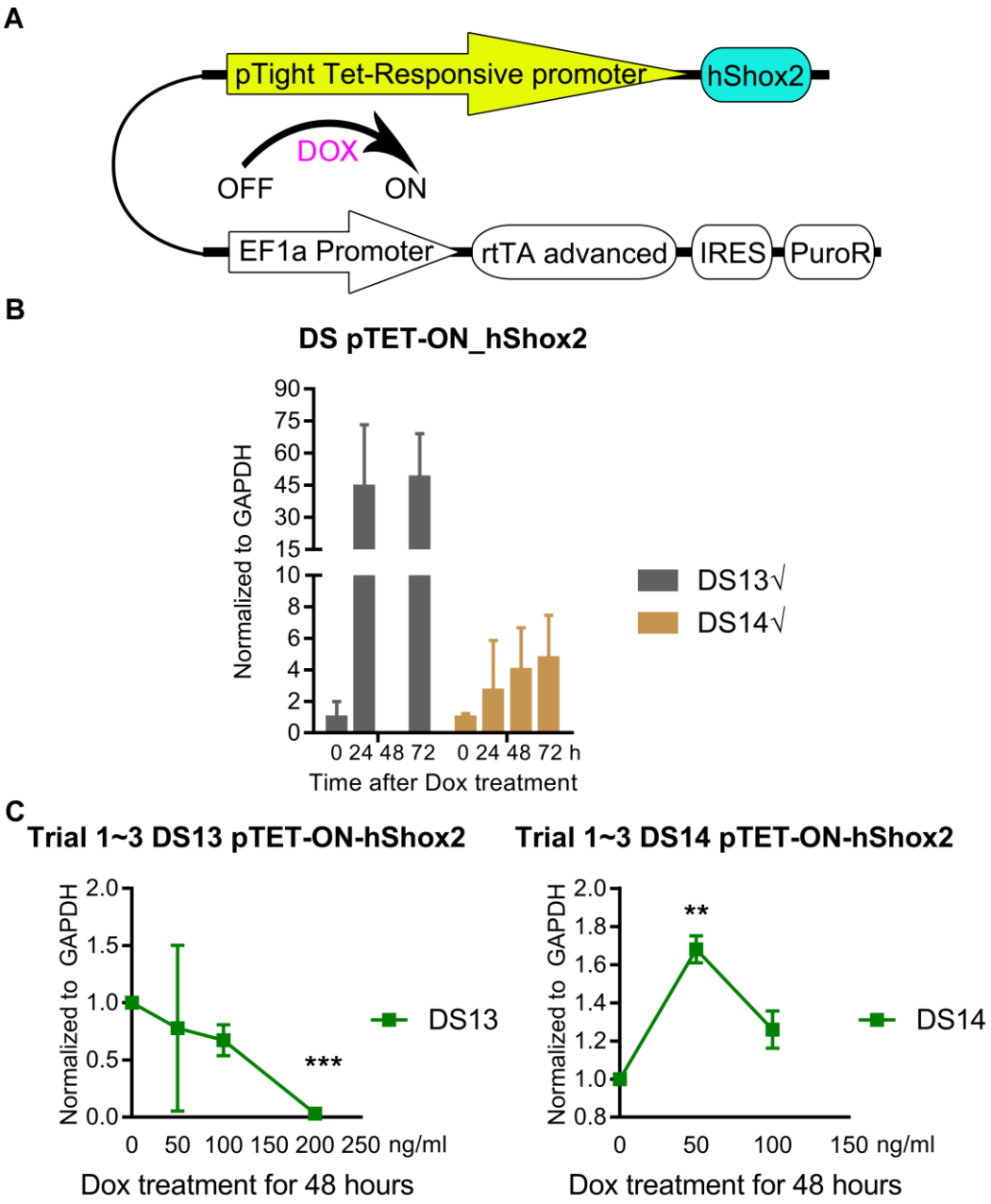

Fig 7.9. Verification of DS13, DS14 pTET-ON-hShox2; αMHC::GFP mouse embryonic stem cell line. Fig 7.9A. Schematic design of pTET-ON-hShox2 Vector, doxycycline-inducible-Shox2-overexpression backbone. Fig 7.9B. DS13 and DS14 mESCs were treated with doxycycline at 1 μg /mL and then collected after 0, 24, 48, 72h. Later qRT-PCR was performed to detect relative expression of Is1. Fig 7.9C. DS13 and DS14 mESCs were treated with doxycycline at 0ng/ml, 50ng/ml, 100ng/ml and 200ng/ml and then collected after 48 hours. Later qRT-PCR was performed to detect relative expression of Shox2. Data represent means ±standard error of 3 independent experiments. Statistical significance was determined by unpaired, two-tailed t-test. **p<0.01, ***p<0.001.

Independent clonal line that conditionally overexpress hTbx18 was established.

To test the role of Tbx18 in SAN development, mESC lines were generated to conditionally overexpress hTbx18. To do this, the open reading frame of hTbx18 was cloned downstream of the TurboRFP motif into the pTripZ vector. This was used to generate lentivirus in which GOI can be overexpressed by the administration of Doxycycline (Fig 7.10A). Another design is to clone Tbx18 ORF into downstream of pTight TET-Responsive promoter into the pTET-ON vector (Fig 7.11A), which drives expression of the insert GOI with administration of Doxycycline.

These vectors can be used to conditionally overexpress all of the key transcriptional regulators of SAN differentiation. Downstream of Tbx5 is Tbx18. Genetic studies in mouse have revealed an essential role for Tbx18 in establishing the SAN [84, 153-155]. However, it has not been shown whether Tbx18 is sufficient for SAN differentiation. To study its role in SAN differentiation, we established one independent, clonal ESC lines (T2), which showed stable upregulation of Tbx18 transcripts in an inducible fashion, as assessed by qRT-PCR at 24, 48 and 72 hours after addition of doxycycline (1 μg /mL) (Fig 7.10B). Other clonal mESC lines (DT2, DT4, DT5, DT7, DT8, DT9 and DT10), DT2 and DT5 showed stable upregulation of Shox2 transcripts as described above (Fig 7.11B). To test the best GOI-inducible dose, DT2 and DT5 mESCs were treated with doxycycline at 0ng/ml, 200ng/ml, 400ng/ml and 800ng/ml and then collected after 48 hours (Fig 7.11C). Later qRT-PCR was performed to detect relative expression of Tbx18. Both DT2 and DT5 did not show upregulation of Tbx18. Other potential cell lines (DT8, DT9 and DT10) will be tested in the future study.

A. Addition of Doxycycline did increase beat rate in T2 EBs

One indication that cardiac cells have adopted the SAN identity, is an increase rate of beating speed. To determine if any of our mESCs could differentiate towards SAN cells in response to increased expression of Tbx18. mESCs were differentiated as EBs and doxycycline added from Day 2 to Day 16 at which point beat rate data was collected and assessed. T2 EBs were tested for increased beat rate with working dose curve of doxycycline (Fig 7.10C). Beating areas were identified based on visual inspection and confirmed by expression of αMHC::GFP. Beat was manually calculated but visual inspection counting beats/minute. Line T2 showed significant increase at 200ng/ml at Day 15. Line T2 will be used for future study.

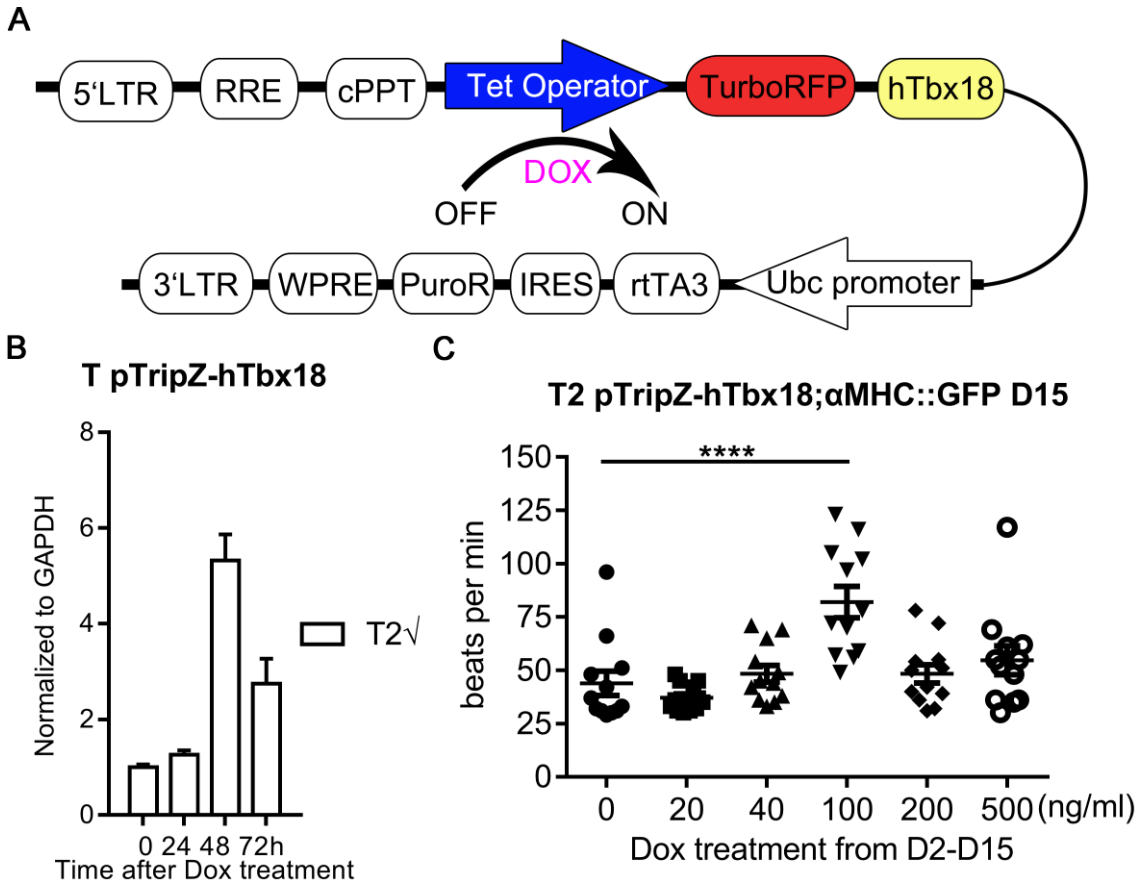

Fig 7.10. Verification of T2 pTripZ-hTbx18; αMHC::GFP mouse embryonic stem cell line. Fig 7.10A. Schematic design of pTripZ-hTbx18 Vector, doxycycline-inducible-Tbx18-overexpression backbone. Fig 7.10B. T2 mESCs were treated with doxycycline at 1 μg /mL and then collected after 0, 24, 48, 72h. Later qRT-PCR was performed to detect relative expression of Isl1. Fig 7.10C. Manual beat data counting of T2 EBs at Day 15 with Doxycycline dose of 0ng/ml, 20ng/ml, 40ng/ml, 100ng/ml, 200ng/ml and 500ng/ml.

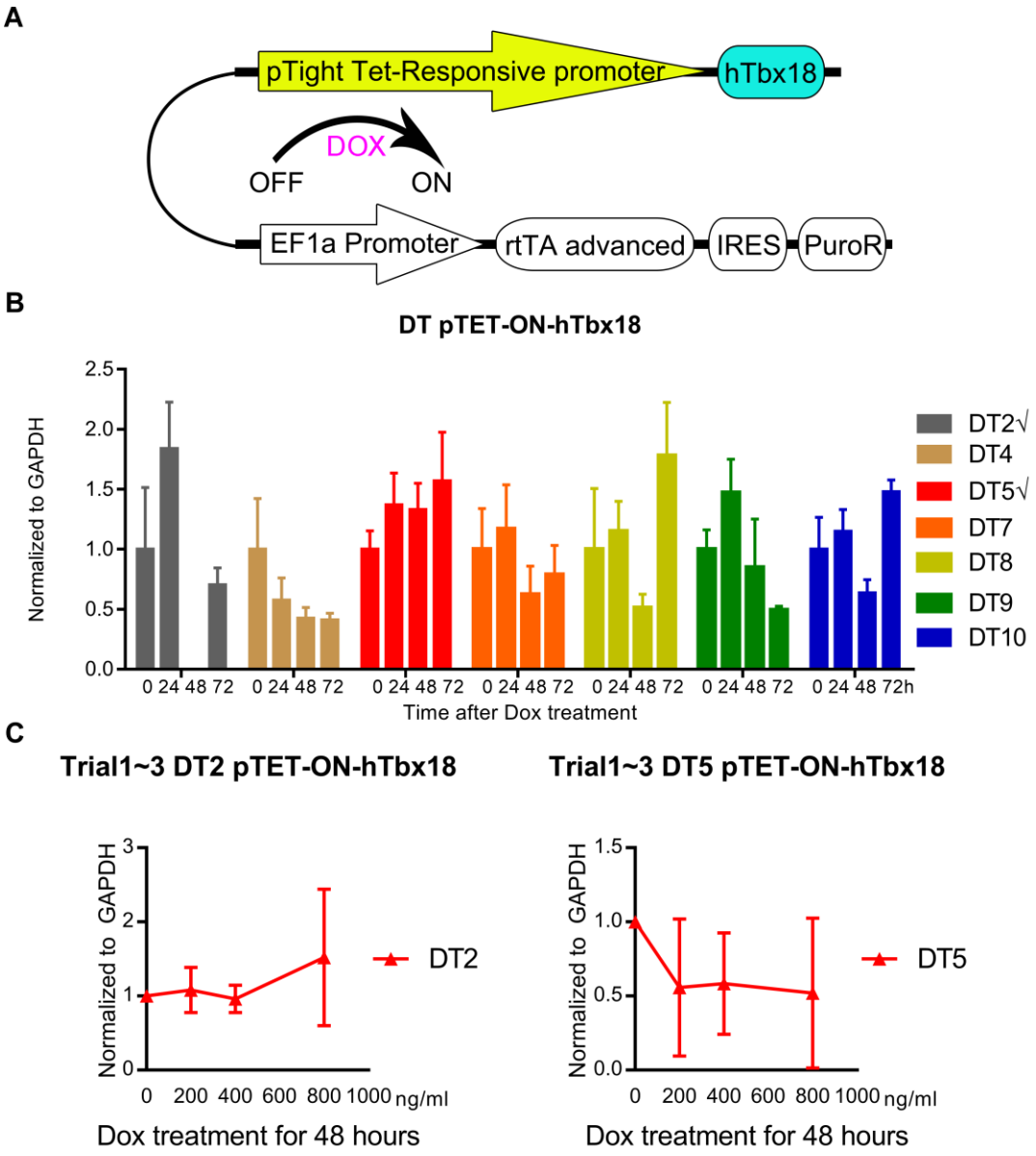

Fig 7.11. Verification of DT2, DT5 pTET-ON-hTbx18; αMHC::GFP mouse embryonic stem cell line. Fig 7.11A. Schematic design of pTET-ON-hTbx18 Vector, doxycycline-inducible-Tbx18-overexpression backbone. Fig 7.11B. DT2, DT4, DT5, DT7, DT8, DT9 and DT10 mESCs were treated with doxycycline at 1 μg /mL and then collected after 0, 24, 48, 72h. Later qRT-PCR was performed to detect relative expression of Tbx18. Fig 7.11C. DT2 and DT5 mESCs were treated with doxycycline at 0ng/ml, 200ng/ml, 400ng/ml and 800ng/ml and then collected after 48 hours. Later qRT-PCR was performed to detect relative expression of Tbx18. Data represent means ± standard error of 3 independent experiments. Statistical significance was determined by unpaired, two-tailed t-test.

Independent clonal lines that conditionally overexpress MAP3K7/TAK1 were established.

To test the role of MAP3K7/TAK1 in SAN development, mESC lines were generated to conditionally overexpress MAP3K7. To do this, the open reading frame of MAP3K7 was cloned downstream of the TurboRFP motif into the pTripZ vector. This was used to generate lentivirus in which GOI can be overexpressed by the administration of Doxycycline (Fig 7.12A). Another design is to clone MAP3K7 ORF into downstream of pTight TET-Responnsive promoter into the pTET-ON vector (Fig 7.13A), which drives expression of the insert GOI with administration of Doxycycline.

These vectors can be used to conditionally overexpress all of the key transcriptional regulators of SAN differentiation. Upstream of Tbx5 is MAP3K7. Genetic studies in mouse have revealed an essential role for MAP3K7 in establishing the SAN [141, 156]. Continuous expression of MAP3K7 directed ES-derived cardiomyocytes into pacemaker fate. However, it has not been shown whether conditional expression of MAP3K7 is sufficient for SAN differentiation. To study its role we established four independent, clonal ESC lines (M8, M10, M11, M14), only M8 which showed stable upregulation of MAP3K7 transcripts in an inducible fashion, as assessed by qRT-PCR at 24, 48 and 72 hours after addition of doxycycline (1 μg /mL) (Fig 7.12B). Other clonal mESC lines (DM1, DM2, DM3, DM5, DM8, DM9, DM10, DM11, DM12 and DM13), DM11 showed stable upregulation of MAP3K7 transcripts as described above (Fig 7.13B). M8 will be used in the subsequent experiments.

A. Addition of Doxycycline did increase beat rate in M8 EBs

One indication that cardiac cells have adopted the SAN identity is an increase rate of beating speed. To determine if any of our mESCs could differentiate towards SAN cells in response to increased expression of MAP3K7. mESCs were differentiated as EBs and doxycycline added from Day 2 to Day 16 at which point beat rate data was collected and assessed. M8 EBs were tested for increased beat rate with working dose curve of doxycycline (Fig 7.12C). Beating areas were identified based on visual inspection and confirmed by expression of αMHC::GFP. Beat was manually calculated but visual inspection counting beats/minute. Line M8 showed significant increase at both 100ng/ml and 200ng/ml at Day 16. Line M8 will be used for future study.

B. Relative MAP3K7 Expression during EB differentiation

Although addition of Dox worked well in M8 or DM11 mESCs, yet regulation of gene expression within differentiating EBs is much more complicated. To test whether addition of Dox also upregulated MAP3K7 transcripts during EB differentiation, EBs were treated with Dox dose of 0ng/ml, 200ng/ml, 500ng/ml, 1000ng/ml and 2000ng/ml from Day 4 to Day 7 (Fig 7.12D&Fig 7.13C). Then EBs were collected at Day 7 and relative MAP3K7 expression was assessed by qRT-PCR. Surprisingly, only M8 EBs treated with Dox dose of 200ng/ml, which was consistent with the dose tested for fast beating cardiomyocytes. Line M8 associated with Dox Dose 200ng/ml will be used for future study. Meanwhile, DM11 EBs treated with 500ng/ml or 2000ng/ml showed significant increase of MAP3K7 transcripts compared to untreated controls. Line DM11 and dose 500ng/ml will be used in the future study.

C. MAP3K7 overexpression did not increase overall cardiac formation

Our data has shown that MAP3K7-overexpressing EBs did not increase overall cardiac differentiation at Day in chapter four. Our next step is to figure out conditional expression of MAP3K7 effect on cardiac formation. To test this, EBs were differentiated with or without the addition of Dox from Day 4 to Day 19 (Fig 7.13D). Cells were isolated at Day 15 and Day 19. The percentage of cardiac differentiation was assessed based on expression of GFP by flow cytometry. DM11 Dox-treated EBs had no significant increase on overall cardiac formation.

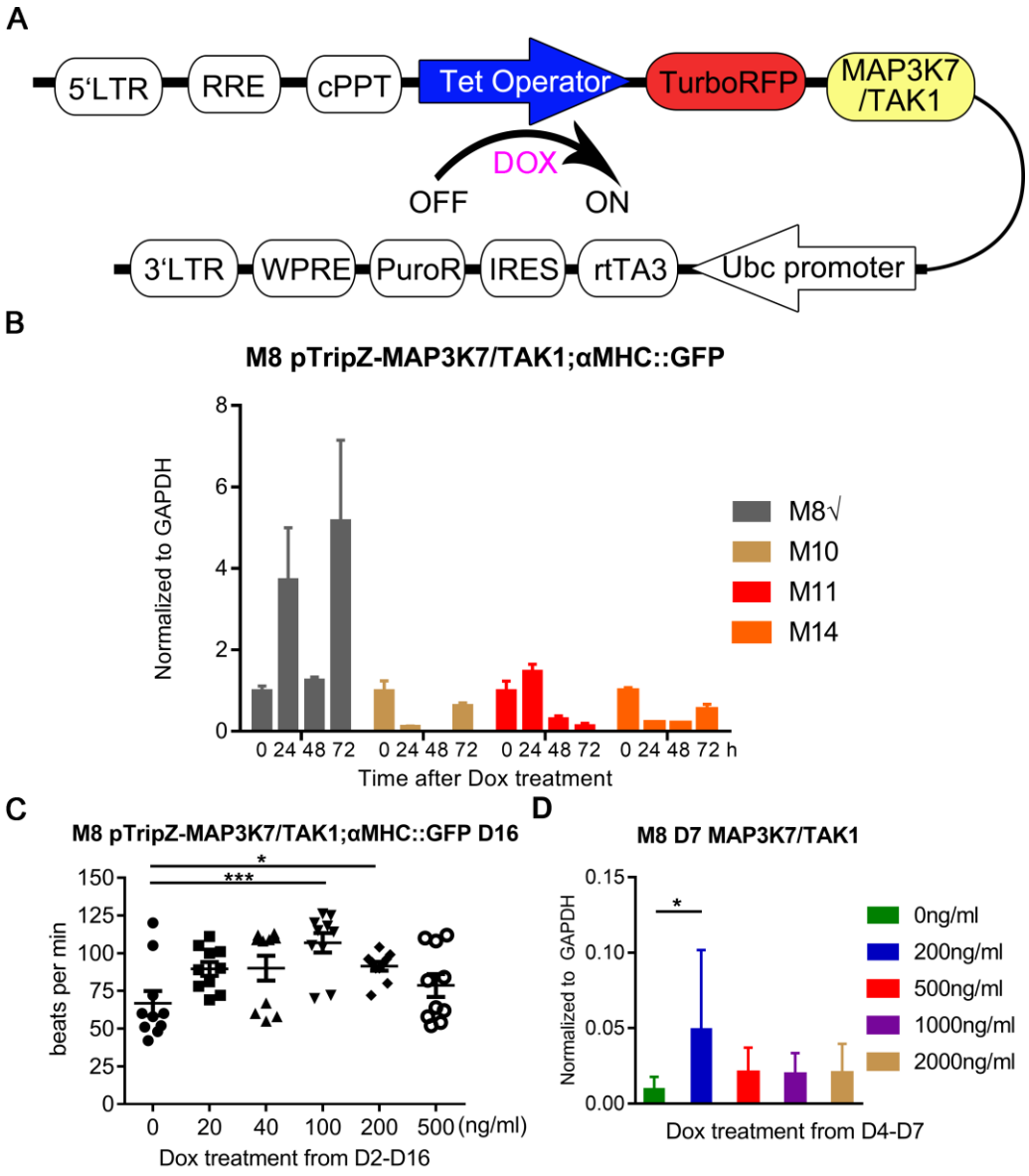

Fig 7.12. Verification of M8 pTripZ-MAP3K7; αMHC::GFP mouse embryonic stem cell line. Fig 7.12A. Schematic design of pTripZ- MAP3K7 Vector, doxycycline-inducible-MAP3K7-overexpression backbone. Fig 7.12B. M8 mESCs were treated with doxycycline at 1 μg /mL and then collected after 0, 24, 48, 72h. Later qRT-PCR was performed to detect relative expression of Isl1. Fig 7.12C. Manual beat data counting of M8 EBs at Day 16 with Doxycycline dose of 0ng/ml, 20ng/ml, 40ng/ml, 100ng/ml, 200ng/ml and 500ng/ml. Fig 7.12D. M8 EBs were treated with Dox dose of 0ng/ml, 200ng/ml, 500ng/ml, 1000ng/ml and 2000ng/ml from Day 4 to Day 7. Then EBs were collected at Day 7 and relative MAP3K7 expression was assessed by qRT-PCR. Data represent means ±standard error of 3 independent experiments. Statistical significance was determined by unpaired, two-tailed t-test. *p<0.05.

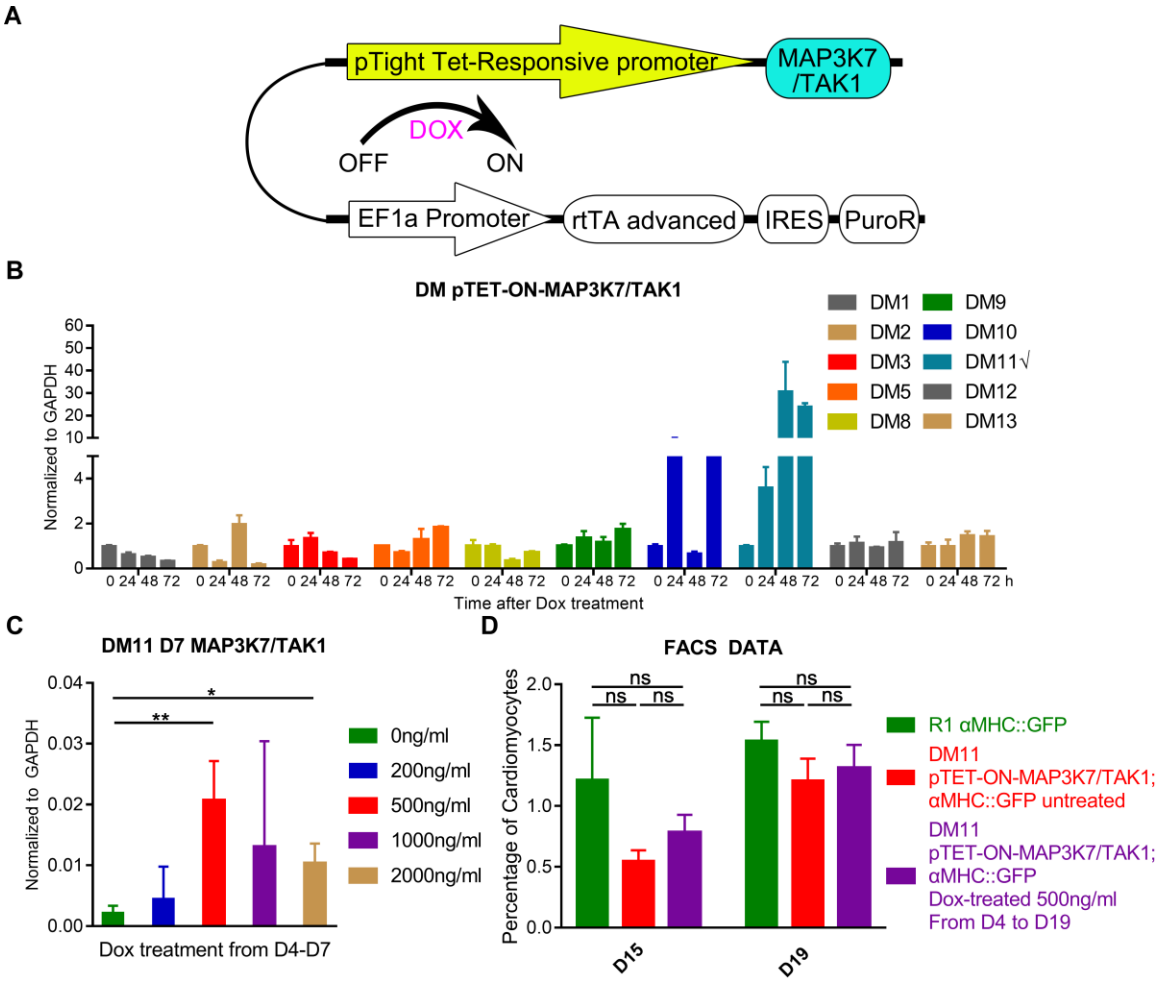

Fig 7.13. Verification of DM11 pTET-ON-MAP3K7; αMHC::GFP mouse embryonic stem cell line. Fig 7.13A. Schematic design of pTET-ON-MAP3K7 Vector, doxycycline-inducible-MAP3K7-overexpression backbone. Fig 7.13B. DM1, DM2, DM3, DM5, DM8, DM9, DM10, DM11, DM12 and DM13 mESCs were treated with doxycycline at 1 μg /mL and then collected after 0, 24, 48, 72h. Later qRT-PCR was performed to detect relative expression of MAP3K7. Fig 7.13C. M8 EBs were treated with Dox dose of 0ng/ml, 200ng/ml, 500ng/ml, 1000ng/ml and 2000ng/ml from Day 4 to Day 7. Then EBs were collected at Day 7 and relative MAP3K7 expression was assessed by qRT-PCR. Fig 7.13 D. EBs were differentiated with or without the addition of Doxycycline from Day 4 to Day 19 and analyzed at Day 15 and Day 19. The percentage of cardiomyocytes was determined by Flow Cytometry Data represent means ± standard error of 3 independent experiments. Statistical significance was determined by unpaired, two-tailed t-test.

Independent clonal lines that conditionally overexpress Tbx5 were established.

To test the role of Tbx5 in SAN development, mESC lines were generated to conditionally overexpress Tbx5. Besides B1, new design is to clone Tbx5 ORF into downstream of pTight TET-Responnsive promoter into the pTET-ON vector (Fig 7.14A), which drives expression of the insert GOI with administration of Doxycycline.

These vectors can be used to conditionally overexpress all of the key transcriptional regulators of SAN differentiation. At the top of this cascade is Tbx5. Genetic studies in mouse have revealed an essential role for Tbx5 in establishing the SAN. However, it has not been shown whether conditional expression of Tbx5 is sufficient for SAN differentiation. To study its role we established four independent, clonal ESC lines (DB3, DB4, DB6, DB7, DB8 and DB10), DB4 and DB6 which showed stable upregulation of Tbx5 transcripts in an inducible fashion, as assessed by qRT-PCR at 24, 48 and 72 hours after addition of doxycycline (1 μg /mL) (Fig 7.14B). To test the best GOI-inducible dose, DB4 and DB6 mESCs were treated with doxycycline at 0ng/ml, 50ng/ml, 100ng/ml and 200ng/ml and then collected after 48 hours (Fig 7.14C). Later qRT-PCR was performed to detect relative expression of Tbx5. Surprisingly, both DB4 and DB6 treated with 100 and 200ng/ml dose of Dox showed upregulation of Tbx5.

A. Relative Tbx5 Expression during EB differentiation

Although addition of Dox worked well in DB4 and DB6 mESCs, yet regulation of gene expression within differentiating EBs is much more complicated. To test whether addition of Dox also upregulated Tbx5 transcripts during EB differentiation, EBs were treated with Dox dose of 0ng/ml, 200ng/ml, 500ng/ml, 1000ng/ml and 2000ng/ml from

Day 4 to Day 7 (Fig 7.14D). Then EBs were collected at Day 7 and relative Tbx5 expression was assessed by qRT-PCR. Surprisingly, DB4 EBs showed upregulation of Tbx5 with dose 500ng/ml and 1000ng/ml, while DB6 showed significant increase of Tbx5 with dose 1000ng/ml and 2000ng/ml. As a result, DB4 with dose 500ng/ml and DB6 with dose 1000ng/ml will be used in the subsequent experiments.

B. Tbx5 overexpression may increase overall cardiac formation

Tbx5 is a key player in cardiac development. Since DB4 and DB6 naturally expresses higher levels of Tbx5 at Day 7 (Fig 7.15A), it might be more active in cardiogenesis. To test this, EBs were differentiated with or without the addition of dox from Day 4 to Day 17 (Fig 7.15B) and from Day 4 to Day 19 (Fig 7.15C). Cells were isolated at Days 15, 17 and 19. The percentage of cardiac differentiation was assessed based on expression of GFP by flow cytometry. Interestingly, at Day 17, both DB4 and DB6 had no significant increase compared to R1, while at Day 15 and Day 19, DB6 untreated EBs had more cardiac cells. DB6 Dox-treated EBs had no significant change.

C. Subtype of Differentiated Cardiomyocytes

Immunocytochemistry (ICC) staining is current standard to figure out cardiac subtype based on protein expression, such as HCN4 and Shox2 for pacemaker marker or Cx43 for ventricular marker. Here four different EBs including R1, MAP3K7/TAK1-overexpressing EBs (pgk:MAP3K7/TAK1; αMHC:mCherry) [141], B1 untreated, B1 Dox-treated were analyzed for HCN4, Shox2 and Cx43 positive cardiomyocytes (Fig 7.16A). MAP3K7/TAK1-overexpressing EBs had more HCH4 and Shox2 positive

cardiomyocytes than R1 EBs, however there was no significant difference either between R1 and DB6, or between DB6 and DB6 dox-treated EBs.

At the same time, whole EBs from R1, DB6 and DB6 Dox-treated group were collected and later assessed by qRT-PCR at Day 17 (Fig 7.16B). DB6 EBs had significant higher levels of MAP3K7 transcripts than the parent cell line R1, while DB6 Dox-treated EBs and DB6 EBs had no significant difference between all these markers.

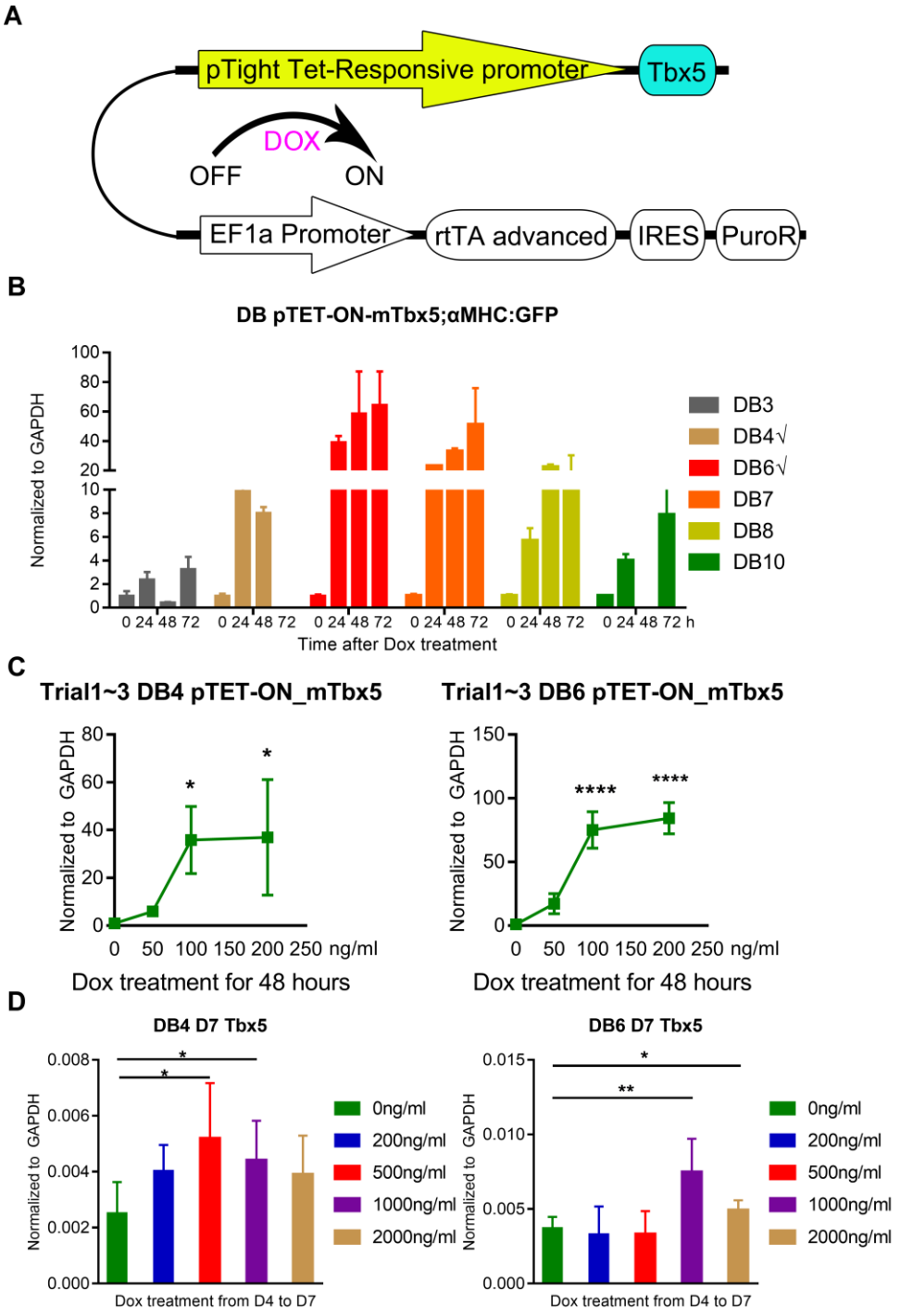

Fig 7.14. Verification of DB4, DB6 pTET-ON-mTbx5; αMHC::GFP mouse embryonic stem cell line. Fig 7.14A. Schematic design of pTET-ON-mTbx5 Vector, doxycycline-inducible-Tbx5-overexpression backbone. Fig 7.14B. DB3, DB4, DB6, DB7, DB8 and DB10 mESCs were treated with doxycycline at 1 μg /mL and then collected after 0, 24, 48, 72h. Later qRT-PCR was performed to detect relative expression of Tbx5. Fig 7.14C. DB4

and DB6 mESCs were treated with doxycycline at 0ng/ml, 50ng/ml, 100ng/ml and 200ng/ml and then collected after 48 hours. Later qRT-PCR was performed to detect relative expression of Tbx5. Fig 7.14D. DB4 and DB6 EBs were treated with Dox dose of 0ng/ml, 200ng/ml, 500ng/ml, 1000ng/ml and 2000ng/ml from Day 4 to Day 7. Then EBs were collected at Day 7 and relative Tbx5 expression was assessed by qRT-PCR. Data represent means ±standard error of 3 independent experiments. Statistical significance was determined by unpaired, two-tailed t-test. *p<0.05, **p<0.01, ****p<0.0001.

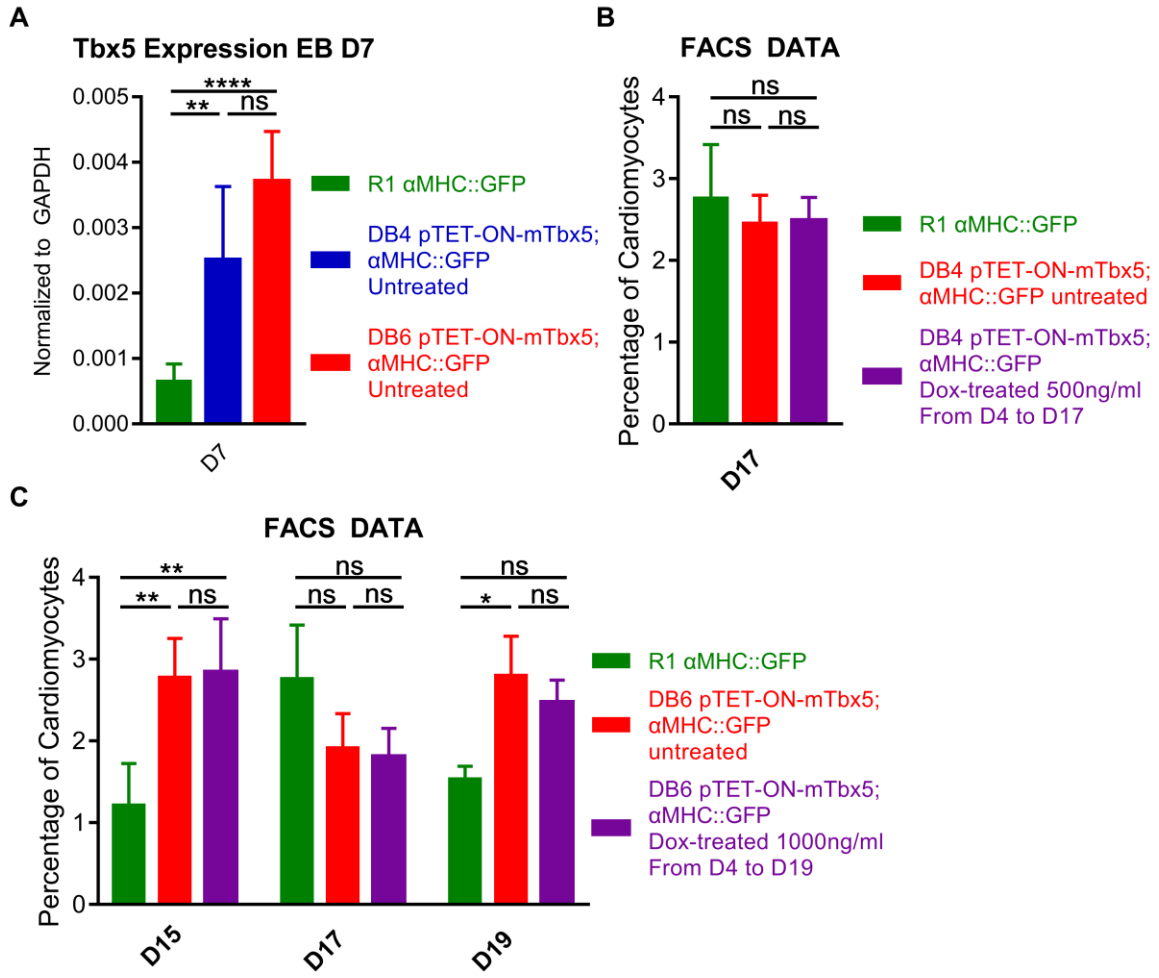

Fig 7.15. Cardiac differentiation analyzed by Flow Cytometry. EBs were collected at Day 7 and assess by qRT-PCR (Fig 7.15A). Fig 7.15B&C. EBs were differentiated with or without the addition of Doxycycline from Day 4 to Day 17 (Fig 7.15B) and from Day 4 to Day 19 (Fig 7.15C). The percentage of cardiomyocytes was determined by Flow Cytometry Data represent means ±standard error of 3 independent experiments. Statistical significance was determined by unpaired, two-tailed t-test. *p<0.05, **p<0.01, ****p<0.0001.

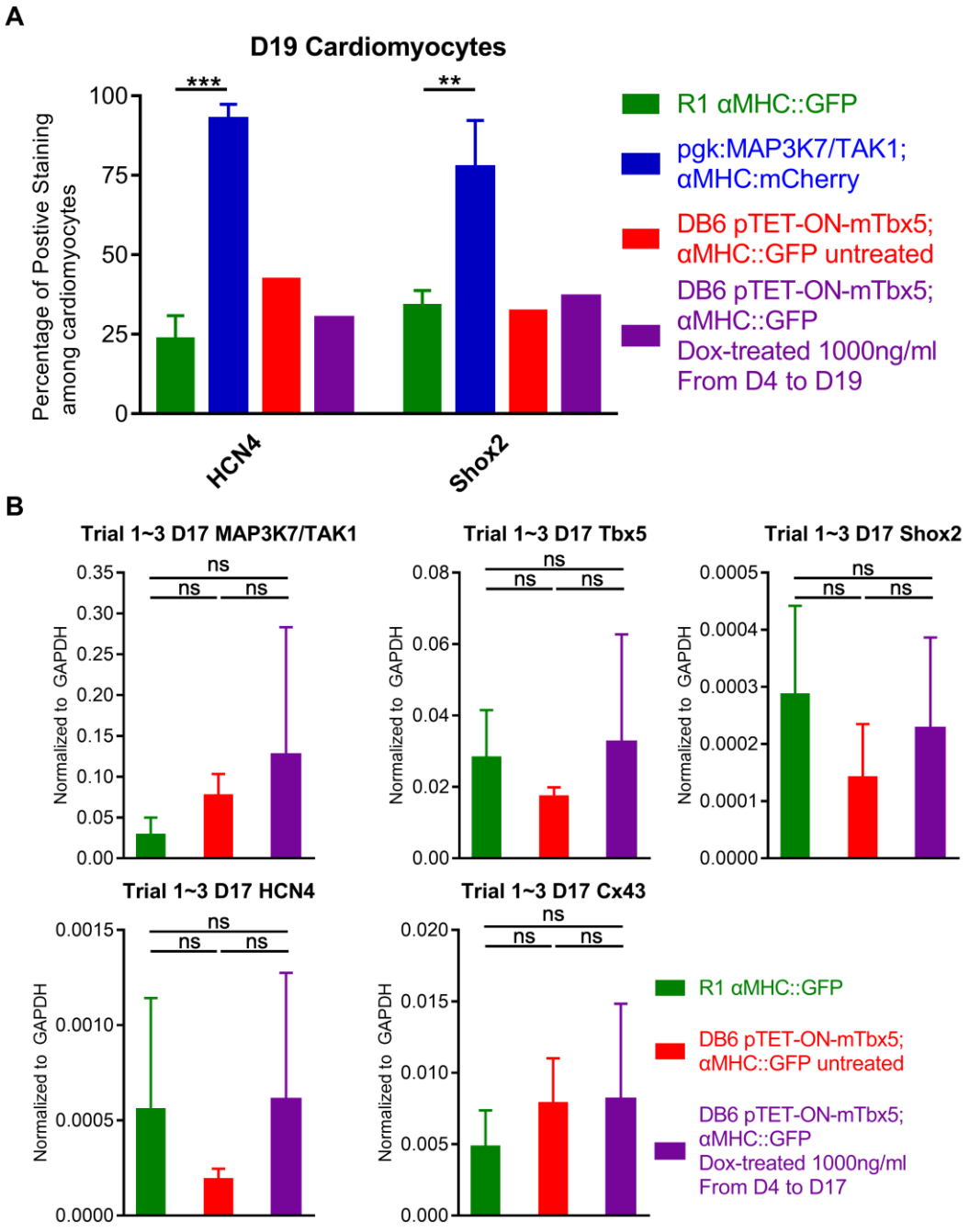

Fig 7.16. The subtype of cardiomyocytes of R1, DB6, DB6 Dox-treated EBs at Day 19 and relative transcripts at Day 17. The percentage of HCN4 and Shox2 positive cardiomyoctes among all cardiomyocytes were analyzed by Immmunocytochemistry and shown in Fig 7.16A, Tbx5, HCN4, Shox2, MAP3K7 and Cx43 transcription were assessed by qRT-PCR and shown in Fig 7.16B. Data represent means ± standard error of 3 independent experiments. Statistical significance was determined by unpaired, two-tailed t-test. **p<0.01, ****p<0.0001.

Summary:

Here, I list all mESCs that I produce and all characteristics of each individual cell line (Table 7.2). For gene Tbx3, pTripZ-mTbx3 X6 and dose of 200ng/ml is the best choice; for gene Isl1, pTripZ-hIsl1 I4 and dose of 500ng/ml is the first choice; for gene, Shox2, pTET-ON-hShox2 DS14 and dose of 50ng/ml is the first choice; for gene Tbx18, pTripZ-hTbx18 T2 and dose of 100ng/ml is the best choice; for gene MAP3K7, pTripZ-MAP3K7 M8 and dose of 200ng/ml is the best choice; for gene Tbx5, pTET-ON-mTbx5 DB6 and dose of 1000ng/ml is the first choice. Taken together, we can study these pacemaker-specific gene in the future project.

Vector Name	Clone	Dox-Inducible ES If Yes, list dose	Dox-Inducible EBs	Increase Beat Rate If Yes, list dose	SAN Gene
pTripZ-mTbx3	X1	Yes, 1000ng/ml	Not Sure	Yes, 200ng/ml	NA
pTripZ-mTbx3	X6	Yes, 1000ng/ml	Yes,200ng/ml	Yes, 200ng/ml	NA
pTET-ON-mTbx3	DX5	Yes, 400ng/ml	NA	NA	NA
pTET-ON-mTbx3	DX9	Yes, 1000ng/ml	NA	NA	NA
pTripZ-hIsl1	I4	Yes, 1000ng/ml	Yes, 500ng/ml	Yes, 500ng/ml	NA
pTET-ON-hIsl1	DI1,DI3	Yes, 1000ng/ml	NA	NA	NA
pTET-ON-hIsl1	DI2,DI7	Yes, 1000ng/ml	NA	NA	NA
pTripZ-hShox2	S2	Yes, 1000ng/ml	NA	No	NA
pTET-ON-hShox2	DS13	Yes, 1000ng/ml	NA	NA	NA
pTET-ON-hShox2	DS14	Yes, 50ng/ml	NA	NA	NA
pTripZ-hTbx18	T2	Yes, 1000ng/ml	NA	Yes, 100ng/ml	NA

pTET-ON-hTbx18	DT2,DT5	Yes, 1000ng/ml	NA	NA	NA
pTripZ-MAP3K7	M8	Yes, 1000ng/ml	Yes, 200ng/ml	Yes, 200ng/ml	NA
pTET-ON-MAP3K7	DM11	Yes, 1000ng/ml	Yes, 500ng/ml	NA	NA
pTET-ON-mTbx5	DB4	Yes, 100ng/ml	Yes, 500ng/ml	NA	NA
pTET-ON-mTbx5	DB6	Yes, 200ng/ml	Yes, 1000ng/ml	NA	Yes

Table 7.2 List of all mESCs that I produce and all characteristics. NA, Not Applicable.

CHAPTER EIGHT

DISCUSSION

A transcriptional cascade that mediates SAN differentiation.

Vincent Christofells elucidated the transcriptional program involved in SAN differentiation from mesodermal precursors in the mouse (Fig 8.1). With the help of transgenic mice and the advancement of lineage tracing techniques, the progenitors of the SAN cells and the transcriptional program directing their differentiation have been well-established [117]. Mommersteeg and colleagues demonstrated that around E8, the sinus venosus develops from $Tbx18^{+}/Nkx2.5^{-}/Isl1^{-}$ progenitors, apart from the rest of the cardiac mesoderm. At E8.5, some of these cells begin to express Islet1, and later at E9.5, a subset within the sinus venosus starts to express Tbx3, a transcription factor (TF) that represses chamber development [118]. Tbx3 is continuously expressed during cardiac development in the forming mature conduction system, comprising both the SAN and the bundle branches of the ventricular conduction system. Shox2, like Tbx18, has an expression pattern complementary to that of Nkx2.5, the TF that activates cardiac chamber formation [113]; Shox2 is a repressor of the Nkx2.5 gene, thus preventing chamber myocardium formation in the SAN, while allowing SAN-specific gene expression, such as Tbx3 and HCN4 [114]. These data suggest that pacemaker cells derive from the activation of a particular genetic pathway in progenitors during cardiogenesis of the SAN.

The Foley lab recently reported that overexpression of MAP3K7/TAK1 in mESC-derived cardiomyocytes faithfully directed cardiac progenitor cells into the SAN lineage.

Most cardiac cells in MAP3K7/TAK1-overexpressing EBs adopted pacemaker markers, cellular morphologies and electrophysiological behaviors characteristics of the SAN fate. MAP3K7/TAK1 proved, by qRT-PCR analysis, to be an upstream regulator of pacemaker specific gene expression (Fig 8.2).

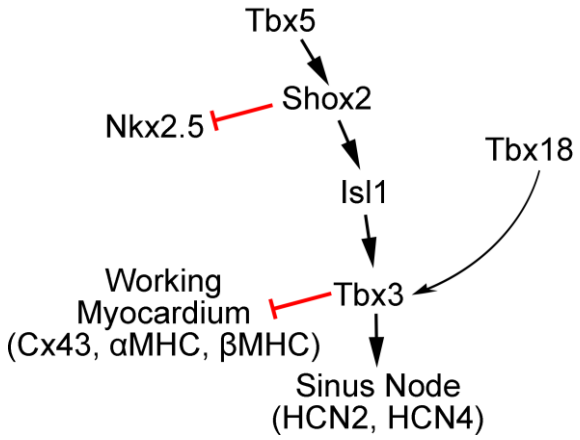

Fig 8.1. Proposed model of TF interactions during SAN differentiation.

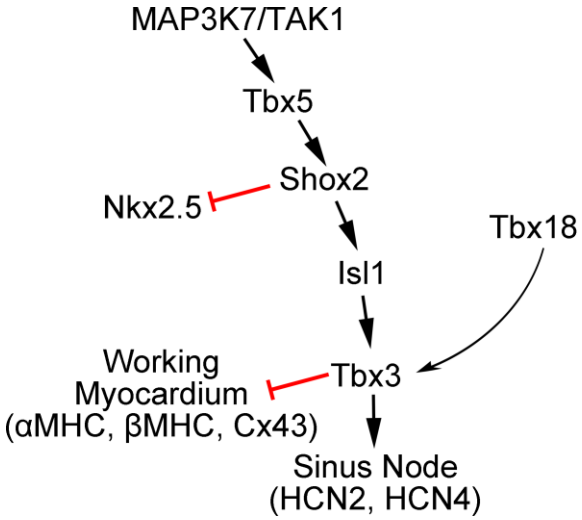

Fig 8.2. Foley lab model of TF interactions during SAN differentiation.

ES cell lines with overexpression of Tbx3, Isl1, Shox2 and Tbx18

In 2013, the Cho lab genetically transduced the TF, Tbx18, into neonatal rat ventricular myocytes (NRVMs), which converted NRVMs into SAN pacemaker-like (SAN) cells [84]. In vivo, gene transfer of Tbx18 in the guinea pig heart yielded ectopic pacemaker activity, restoring a bradycardic phenotype [84]. One year later, the David lab showed that pure populations of physiologically and pharmacologically functional pacemaker cells could be obtained by overexpressing the SAN-inducing TF, Tbx3, in mouse embryonic stem cells (mESCs); these were differentiated as embryoid bodies (EBs), and cardiomyocytes were purified based on an Myh6 promoter-based antibiotic selection [157]. In 2015, the Cho lab demonstrated that TF, Shox2, overexpression during EB differentiation of mESCs resulted in upregulation of the pacemaker genetic program [151]. Similarly, the TF, Isl1 overexpression in mESCs was shown to promote differentiation of cardiomyocytes with electrophysiological profiles typical of pacemaker cells [149]. Taken together, these data suggest that TFs can activate (or select for) the differentiation of SAN cells from ESCs. However, these studies do not completely address all criteria for SAN cell differentiation and, in most cases, the efficiency of SAN conversion was low [151, 157]. Additionally, purported pacemaker cells in some cases expressed the ventricular inward rectifier Ik1 [151] suggesting that these had hybrid ventricular/SAN characteristics. Also some of these cells did not express physiologically normal levels or the pacemaker-specific inward funny (If) current suggesting that they were immature SAN-like cells [157]. Biological pacing in this model peaked around day 7 and waned by day 14 due to the

declining heart rate [84], showing that biological pacing was not successfully maintained in the absence of these transgenes.

These suggest that TFs downstream of Tbx5 were not sufficient for permanent conversion of ES cells to the pacemaker fate. To determine whether Tbx5 could activate pacemaker fates I made a cell line to conditionally overexpress Tbx5 (B1).

Data Interpretation from Tbx5-Overexpressing B1 EBs

From beat data at D19 and D21, we observed something different in B1 and B1 Dox-treated EBs (Fig 8.3A). At the same time, we checked the relative Tbx5 transcripts at D19 and D21 (Fig 8.3B). Interesting, B1 Dox-treated EBs had more Tbx5 transcripts at D19 and less Tbx5 transcripts at Day 21, compared to B1 untreated EBs, meanwhile, B1 treated EBs had faster beating cells than B1 untreated EBs only at Day 21, not at Day 19. These data suggested that the loss of Tbx5 in B1 Dox-treated EBs might be the reason for fast beating cardiomyocytes. Tbx5 may be lost in adult mature cardiomyocytes.

Next, to figure out the expression of all downstream marker of Tbx5, such as Shox2, Isl1, Tbx3, Tbx18, HCN4 and also ventricular marker Nkx2.5 and Cx43 (Fig 8.4). Compared to R1 wild type, the Tbx5 overexpressing cell line B1 had a pattern that activated downstream Shox2, Isl1, Tbx3, Tbx18, HCN4, but did not inhibit Nkx2.5 and Cx43 transcripts. Upstream MAP3K7/TAK1 did not change among R1, B1, B1 Dox-treated EBs.

In order to figure out the subtype of cardiomyocytes of R1, MAP3K7/TAK1-overexpressiong, B1, B1 Dox-treated EBs, ICC staining was performed on these four groups (Fig 8.5). To our surprise, either B1 Dox-treated EBs or B1 untreated EBs did not

adopt HCN4 or Shox2 pacemaker phenotype even with increased HCN4 and Shox2 transcripts. In other words, cardiac cells derived from B1 or B1 Dox-treated EBs did not express transcription factors associated with the SAN fate. Meanwhile, B1 and B1 Dox-treated EBs had less Cx43 positive population compared to R1 ventricle phenotype, more Cx43 cardiac cells compared to MAP3K7/TAK1 pacemaker phenotype. Surprisingly, compare to B1 untreated EBs, B1 Dox-treated EBs had less Cx43 positive myocytes, which explained why fast beating myocytes in B1 Box-treated EBs were found at Day 21.These data suggested that B1 and B1 Dox-treated EBs might acquire atrial cardiac fate.

Recent study has shown that lentiviral delivery of Cx43 ectopic expression in myocardial scar area resulted in increased conduction velocities in the infarct and its border zone and during long-time anti-ventricular tachycardia protection [158]. Optical mapping of hearts transduced by a Cx43 overexpression lentivirus revealed enhanced conduction velocity within the scar, indicating Cx43-mediated electrical coupling between myocytes and myofibroblasts. The Cx43 protein expression in myofibroblast surrounding the myocytes is unknown. Further experiments need to test this assumption. This is another explanation why B1 Dox-treated EBs beats much faster than B1 untreated EBs. Furthermore, targeted mutation of Mef2c, downstream of MAP3K7/TAK1, resulted in a small left ventricle and complete loss of the right ventricle. Tbx5 was normally expressed throughout cardiac crescent but become restricted to sinoatrial region during linear heart tube formation. In Mef2c-/- embryos, Tbx5 was ectopically and anteriorly expressed in the primitive Mef2c-/- ventricle [159].

Cardiac cells differentiated from Tbx5-overexpression B1 cell line did activated enhanced expression of Shox2 and HCN4, however there was no significant difference of HCN4 or Shox2 positive population among R1, B1, B1 Dox-treated cardiac cells as assessed by ICC. Due to RNA analysis from whole EBs, including cardiomyocytes and non-cardiomyocytes, ICC staining only focused on authentic myocytes. This means untargeted HCN4 and Shox2 ectopic expression in non-myocytes.

In summary, Tbx5 is required for cardiac formation generally and is sufficient to activate Shox2, Tbx3, Tbx18 and HCN4 transcripts but its expression alone does not inhibits Nkx2.5 and Cx43 transcripts. Together these data suggest that Tbx5 cannot activate SAN differentiation alone but instead must synergize with other factors (Fig 8.6).

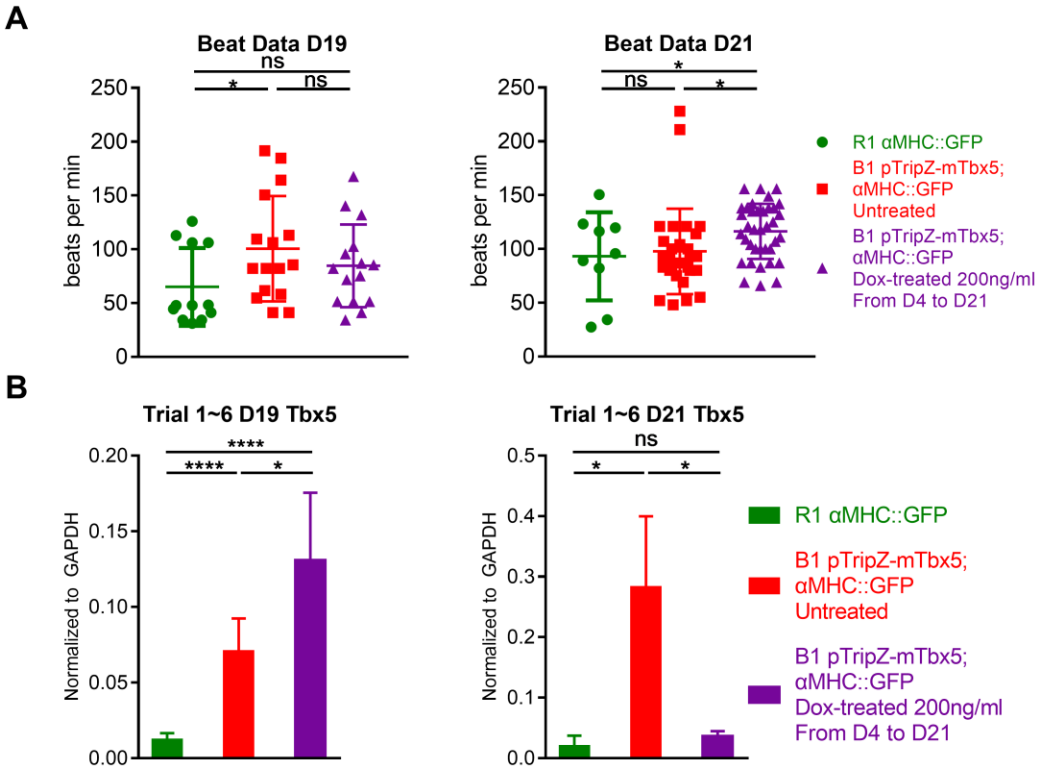

Fig 8.3. Beat Data and Tbx5 transcripts at Day 19 and Day 21 and subtype of cardiomyocytes at Day 21. Fig 8.3A. Using MATLAB automation to calculate cardiac beats of R1, B1 and B1 Dox-treated EBs at Day 19 and Day 21. Fig 8.3B. The relative Tbx5 transcripts among R1, B1 and B1 Dox-treated EBs by qRT-PCR. Data represent means ± standard error of 6 independent experiments. Statistical significance was determined by unpaired, two-tailed t-test. *p<0.05, ***p<0.001, ****p<0.0001.

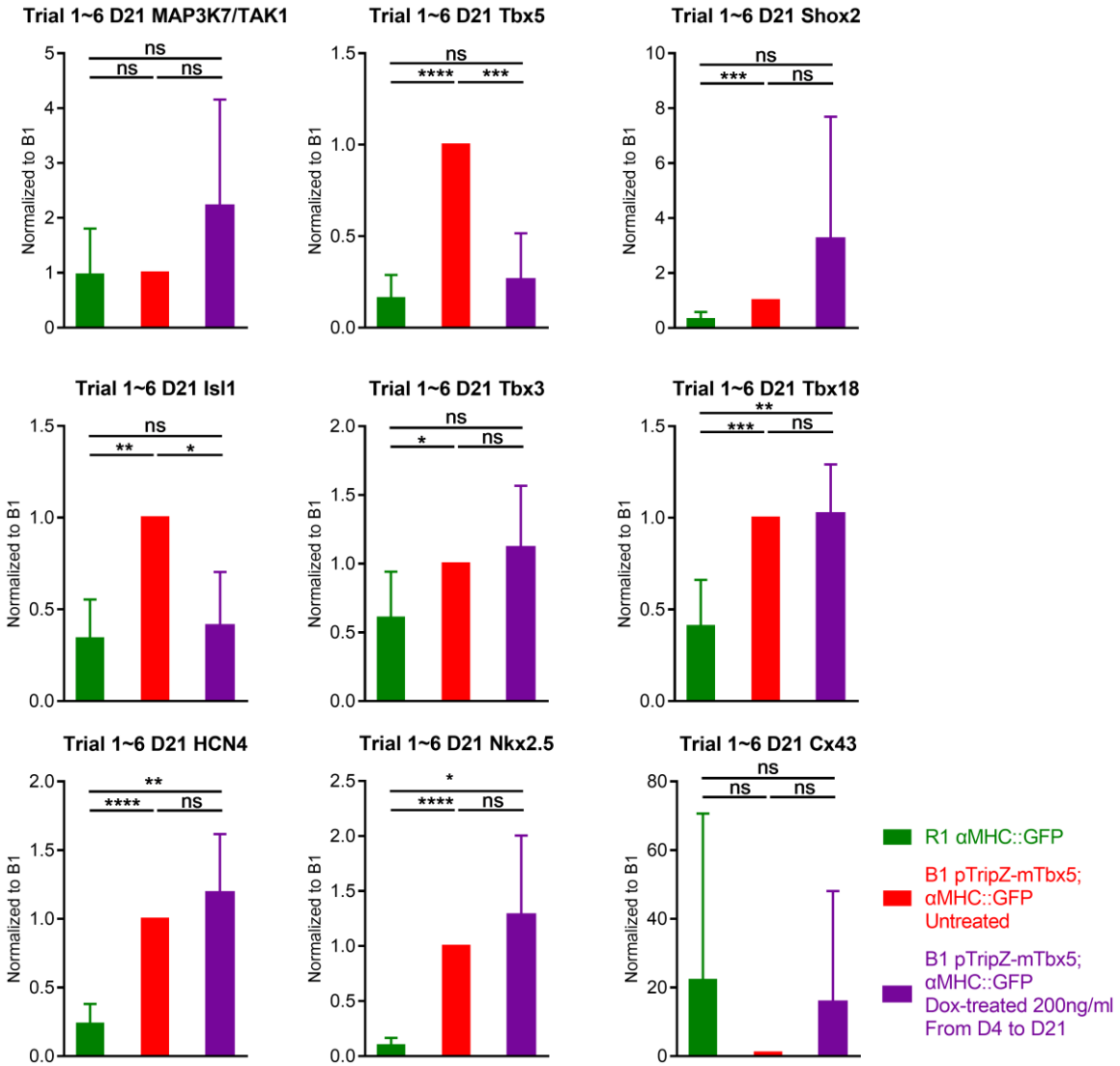

Fig 8.4. The relative transcripts of R1, B1, B1 Dox-treated EBs at Day 21. MAP3K7/TAK1, Tbx5, Shox2, Tbx3, Tbx18, HCN4, Nkx2.5, Isl1 and Cx43 transcription were assessed by qRT-PCR. Data represent means ± standard error of 6 independent experiments, normalized to B1. Statistical significance was determined by unpaired, two-tailed t-test. *p<0.05, **p<0.01, ***p<0.001, ****p<0.0001.

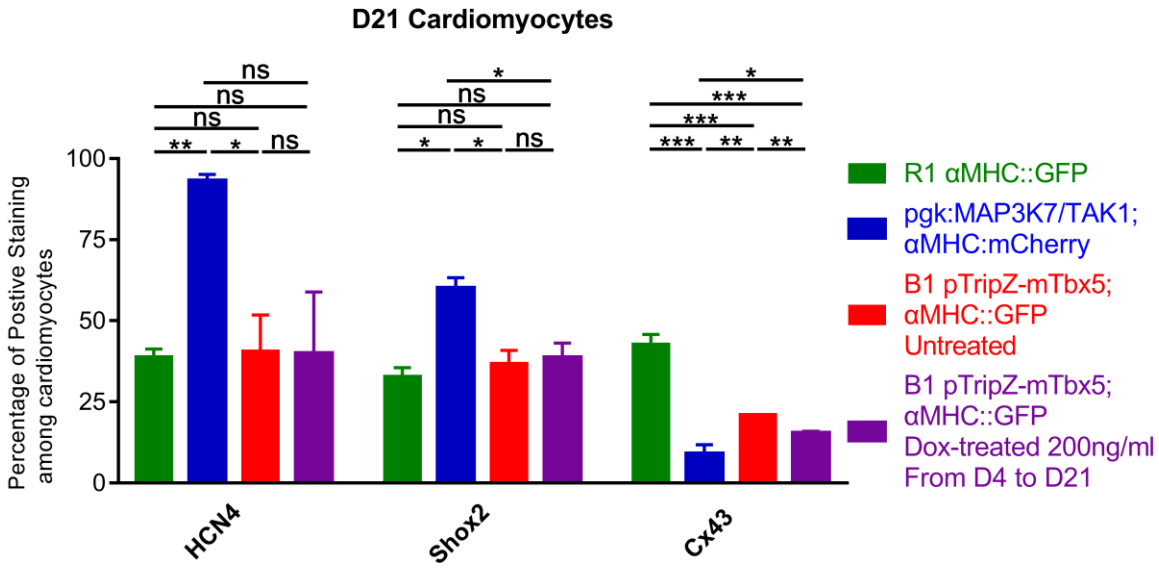

Fig 8.5. The subtype of cardiomyocytes of R1, MAP3K7/TAK1 overexpressing, B1, B1 Dox-treated EBs at Day 21. The percentage of HCN4, Shox2 and Cx43 positive cardiomyoctes among all cardiomyocytes were analyzed by ICC. Data represent means ± standard error of 3 independent experiments. Statistical significance was determined by unpaired, two-tailed t-test. *p<0.05, **p<0.01, ***p<0.001.

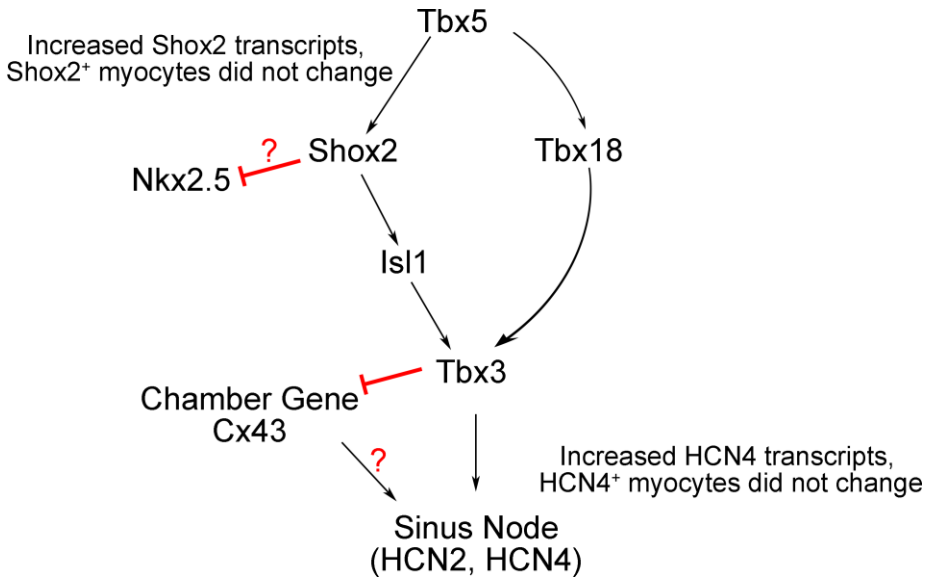

Fig 8.6. Sufficient expression of Tbx5 activates Shox2, Isl1, Tbx3, Tbx18 and HCN4 transcripts, but do not inhibits Nkx2.5 and Cx43 transcripts.

CHAPTER NINE

FUTURE RESEARCH

In the field of regenerative medicine, protocols for lineage specific differentiation of cardiomyocytes have promising applications. At first, they will provide the tools to find out new markers for SAN fate during differentiation. Second, these well-characterized cardiac cells could be used as a basis for pharmacological screening on pacemaker cells especially derived from patient-specific iPS cells. This will allow us to test the effect of new designed drugs on pacemaker cells. Finally, these cells could serve as the basis for biological pacemaker development. Unlike skin or skeleton muscle, adult mammal hearts have little or no capability to regenerate themselves after myocardial infarction. Furthermore, myocardial infarction causes the formation of apoptotic and necrotic myocytes that would be replaced by myofibroblasts and scar tissue in the end. The SAN dysfunction results in bradycardia, arrhythmia and eventually heart failure.

REFERENCE

1. Hoyert, D.L. and J. Xu, *Deaths; Preliminary data for 2011*. 2012.
2. Bergmann, O., et al., *Evidence for cardiomyocyte renewal in humans.* Science, 2009. **324**(5923): p. 98-102.
3. Andersen, D.C., et al., *Do neonatal mouse hearts regenerate following heart apex resection?* Stem cell reports, 2014. **2**(4): p. 406-413.
4. Beltrami, C.A., et al., *Structural basis of end-stage failure in ischemic cardiomyopathy in humans.* Circulation, 1994. **89**(1): p. 151-163.
5. Hsieh, P.C., et al., *Evidence from a genetic fate-mapping study that stem cells refresh adult mammalian cardiomyocytes after injury.* Nature medicine, 2007. **13**(8): p. 970.
6. Mummery, C., et al., *Differentiation of human embryonic stem cells to cardiomyocytes: role of coculture with visceral endoderm-like cells.* Circulation, 2003. **107**(21): p. 2733-40.
7. Laflamme, M.A., et al., *Cardiomyocytes derived from human embryonic stem cells in pro-survival factors enhance function of infarcted rat hearts.* Nat Biotechnol, 2007. **25**(9): p. 1015-24.
8. Yang, L., et al., *Human cardiovascular progenitor cells develop from a KDR+ embryonic-stem-cell-derived population.* Nature, 2008. **453**(7194): p. 524-8.
9. Moretti, A., et al., *Multipotent embryonic isl1+ progenitor cells lead to cardiac, smooth muscle, and endothelial cell diversification.* Cell, 2006. **127**(6): p. 1151-65.
10. Meilhac, S.M., et al., *The clonal origin of myocardial cells in different regions of the embryonic mouse heart.* Dev Cell, 2004. **6**(5): p. 685-98.
11. Cai, C.L., et al., *Isl1 identifies a cardiac progenitor population that proliferates prior to differentiation and contributes a majority of cells to the heart.* Dev Cell, 2003. **5**(6): p. 877-89.
12. Kelly, R.G., N.A. Brown, and M.E. Buckingham, *The arterial pole of the mouse heart forms from Fgf10-expressing cells in pharyngeal mesoderm.* Dev Cell, 2001. **1**(3): p. 435-40.
13. Qyang, Y., et al., *The renewal and differentiation of Isl1+ cardiovascular progenitors are controlled by a Wnt/beta-catenin pathway.* Cell Stem Cell, 2007. **1**(2): p. 165-79.
14. Zaffran, S., et al., *Right ventricular myocardium derives from the anterior heart field.* Circ Res, 2004. **95**(3): p. 261-8.
15. Waldo, K., et al., *Cardiac neural crest cells provide new insight into septation of the cardiac outflow tract: aortic sac to ventricular septal closure.* Developmental biology, 1998. **196**(2): p. 129-144.
16. Foley, A., *Cardiac lineage selection: integrating biological complexity into computational models.* Wiley Interdisciplinary Reviews: Systems Biology and Medicine, 2009. **1**(3): p. 334-347.

17. Guzzo, R.M., et al., *Signaling pathways in embryonic heart induction.* Advances in Developmental Biology, 2007. **18**: p. 117-151.
18. Eisenberg, C.A., R.G. Gourdie, and L.M. Eisenberg, *Wnt-11 is expressed in early avian mesoderm and required for the differentiation of the quail mesoderm cell line QCE-6.* Development, 1997. **124**(2): p. 525-536.
19. Heasman, J., et al., *Overexpression of cadherins and underexpression of beta-catenin inhibit dorsal mesoderm induction in early Xenopus embryos.* Cell, 1994. **79**(5): p. 791-803.
20. Zorn, A.M., K. Butler, and J. Gurdon, *Anterior Endomesoderm Specification inXenopusby Wnt/β-catenin and TGF-β Signalling Pathways.* Developmental biology, 1999. **209**(2): p. 282-297.
21. Christian, J.L., et al., *Xwnt-8, a Xenopus Wnt-1/int-1-related gene responsive to mesoderm-inducing growth factors, may play a role in ventral mesodermal patterning during embryogenesis.* Development, 1991. **111**(4): p. 1045-1055.
22. Kofron, M., et al., *Mesoderm induction in Xenopus is a zygotic event regulated by maternal VegT via TGFbeta growth factors.* Development, 1999. **126**(24): p. 5759-5770.
23. Yamaguchi, K., et al., *XIAP, a cellular member of the inhibitor of apoptosis protein family, links the receptors to TAB1-TAK1 in the BMP signaling pathway.* EMBO J, 1999. **18**(1): p. 179-87.
24. Kimelman, D. and M. Kirschner, *Synergistic induction of mesoderm by FGF and TGF-β and the identification of an mRNA coding for FGF in the early Xenopus embryo.* Cell, 1987. **51**(5): p. 869-877.
25. Pfendler, K.C., et al., *Nodal and bone morphogenetic protein 5 interact in murine mesoderm formation and implantation.* genesis, 2000. **28**(1): p. 1-14.
26. Rodaway, A., et al., *Induction of the mesendoderm in the zebrafish germ ring by yolk cell-derived TGF-beta family signals and discrimination of mesoderm and endoderm by FGF.* Development, 1999. **126**(14): p. 3067-3078.
27. Rosa, F., et al., *Mesoderm induction in amphibians: the role of TGF-beta 2-like factors.* Science, 1988. **239**(4841): p. 783-785.
28. Tam, P. and R. Beddington, *The formation of mesodermal tissues in the mouse embryo during gastrulation and early organogenesis.* Development, 1987. **99**(1): p. 109-126.
29. Tam, P., et al., *The allocation of epiblast cells to the embryonic heart and other mesodermal lineages: the role of ingression and tissue movement during gastrulation.* Development, 1997. **124**(9): p. 1631-1642.
30. Lickert, H., et al., *Formation of multiple hearts in mice following deletion of β-catenin in the embryonic endoderm.* Developmental cell, 2002. **3**(2): p. 171-181.
31. Marvin, M.J., et al., *Inhibition of Wnt activity induces heart formation from posterior mesoderm.* Genes Dev, 2001. **15**(3): p. 316-27.
32. Schneider, V.A. and M. Mercola, *Wnt antagonism initiates cardiogenesis in Xenopus laevis.* Genes & development, 2001. **15**(3): p. 304-315.

33. Nakamura, T., et al., *A Wnt-and β-catenin-dependent pathway for mammalian cardiac myogenesis.* Proceedings of the National Academy of Sciences, 2003. **100**(10): p. 5834-5839.
34. Naito, A.T., et al., *Developmental stage-specific biphasic roles of Wnt/beta-catenin signaling in cardiomyogenesis and hematopoiesis.* Proc Natl Acad Sci U S A, 2006. **103**(52): p. 19812-7.
35. Ueno, S., et al., *Biphasic role for Wnt/beta-catenin signaling in cardiac specification in zebrafish and embryonic stem cells.* Proc Natl Acad Sci U S A, 2007. **104**(23): p. 9685-90.
36. Gadue, P., et al., *Wnt and TGF-beta signaling are required for the induction of an in vitro model of primitive streak formation using embryonic stem cells.* Proc Natl Acad Sci U S A, 2006. **103**(45): p. 16806-11.
37. Behfar, A., et al., *Stem cell differentiation requires a paracrine pathway in the heart.* The FASEB Journal, 2002. **16**(12): p. 1558-1566.
38. Goumans, M.-J. and C. Mummery, *Functional analysis of the TGFbeta receptor/Smad pathway through gene ablation in mice.* International Journal of Developmental Biology, 2000. **44**(3): p. 253-265.
39. Jamali, M., et al., *BMP signaling regulates Nkx2‐5 activity during cardiomyogenesis.* FEBS letters, 2001. **509**(1): p. 126-130.
40. Lin, L., et al., *β-catenin directly regulates Islet1 expression in cardiovascular progenitors and is required for multiple aspects of cardiogenesis.* Proceedings of the National Academy of Sciences, 2007. **104**(22): p. 9313-9318.
41. Takei, S., et al., *Bone morphogenetic protein-4 promotes induction of cardiomyocytes from human embryonic stem cells in serum-based embryoid body development.* American Journal of Physiology-Heart and Circulatory Physiology, 2009.
42. Willems, E. and L. Leyns, *Patterning of mouse embryonic stem cell-derived pan-mesoderm by Activin A/Nodal and Bmp4 signaling requires Fibroblast Growth Factor activity.* Differentiation, 2008. **76**(7): p. 745-759.
43. Yuasa, S., et al., *Transient inhibition of BMP signaling by Noggin induces cardiomyocyte differentiation of mouse embryonic stem cells.* Nature biotechnology, 2005. **23**(5): p. 607.
44. Mjaatvedt, C., et al., *The outflow tract of the heart is recruited from a novel heart-forming field.* Developmental biology, 2001. **238**(1): p. 97-109.
45. Waldo, K.L., et al., *Conotruncal myocardium arises from a secondary heart field.* Development, 2001. **128**(16): p. 3179-3188.
46. Saga, Y., S. Kitajima, and S. Miyagawa-Tomita, *Mesp1 expression is the earliest sign of cardiovascular development.* Trends in cardiovascular medicine, 2000. **10**(8): p. 345-352.
47. Saga, Y., et al., *MesP1 is expressed in the heart precursor cells and required for the formation of a single heart tube.* Development, 1999. **126**(15): p. 3437-3447.
48. Kitajima, S., et al., *MesP1 and MesP2 are essential for the development of cardiac mesoderm.* Development, 2000. **127**(15): p. 3215-3226.

49. Bondue, A., et al., *Mesp1 acts as a master regulator of multipotent cardiovascular progenitor specification.* Cell stem cell, 2008. **3**(1): p. 69-84.
50. Ma, Q., B. Zhou, and W.T. Pu, *Reassessment of Isl1 and Nkx2-5 cardiac fate maps using a Gata4-based reporter of Cre activity.* Developmental biology, 2008. **323**(1): p. 98-104.
51. Spater, D., et al., *A HCN4+ cardiomyogenic progenitor derived from the first heart field and human pluripotent stem cells.* Nat Cell Biol, 2013. **15**(9): p. 1098-106.
52. Wu, S.M., et al., *Developmental origin of a bipotential myocardial and smooth muscle cell precursor in the mammalian heart.* Cell, 2006. **127**(6): p. 1137-1150.
53. Bu, L., et al., *Human ISL1 heart progenitors generate diverse multipotent cardiovascular cell lineages.* Nature, 2009. **460**(7251): p. 113-7.
54. Laugwitz, K.-L., et al., *Postnatal isl1+ cardioblasts enter fully differentiated cardiomyocyte lineages.* Nature, 2005. **433**(7026): p. 647.
55. Sun, Y., et al., *Islet 1 is expressed in distinct cardiovascular lineages, including pacemaker and coronary vascular cells.* Dev Biol, 2007. **304**(1): p. 286-96.
56. Laugwitz, K.L., et al., *Postnatal isl1+ cardioblasts enter fully differentiated cardiomyocyte lineages.* Nature, 2005. **433**(7026): p. 647-53.
57. Ema, M., S. Takahashi, and J. Rossant, *Deletion of the selection cassette, but not cis-acting elements, in targeted Flk1-lacZ allele reveals Flk1 expression in multipotent mesodermal progenitors.* Blood, 2006. **107**(1): p. 111-117.
58. Motoike, T., et al., *Evidence for novel fate of Flk1+ progenitor: contribution to muscle lineage.* genesis, 2003. **35**(3): p. 153-159.
59. Kattman, S.J., E.D. Adler, and G.M. Keller, *Specification of multipotential cardiovascular progenitor cells during embryonic stem cell differentiation and embryonic development.* Trends in cardiovascular medicine, 2007. **17**(7): p. 240-246.
60. Kattman, S.J., T.L. Huber, and G.M. Keller, *Multipotent flk-1+ cardiovascular progenitor cells give rise to the cardiomyocyte, endothelial, and vascular smooth muscle lineages.* Developmental cell, 2006. **11**(5): p. 723-732.
61. Christoforou, N., et al., *Mouse ES cell–derived cardiac precursor cells are multipotent and facilitate identification of novel cardiac genes.* The Journal of clinical investigation, 2008. **118**(3): p. 894-903.
62. Nelson, T.J., et al., *CXCR4+/FLK‐1+ biomarkers select a cardiopoietic lineage from embryonic stem cells.* Stem cells, 2008. **26**(6): p. 1464-1473.
63. He, J.-Q., et al., *Human embryonic stem cells develop into multiple types of cardiac myocytes.* Circulation research, 2003. **93**(1): p. 32-39.
64. Kolossov, E., et al., *Identification and characterization of embryonic stem cell-derived pacemaker and atrial cardiomyocytes.* The FASEB journal, 2005. **19**(6): p. 577-579.
65. Maltsev, V.A., et al., *Cardiomyocytes differentiated in vitro from embryonic stem cells developmentally express cardiac-specific genes and ionic currents.* Circulation research, 1994. **75**(2): p. 233-244.

66. Chong, J.J., et al., *Human embryonic-stem-cell-derived cardiomyocytes regenerate non-human primate hearts.* Nature, 2014. **510**(7504): p. 273.
67. Yang, X., L. Pabon, and C.E. Murry, *Engineering adolescence: maturation of human pluripotent stem cell-derived cardiomyocytes.* Circ Res, 2014. **114**(3): p. 511-23.
68. Garcia‐Martinez, V., I.S. Alvarez, and G.C. Schoenwolf, *Locations of the ectodermal and nonectodermal subdivisions of the epiblast at stages 3 and 4 of avian gastrulation and neurulation.* Journal of Experimental Zoology, 1993. **267**(4): p. 431-446.
69. Stainier, D., R.K. Lee, and M.C. Fishman, *Cardiovascular development in the zebrafish. I. Myocardial fate map and heart tube formation.* Development, 1993. **119**(1): p. 31-40.
70. Yutzey, K.E., M. Gannon, and D. Bader, *Diversification of cardiomyogenic cell lineages in vitro.* Developmental biology, 1995. **170**(2): p. 531-541.
71. Yutzey, K.E., J.T. Rhee, and D. Bader, *Expression of the atrial-specific myosin heavy chain AMHC1 and the establishment of anteroposterior polarity in the developing chicken heart.* Development, 1994. **120**(4): p. 871-883.
72. Satin, J., S. Fujii, and R.L. DeHaan, *Development of cardiac beat rate in early chick embryos is regulated by regional cues.* Developmental biology, 1988. **129**(1): p. 103-113.
73. Wang, J., et al., *Effect of engineered anisotropy on the susceptibility of human pluripotent stem cell-derived ventricular cardiomyocytes to arrhythmias.* Biomaterials, 2013. **34**(35): p. 8878-8886.
74. Karakikes, I., et al., *Small molecule‐mediated directed differentiation of human embryonic stem cells toward ventricular cardiomyocytes.* Stem cells translational medicine, 2014. **3**(1): p. 18-31.
75. Weng, Z., et al., *A simple, cost-effective but highly efficient system for deriving ventricular cardiomyocytes from human pluripotent stem cells.* Stem cells and development, 2014. **23**(14): p. 1704-1716.
76. Takahashi, K. and S. Yamanaka, *Induction of pluripotent stem cells from mouse embryonic and adult fibroblast cultures by defined factors.* Cell, 2006. **126**(4): p. 663-76.
77. Halder, G., P. Callaerts, and W.J. Gehring, *Induction of ectopic eyes by targeted expression of the eyeless gene in Drosophila.* Science, 1995. **267**(5205): p. 1788-1792.
78. Davis, R.L., H. Weintraub, and A.B. Lassar, *Expression of a single transfected cDNA converts fibroblasts to myoblasts.* Cell, 1987. **51**(6): p. 987-1000.
79. Lassar, A.B., B.M. Paterson, and H. Weintraub, *Transfection of a DNA locus that mediates the conversion of 10T12 fibroblasts to myoblasts.* Cell, 1986. **47**(5): p. 649-656.
80. Ieda, M., et al., *Direct reprogramming of fibroblasts into functional cardiomyocytes by defined factors.* Cell, 2010. **142**(3): p. 375-386.
81. Qian, L., et al., *In vivo reprogramming of murine cardiac fibroblasts into induced cardiomyocytes.* Nature, 2012. **485**(7400): p. 593.

82. Chen, J.X., et al., *Inefficient reprogramming of fibroblasts into cardiomyocytes using Gata4, Mef2c, and Tbx5.* Circulation research, 2012. **111**(1): p. 50-55.
83. Fu, J.-D., et al., *Direct reprogramming of human fibroblasts toward a cardiomyocyte-like state.* Stem cell reports, 2013. **1**(3): p. 235-247.
84. Kapoor, N., et al., *Direct conversion of quiescent cardiomyocytes to pacemaker cells by expression of Tbx18.* Nat Biotechnol, 2013. **31**(1): p. 54-62.
85. Boudou, T., et al., *A microfabricated platform to measure and manipulate the mechanics of engineered cardiac microtissues.* Tissue Eng Part A, 2012. **18**(9-10): p. 910-9.
86. Vunjak-Novakovic, G., et al., *Bioengineering heart muscle: a paradigm for regenerative medicine.* Annu Rev Biomed Eng, 2011. **13**: p. 245-67.
87. Kofidis, T., et al., *Novel injectable bioartificial tissue facilitates targeted, less invasive, large-scale tissue restoration on the beating heart after myocardial injury.* Circulation, 2005. **112**(9_supplement): p. I-173-I-177.
88. Zhang, Y., et al., *Collagen-based matrices improve the delivery of transplanted circulating progenitor cells: development and demonstration by ex vivo radionuclide cell labeling and in vivo tracking with positron-emission tomography.* Circulation: Cardiovascular Imaging, 2008. **1**(3): p. 197-204.
89. Roura, S., et al., *Human umbilical cord blood-derived mesenchymal stem cells promote vascular growth in vivo.* PloS one, 2012. **7**(11): p. e49447.
90. Jia, J., et al., *Engineering alginate as bioink for bioprinting.* Acta biomaterialia, 2014. **10**(10): p. 4323-4331.
91. Kraehenbuehl, T.P., et al., *Three-dimensional extracellular matrix-directed cardioprogenitor differentiation: systematic modulation of a synthetic cell-responsive PEG-hydrogel.* Biomaterials, 2008. **29**(18): p. 2757-2766.
92. Dobner, S., et al., *A synthetic non-degradable polyethylene glycol hydrogel retards adverse post-infarct left ventricular remodeling.* J Card Fail, 2009. **15**(7): p. 629-36.
93. Paul, A., et al., *Injectable graphene oxide/hydrogel-based angiogenic gene delivery system for vasculogenesis and cardiac repair.* ACS Nano, 2014. **8**(8): p. 8050-62.
94. Duan, B., et al., *Three-dimensional printed trileaflet valve conduits using biological hydrogels and human valve interstitial cells.* Acta biomaterialia, 2013.
95. Landa, N., et al., *Effect of injectable alginate implant on cardiac remodeling and function after recent and old infarcts in rat.* Circulation, 2008. **117**(11): p. 1388.
96. Leor, J., et al., *Intracoronary injection of in situ forming alginate hydrogel reverses left ventricular remodeling after myocardial infarction in Swine.* Journal of the American College of Cardiology, 2009. **54**(11): p. 1014-1023.
97. Christman, K.L., et al., *Injectable fibrin scaffold improves cell transplant survival, reduces infarct expansion, and induces neovasculature formation in ischemic myocardium.* Journal of the American College of Cardiology, 2004. **44**(3): p. 654-660.

98. Godier-Furnémont, A.F., et al., *Composite scaffold provides a cell delivery platform for cardiovascular repair.* Proceedings of the National Academy of Sciences, 2011. **108**(19): p. 7974-7979.
99. Singelyn, J.M., et al., *Catheter-deliverable hydrogel derived from decellularized ventricular extracellular matrix increases endogenous cardiomyocytes and preserves cardiac function post-myocardial infarction.* Journal of the American College of Cardiology, 2012. **59**(8): p. 751-763.
100. Duan, Y., et al., *Hybrid gel composed of native heart matrix and collagen induces cardiac differentiation of human embryonic stem cells without supplemental growth factors.* J Cardiovasc Transl Res, 2011. **4**(5): p. 605-15.
101. Cui, X. and T. Boland, *Human microvasculature fabrication using thermal inkjet printing technology.* Biomaterials, 2009. **30**(31): p. 6221-6227.
102. Vollert, I., et al., *In vitro perfusion of engineered heart tissue through endothelialized channels.* Tissue Eng Part A, 2014. **20**(3-4): p. 854-63.
103. Vukadinovic-Nikolic, Z., et al., *Generation of Bioartificial Heart Tissue by Combining a Three-Dimensional Gel-Based Cardiac Construct with Decellularized Small Intestinal Submucosa.* Tissue Engineering Part A, 2013.
104. Ott, H.C., et al., *Perfusion-decellularized matrix: using nature's platform to engineer a bioartificial heart.* Nat Med, 2008. **14**(2): p. 213-21.
105. Lu, T.Y., et al., *Repopulation of decellularized mouse heart with human induced pluripotent stem cell-derived cardiovascular progenitor cells.* Nat Commun, 2013. **4**: p. 2307.
106. van Weerd, J.H. and V.M. Christoffels, *The formation and function of the cardiac conduction system.* Development, 2016. **143**(2): p. 197-210.
107. Christoffels, V.M., et al., *Development of the pacemaker tissues of the heart.* Circulation research, 2010. **106**(2): p. 240-254.
108. Puskaric, S., et al., *Shox2 mediates Tbx5 activity by regulating Bmp4 in the pacemaker region of the developing heart.* Human molecular genetics, 2010. **19**(23): p. 4625-4633.
109. Mori, A.D., et al., *Tbx5-dependent rheostatic control of cardiac gene expression and morphogenesis.* Developmental biology, 2006. **297**(2): p. 566-586.
110. Schott, J.J., et al., *Congenital heart disease caused by mutations in the transcription factor NKX2-5.* Science, 1998. **281**(5373): p. 108-11.
111. Basson, C.T., et al., *Mutations in human TBX5 [corrected] cause limb and cardiac malformation in Holt-Oram syndrome.* Nat Genet, 1997. **15**(1): p. 30-5.
112. Li, Q.Y., et al., *Holt-Oram syndrome is caused by mutations in TBX5, a member of the Brachyury (T) gene family.* Nature genetics, 1997. **15**(1): p. 21.
113. Liu, H., et al., *The role of Shox2 in SAN development and function.* Pediatr Cardiol, 2012. **33**(6): p. 882-9.
114. Espinoza-Lewis, R.A., et al., *Shox2 is essential for the differentiation of cardiac pacemaker cells by repressing Nkx2-5.* Dev Biol, 2009. **327**(2): p. 376-85.
115. Hashem, S.I., et al., *Shox2 regulates the pacemaker gene program in embryoid bodies.* Stem cells and development, 2013. **22**(21): p. 2915-2926.

116. Blaschke, R.J., et al., *Targeted mutation reveals essential functions of the homeodomain transcription factor Shox2 in sinoatrial and pacemaking development.* Circulation, 2007. **115**(14): p. 1830-8.
117. Mommersteeg, M.T., et al., *The sinus venosus progenitors separate and diversify from the first and second heart fields early in development.* Cardiovasc Res, 2010. **87**(1): p. 92-101.
118. Hoogaars, W.M., et al., *The transcriptional repressor Tbx3 delineates the developing central conduction system of the heart.* Cardiovascular research, 2004. **62**(3): p. 489-499.
119. Wiese, C., et al., *Formation of the sinus node head and differentiation of sinus node myocardium are independently regulated by Tbx18 and Tbx3.* Circ Res, 2009. **104**(3): p. 388-97.
120. Mommersteeg, M.T., et al., *Molecular pathway for the localized formation of the sinoatrial node.* Circ Res, 2007. **100**(3): p. 354-62.
121. Hoogaars, W.M., et al., *Tbx3 controls the sinoatrial node gene program and imposes pacemaker function on the atria.* Genes Dev, 2007. **21**(9): p. 1098-112.
122. Bakker, M.L., et al., *T-box transcription factor TBX3 reprogrammes mature cardiac myocytes into pacemaker-like cells.* Cardiovascular research, 2012. **94**(3): p. 439-449.
123. Garcia-Frigola, C., Y. Shi, and S.M. Evans, *Expression of the hyperpolarization-activated cyclic nucleotide-gated cation channel HCN4 during mouse heart development.* Gene Expression Patterns, 2003. **3**(6): p. 777-783.
124. Liang, X., et al., *HCN4 dynamically marks the first heart field and conduction system precursors.* Circulation research, 2013. **113**(4): p. 399-407.
125. Christoffels, V.M., et al., *Formation of the venous pole of the heart from an Nkx2–5–negative precursor population requires Tbx18.* Circulation research, 2006. **98**(12): p. 1555-1563.
126. Horsthuis, T., et al., *Gene expression profiling of the forming atrioventricular node using a novel tbx3-based node-specific transgenic reporter.* Circ Res, 2009. **105**(1): p. 61-9.
127. Christoffels, V.M., et al., *T-box transcription factor Tbx2 represses differentiation and formation of the cardiac chambers.* Dev Dyn, 2004. **229**(4): p. 763-70.
128. Harrelson, Z., et al., *Tbx2 is essential for patterning the atrioventricular canal and for morphogenesis of the outflow tract during heart development.* Development, 2004. **131**(20): p. 5041-5052.
129. Aanhaanen, W.T., et al., *Defective Tbx2-dependent patterning of the atrioventricular canal myocardium causes accessory pathway formation in mice.* The Journal of clinical investigation, 2011. **121**(2): p. 534-544.
130. Singh, R., et al., *Tbx2 and Tbx3 induce atrioventricular myocardial development and endocardial cushion formation.* Cellular and Molecular Life Sciences, 2012. **69**(8): p. 1377-1389.
131. Boogerd, K.-J., et al., *Msx1 and Msx2 are functional interacting partners of T-box factors in the regulation of Connexin43.* Cardiovascular research, 2008. **78**(3): p. 485-493.

132. Chen, Y.-H., et al., *Msx1 and Msx2 are required for endothelial-mesenchymal transformation of the atrioventricular cushions and patterning of the atrioventricular myocardium.* BMC developmental biology, 2008. **8**(1): p. 75.
133. van den Boogaard, M., et al., *Genetic variation in T-box binding element functionally affects SCN5A/SCN10A enhancer.* The Journal of clinical investigation, 2012. **122**(7): p. 2519-2530.
134. Habets, P.E., et al., *Cooperative action of Tbx2 and Nkx2. 5 inhibits ANF expression in the atrioventricular canal: implications for cardiac chamber formation.* Genes & development, 2002. **16**(10): p. 1234-1246.
135. Rentschler, S., et al., *Visualization and functional characterization of the developing murine cardiac conduction system.* Development, 2001. **128**(10): p. 1785-1792.
136. Miquerol, L., et al., *Biphasic development of the mammalian ventricular conduction system.* Circulation research, 2010. **107**(1): p. 153.
137. Miquerol, L., et al., *Resolving cell lineage contributions to the ventricular conduction system with a Cx40‐GFP allele: A dual contribution of the first and second heart fields.* Developmental Dynamics, 2013. **242**(6): p. 665-677.
138. Herrmann, J., et al., *Contemporary Reviews in Cardiovascular Medicine.* 2016.
139. Brown, K., et al., *eXtraembryonic ENdoderm (XEN) stem cells produce factors that activate heart formation.* PLoS One, 2010. **5**(10): p. e13446.
140. Liu, W., et al., *Nodal mutant eXtraembryonic ENdoderm (XEN) stem cells upregulate markers for the anterior visceral endoderm and impact the timing of cardiac differentiation in mouse embryoid bodies.* Biology open, 2012: p. BIO2012038.
141. Brown, K., et al., *Overexpression of Map3k7 activates sinoatrial node-like differentiation in mouse ES-derived cardiomyocytes.* PLoS One, 2017. **12**(12): p. e0189818.
142. Bajpai, R. and A. Terskikh, *Genetic manipulation of human embryonic stem cells: lentivirus vectors*, in *Human Stem Cell Manual*. 2007, Elsevier. p. 255-266.
143. Reno, A., et al. *Quantification of Cardiomyocyte Beating Frequency Using Fourier Transform Analysis*. in *Photonics*. 2018. Multidisciplinary Digital Publishing Institute.
144. Kwon, G.S., et al., *Tg (Afp‐GFP) expression marks primitive and definitive endoderm lineages during mouse development.* Developmental dynamics: an official publication of the American Association of Anatomists, 2006. **235**(9): p. 2549-2558.
145. Kwon, G.S., M. Viotti, and A.-K. Hadjantonakis, *The endoderm of the mouse embryo arises by dynamic widespread intercalation of embryonic and extraembryonic lineages.* Developmental cell, 2008. **15**(4): p. 509-520.
146. Brown, K., et al., *A comparative analysis of extra-embryonic endoderm cell lines.* PLoS One, 2010. **5**(8): p. e12016.
147. Zhu, L., et al., *Cerberus regulates left–right asymmetry of the embryonic head and heart.* Current Biology, 1999. **9**(17): p. 931-938.

148. Mohan, R.A., et al., *Embryonic Tbx3(+) cardiomyocytes form the mature cardiac conduction system by progressive fate restriction.* Development, 2018. **145**(17).
149. Dorn, T., et al., *Direct nkx2-5 transcriptional repression of isl1 controls cardiomyocyte subtype identity.* Stem Cells, 2015. **33**(4): p. 1113-29.
150. Liang, X., et al., *Transcription factor ISL1 is essential for pacemaker development and function.* The Journal of clinical investigation, 2015. **125**(8): p. 3256.
151. Ionta, V., et al., *SHOX2 overexpression favors differentiation of embryonic stem cells into cardiac pacemaker cells, improving biological pacing ability.* Stem Cell Reports, 2015. **4**(1): p. 129-42.
152. Ye, W., et al., *A common Shox2-Nkx2-5 antagonistic mechanism primes the pacemaking cell fate in the pulmonary vein myocardium and sinoatrial node.* Development, 2015.
153. Chen, L., et al., *Tbx18-dependent differentiation of brown adipose tissue-derived stem cells toward cardiac pacemaker cells.* Molecular and cellular biochemistry, 2017. **433**(1-2): p. 61-77.
154. Choudhury, M., et al., *TBX18 overexpression enhances pacemaker function in a rat subsidiary atrial pacemaker model of sick sinus syndrome.* J Physiol, 2018.
155. Li, Y., et al., *Transcription factor TBX18 promotes adult rat bone mesenchymal stem cell differentiation to biological pacemaker cells.* Int J Mol Med, 2018. **41**(2): p. 845-851.
156. Jadrich, J.L., M.B. O'Connor, and E. Coucouvanis, *The TGF beta activated kinase TAK1 regulates vascular development in vivo.* Development, 2006. **133**(8): p. 1529-41.
157. Jung, J.J., et al., *Programming and isolation of highly pure physiologically and pharmacologically functional sinus-nodal bodies from pluripotent stem cells.* Stem Cell Reports, 2014. **2**(5): p. 592-605.
158. Roell, W., et al., *Overexpression of Cx43 in cells of the myocardial scar: Correction of post-infarct arrhythmias through heterotypic cell-cell coupling.* Scientific reports, 2018. **8**(1): p. 7145.
159. Vong, L., et al., *MEF2C is required for the normal allocation of cells between the ventricular and sinoatrial precursors of the primary heart field.* Developmental dynamics, 2006. **235**(7): p. 1809-1821.